




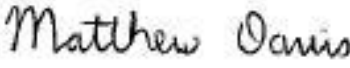
Central Waitemata Harbour Contaminant Study

Harbour Hydrodynamic, Wave and
Sediment Transport Model
Implementation and Calibration

December

TR 2008/037

Technical Report, first edition.

Reviewed by:	Approved for ARC publication by:
	
Name: Hayden Easton	Name: Matthew Davis
Position: Team Leader Stormwater Action Team	Position: Group Manager Partnerships & Community Programmes
Organisation: Auckland Regional Council	Organisation: Auckland Regional Council
Date: 12 December 2009	Date: 18 December 2009

Recommended Citation:

OLDMAN, J.; GORMAN, R.; LEWIS, M., 2008. Central Waitemata Harbour Contaminant Study. Harbour Hydrodynamic, Wave and Sediment Transport Model Implementation and Calibration. Prepared by NIWA Ltd for Auckland Regional Council. Auckland Regional Council Technical Report 2008/037.

© 2008 Auckland Regional Council

This publication is provided strictly subject to Auckland Regional Council's (ARC) copyright and other intellectual property rights (if any) in the publication. Users of the publication may only access, reproduce and use the publication, in a secure digital medium or hard copy, for responsible genuine non-commercial purposes relating to personal, public service or educational purposes, provided that the publication is only ever accurately reproduced and proper attribution of its source, publication date and authorship is attached to any use or reproduction. This publication must not be used in any way for any commercial purpose without the prior written consent of ARC. ARC does not give any warranty whatsoever, including without limitation, as to the availability, accuracy, completeness, currency or reliability of the information or data (including third party data) made available via the publication and expressly disclaim (to the maximum extent permitted in law) all liability for any damage or loss resulting from your use of, or reliance on the publication or the information and data provided via the publication. The publication and information and data contained within it are provided on an "as is" basis.

Central Waitemata Harbour Contaminant Study. Harbour Hydrodynamic, Wave and Sediment Transport Model Implementation and Calibration

John Oldman
Richard Gorman
Matt Lewis

Prepared for
Auckland Regional Council

NIWA Client Report: HAM2007-102
June 2007

NIWA Projects: ARC06217 and ARC07236
National Institute of Water & Atmospheric Research Ltd
Gate 10, Silverdale Road, Hamilton
P O Box 11115, Hamilton, New Zealand
Phone +64-7-856 7026, Fax +64-7-856 0151
www.niwa.co.nz

Reviewed by:



Scott Stephens, NIWA

Approved for release by:



Malcolm Green, NIWA

Preface

The Waitemata Harbour is comprised of tidal creeks, embayments and the central basin. The harbour receives sediment and stormwater chemical contaminant run-off from urban and rural land from a number of subcatchments, which can adversely affect the ecology. An earlier study examined long-term accumulation of sediment and stormwater chemical contaminants in the Upper Waitemata Harbour. However, previously little was known about the existing and long-term accumulation of sediment and stormwater chemical contaminants in the central harbour. The Central Waitemata Harbour Contaminant Study was commissioned to improve understanding of these issues. This study is part of the 10-year Stormwater Action Plan to increase knowledge and improve stormwater management outcomes in the region. The work was undertaken by the National Institute of Water and Atmospheric Research (NIWA).

The scope of the study entailed:

- 1) field investigation,
- 2) development of a suite of computer models for
 - a. urban and rural catchment sediment and chemical contaminant loads,
 - b. harbour hydrodynamics and
 - c. harbour sediment and contaminant dispersion and accumulation,
- 3) application of the suite of computer models to project the likely fate of sediment, copper and zinc discharged into the central harbour over the 100-year period 2001 to 2100, and
- 4) conversion of the suite of computer models into a desktop tool that can be readily used to further assess the effects of different stormwater management interventions on sediment and stormwater chemical contaminant accumulation in the central harbour over the 100-year period.

The study is limited to assessment of long-term accumulation of sediment, copper and zinc in large-scale harbour depositional zones. The potential for adverse ecological effects from copper and zinc in the harbour sediments was assessed against sediment quality guidelines for chemical contaminants.

The study and tools developed address large-scale and long timeframes and consequently cannot be used to assess changes and impacts from small subcatchments or landuse developments, for example. Furthermore, the study does not assess ecological effects of discrete storm events or long-term chronic or sub-lethal ecological effects arising from the cocktail of urban contaminants and sediment.

The range of factors and contaminants influencing the ecology means that adverse ecological effects may occur at levels below contaminant guideline values for individual chemical contaminants (i.e., additive effects due to exposure to multiple contaminants may be occurring).

Existing data and data collected for the study were used to calibrate the individual computer models. The combined suite of models was calibrated against historic sedimentation and copper and zinc accumulation rates, derived from sediment cores collected from the harbour.

Four scenarios were modelled: a baseline scenario and three general stormwater management intervention scenarios.

The baseline scenario assumed current projections (at the time of the study) of

- future population growth,
- future landuse changes,
- expected changes in building roof materials,
- projected vehicle use, and
- existing stormwater treatment.

The three general stormwater management intervention scenarios evaluated were:

- 1) source control of zinc by painting existing unpainted and poorly painted galvanised steel industrial building roofs;
- 2) additional stormwater treatment, including:
 - raingardens on roads carrying more than 20,000 vehicles per day and on paved industrial sites,
 - silt fences and hay bales for residential infill building sites and
 - pond / wetland trains treating twenty per cent of catchment area; and
- 3) combinations of the two previous scenarios.

International Peer Review Panel

The study was subject to internal officer and international peer review. The review was undertaken in stages during the study, which allowed incorporation of feedback and completion of a robust study. The review found:

- a state-of-the-art study on par with similar international studies,
- uncertainties that remain about the sediment and contaminant dynamics within tidal creeks / estuaries, and
- inherent uncertainties when projecting out 100 years.

Key Findings of the Study

Several key findings can be ascertained from the results and consideration of the study within the context of the wider Stormwater Action Plan aim to improve stormwater outcomes:

- Henderson Creek (which drains the largest subcatchment and with the largest urban area, as well as substantial areas of rural land) contributes the largest loads of sediment, copper and zinc to the Central Waitemata Harbour. The second largest loads come from the Upper Waitemata Harbour.
- Substantial proportions of the subcatchment sediment, copper and zinc loads are accumulating in the Henderson, Whau, Meola and Motions tidal creeks and in the Shoal Bay, Hobson Bay and Waterview embayments.
- Central Waitemata Harbour bed sediment concentrations of copper and zinc are not expected to reach toxic levels based on current assumptions of future trends in urban landuse and activities.
- Zinc source control targeting industrial building roofs produced limited reduction of zinc accumulation rates in the harbour because industrial areas cover only a small proportion of the catchment area and most unpainted galvanised steel roofs are expected to be replaced with other materials within the next 25 to 50 years.
- Given that the modelling approach used large-scale depositional zones and long timeframes, differences can be expected from the modelling projections and stormwater management interventions contained within these reports versus consideration of smaller depositional areas and local interventions. (For example, whereas the study addresses the Whau River as a whole, differences exist within parts of the Whau River that may merit a different magnitude or type of intervention than may be inferred from considering the Whau River and its long-term contaminant trends as a whole.) As a consequence, these local situations may merit further investigation and assessment to determine the best manner in which to intervene and make improvements in the short and long terms.

Research and Investigation Questions

From consideration of the study and results, the following issues have been identified that require further research and investigation:

- Sediment and chemical contaminant dynamics within tidal creeks.
- The magnitude and particular locations of stormwater management interventions required to arrest sediment, copper and zinc accumulation in tidal creeks and embayments, including possible remediation / restoration opportunities.
- The fate of other contaminants derived from urban sources.
- The chronic / sub-lethal effects of marine animal exposure to the cocktail of urban contaminants and other stressors such sediment deposition, changing sediment particle size distribution and elevated suspended sediment loads.
- Ecosystem health and connectivity issues between tidal creeks and the central basin of the harbour, and the wider Hauraki Gulf.

Technical reports

The study has produced a series of technical reports:

Technical Report TR2008/032
Central Waitemata Harbour Contaminant Study. Landuse Scenarios.

Technical Report TR2008/033
Central Waitemata Harbour Contaminant Study. Background Metal Concentrations in Soils: Methods and Results.

Technical Report TR2008/034
Central Waitemata Harbour Contaminant Study. Harbour Sediments.

Technical Report TR2008/035
Central Waitemata Harbour Contaminant Study. Trace Metal Concentrations in Harbour Sediments.

Technical Report TR2008/036
Central Waitemata Harbour Contaminant Study. Hydrodynamics and Sediment Transport Fieldwork.

Technical Report TR2008/037
Central Waitemata Harbour Contaminant Study. Harbour Hydrodynamics, Wave and Sediment Transport Model Implementation and Calibration.

Technical Report TR2008/038
Central Waitemata Harbour Contaminant Study. Development of the Contaminant Load Model.

Technical Report TR2008/039
Central Waitemata Harbour Contaminant Study. Predictions of Stormwater Contaminant Loads.

Technical Report TR2008/040
Central Waitemata Harbour Contaminant Study. GLEAMS Model Structure, Setup and Data Requirements.

Technical Report TR2008/041
Central Waitemata Harbour Contaminant Study. GLEAMS Model Results for Rural and Earthworks Sediment Loads.

Technical Report TR2008/042
Central Waitemata Harbour Contaminant Study. USC-3 Model Description, Implementation and Calibration.

Technical Report TR2008/043
Central Waitemata Harbour Contaminant Study. Predictions of Sediment, Zinc and Copper Accumulation under Future Development Scenario 1.

Technical Report TR2008/044
Central Waitemata Harbour Contaminant Study. Predictions of Sediment, Zinc and Copper Accumulation under Future Development Scenarios 2, 3 and 4.

Technical Report TR2009/109
Central Waitemata Harbour Contaminant Study. Rainfall Analysis.

Contents

1	Executive Summary	1
2	Introduction	2
2.1	Study aims	2
2.2	Model suite	2
2.3	This report	3
3	Mesh Development	8
4	Formulation of Processes Simulated by the MIKE3 Models	15
4.1	Mesh flooding and drying	15
4.2	Bed shear stress	15
4.3	Currents	17
4.4	Salinity	18
4.5	Sediment transport	18
4.5.1	Deposition	19
4.5.2	Erosion	19
5	Model Calibration	20
5.1	Water surface elevation	20
5.2	Currents	24
5.3	Salinity	32
5.4	Waves	46
5.4.1	SWAN model application to the Central Waitemata Harbour	46
5.4.2	Calibration simulations	46
5.4.3	Comparison with measurements	47
5.5	Suspended sediment concentration	55
6	References	74
7	Appendix 1: LIDAR Data Processing	76
8	Appendix 2: Mesh Detail	78

1 Executive Summary

The overall aim of the Central Waitemata Harbour (CWH) Contaminant Study is to model contaminant accumulation (sediment, zinc, copper) within the harbour for the purposes of, amongst other things, identifying significant contaminant sources, and testing efficacy of stormwater treatment and zinc source control of industrial roofs. The objective is to predict (using models) contaminant build up and movement in the CWH.

This report describes the implementation and calibration of three models being used in the study: an estuarine hydrodynamic model, a wave model, and a sediment-transport model. Together these simulate the dispersal of contaminants and sediments by physical processes such as tidal currents and waves.

The particular models used in the study are the DHI Water and Environment (DHI) MIKE3 FM hydrodynamic model, the DHI MIKE3 MT sediment transport model, and the SWAN wave model.

The bathymetry of the Regional Harbour Model (RHM), which has been previously calibrated for the Auckland Regional Council (ARC), was used as the basis for the mesh developed for this study. To provide extra resolution in tidal creeks and on intertidal flats, the RHM bathymetry was augmented by LIDAR data supplied by the ARC.

Calibration of the models was primarily based on field data collected between February and June 2006, augmented by archived data from previous modelling studies.

The hydrodynamic model provided excellent predictions of water surface elevations and tidal currents. The model is a good predictor of tidal- and wind-driven currents, but does not resolve some small-scale temporal fluctuations in currents. Predicted wave heights agreed well with measurements, but predicted mean wave periods were generally smaller than corresponding measured values.

The model provides good estimates of the horizontal and vertical mixing of freshwater discharged from the catchment into the harbour. This is important for predicting dispersal of catchment-derived sediments and contaminants delivered to the harbour in freshwater run-off.

Measurements of suspended sediment concentration from several sites were used to calibrate the MIKE3 MT sediment transport model. The resuspension and transport of three constituent particle sizes (12, 40 and 125 μm) were simulated by the model. The constituent concentrations were combined to yield a total concentration, which was compared to measurements. The calibration process consisted of adjusting deposition and erosion thresholds and the erosion rate to achieve a good match between measured and predicted concentrations. The calibrated model was able to satisfactorily reproduce the measurements of suspended sediment concentration under tides alone, under weak winds that enhanced non-tidal circulation, and under strong winds that generated waves. The MIKE3 MT model is properly constituted for the 12 and 40 μm fractions, but not necessarily the 125 μm fraction. Nevertheless, the 125 μm concentrations predicted by the model agree well with a reference-concentration model more normally applied to this fraction. In any case, the 125 μm fraction constitutes (correctly) only a small fraction of the predicted total suspended-sediment load.

2 Introduction

Modelling and empirical data indicate that stormwater contaminants are rapidly accumulating in the highly urbanised side branches of the Central Waitemata Harbour (CWH). However, there is no clear understanding of the fate of contaminants exported from these side branches into the main body of the harbour, or that of contaminants discharged directly into the harbour.

The main aim of the study is to model contaminant (zinc, copper) and sediment accumulation within the CWH for the purposes of, amongst other things, identifying significant contaminant sources, and testing efficacy of stormwater treatment and zinc source control of industrial roofs.

2.1 Study aims

The study aims to:

- predict contaminant loads based on past, present and future land use and population growth for each sub-catchment discharging into the CWH, allowing for stormwater treatment and zinc source control of industrial roofs;
- predict dispersal and accumulation (or loss) of sediment and stormwater contaminants in the CWH;
- calibrate and validate the dispersal/accumulation model;
- apply the various models to predict catchment contaminant loads and accumulation of copper, zinc and sediment in the CWH under specific scenarios that depict various combinations of projected land use/population growth, stormwater treatment efficiency, and zinc source control of industrial roofs;
- determine from the model predictions the relative contributions of sediment and contaminant from individual sub-catchments and local authorities;
- provide an assessment of the environmental consequences of model outputs;
- provide technical reports on each component of the work; and
- provide a desktop application suitable.

2.2 Model suite

The study centres on the application of three models that are linked to each other in a single suite:

- The GLEAMS sediment-generation model, which predicts sediment erosion from the land and transport down the stream channel network. Predictions of sediment supply are necessary because, ultimately, sediment eroded from the land dilutes

the concentration of contaminants in the bed sediments of the harbour, making them less harmful to biota¹.

- The CLM contaminant/sediment-generation model, which predicts sediment and contaminant concentrations (including zinc, copper) in stormwater at a point source, in urban streams, or at end-of-pipe where stormwater discharges into the receiving environment.
- The USC-3 (Urban Stormwater Contaminant) contaminant/sediment accumulation model, which predicts sedimentation and accumulation of contaminants (including zinc, copper) in the bed sediments of the estuary. Underlying the USC-3 model is yet another model: an estuarine sediment-transport model, which simulates the dispersal of contaminants/sediments by physical processes such as tidal currents and waves.

2.3 This report

This report documents the implementation, calibration and validation of the harbour hydrodynamic model, the wave model and the sediment-transport model that underpin the USC model. The particular models used in the study are the DHI Water and Environment (DHI) MIKE3 FM hydrodynamic model, the DHI MIKE3 MT sediment transport model (www.dhigroup.com), and the SWAN wave model (Holthuijsen et al. 1993). Together, these simulate tidal propagation within the harbour, tide- and wind-driven currents, freshwater mixing, waves, and sediment transport and deposition. SWAN uses the water levels and current fields predicted by the MIKE3 FM model in predicting wind-generated waves. The predicted wave heights, periods and directions are in turn used to quantify wave-induced bed shear stress, which then transports sediments in the MIKE3 MT model.

Data from fieldwork conducted between 30 March and 24 July 2007 (Oldman et al. 2008) are used along with archived data to calibrate and validate the models against a range of conditions. The sites where data were collected for calibrating the models are shown in Figures 1a–c. An analysis of the long-term rainfall record for Auckland showed that the period April–July is the third-highest ranked period in terms of the number of days of rain. Rain fell on 63 % of the days in the deployment period, which is higher than the long-term average number of rain days for Auckland (40 %). Data collected during the field programme should therefore provide a reasonable test of the models in terms of their ability to simulate conditions within the Waitemata Harbour during rain events.

The MIKE3 FM model solves the three-dimensional incompressible Reynolds-averaged Navier–Stokes equations on a finite-element irregular mesh. The model consists of continuity, momentum, temperature, salinity and density equations with turbulent closure schemes. MIKE3 FM performs spatial discretisation of the equations using a cell-centred finite-volume method. In the horizontal plane an unstructured grid is used, while in the vertical domain a structured discretisation is used.

¹ The term “contaminant” is used herein to mean chemical contaminants such as zinc and copper, and “sediments” are referred to separately.

The MIKE3 MT model is a combined multi-fraction and multi-layer model that describes erosion, transport and deposition of mud or sand/mud mixtures under the action of currents and waves.

The SWAN wave model is a spectral wave model particularly intended for shallow-water applications in coastal and estuarine environments. It describes the sea state in terms of the amount of energy associated with each wave frequency and propagation direction. The model computes the evolution of the wave spectrum by accounting for the input, transfer and loss of energy through various physical processes.

Ideally, models should be validated against an independent dataset obtained under substantially different conditions than the conditions under which the calibration dataset was obtained. Where possible this has been done. For example, the FM model is calibrated against current data collected in 2007, and then validated against data collected in 2001 and 2002. Where independent data is not available (eg, suspended sediment concentration), the model is calibrated for a broad range of forcings (eg, the model for predicting suspended sediment concentration is calibrated for tides alone, tides plus waves, and spring and neap tides).

Figure 1a

DOBIE wave gauge sites used for calibrating the MIKE 3 FM and SWAN wave models. All DOBIEs measured water levels, optical backscatter and waves. DOBIEs at sites 2, 3, 5, 7 and 8 (●) also measured conductivity and temperature.



Figure 1b

Sites for conductivity–temperature–depth surveys carried out 14–16 June 2006.



Figure 1c

Current meter sites used for calibrating the MIKE3 FM model.



3 Mesh Development

The first step in model implementation is to define the limits of the model domain and develop a mesh that has element resolution appropriate to the underlying bathymetry and the physical processes being modelled.

Because this study is focusing on the delivery of catchment sediments to the wider harbour the mesh needed to be well-defined near the catchment outlets. These outlets were identified following consultation with the ARC and are shown in Figure 1 and tabulated in Table 1.

Because the delivery of catchment sediment is very dependent on tidal creek dynamics, a high-resolution mesh was also required within tidal creeks. The following catchment outlets are deemed to discharge into tidal creeks: Henderson Creek, Hobsons Bay and the Whau River (Figure 1).

The mesh also needed to resolve the main channels of the harbour; in these areas the mesh elements must be smaller than the channel dimensions.

The intertidal areas of the harbour need to be well defined so that flooding and drying of these areas is well represented within the model. This becomes particularly important when considering the resuspension and transport of intertidal bed sediments.

Because of the number of elements needed to resolve the tidal creeks and intertidal areas and the computational restrictions that this imposes, the vertical layout of the mesh was defined as five equidistant layers.

Figure 1
Catchment outlet locations.

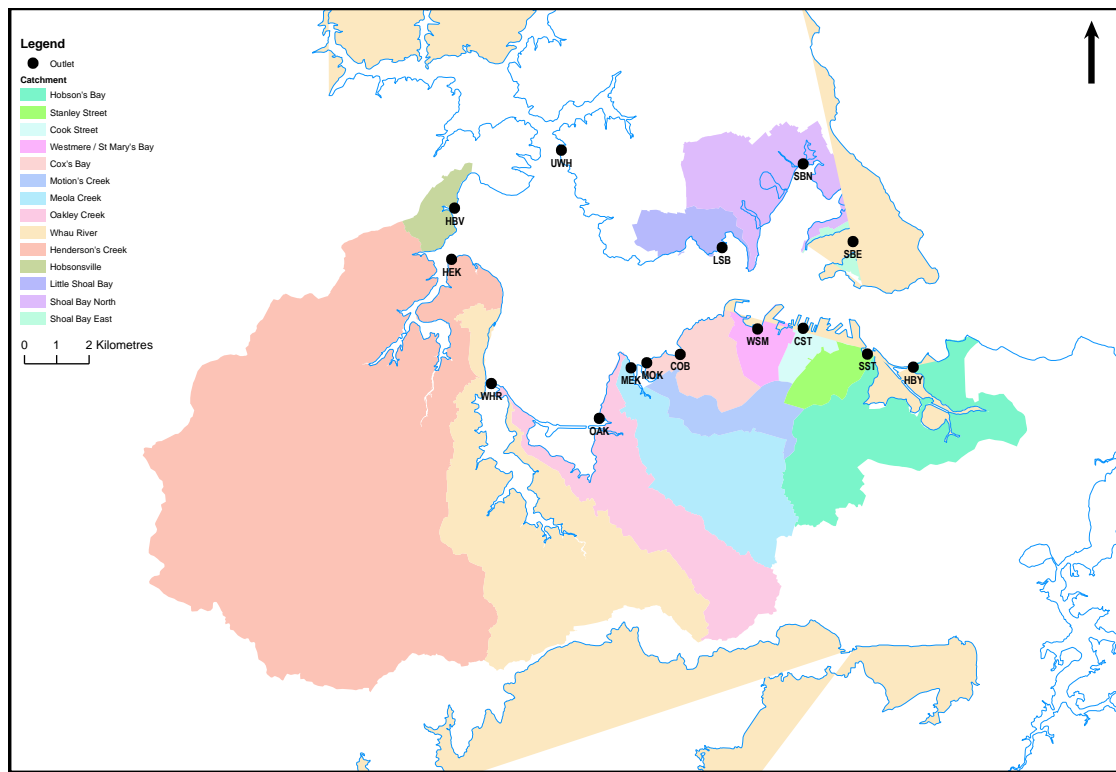


Table 1

Catchment outlet numbers, names and codes.

Catchment outlet number	Catchment outlet name	Catchment outlet code
1	Hobsons Bay	HBV
2	Stanley St	SST
3	Cook St	CST
4	Westmere/St. Mary's Bay	WSM
5	Cox's Bay	COB
6	Motions Creek	MOK
7	Meola Creek	MEK
8	Oakley Creek	OAK
9	Whau River	WHR
10	Henderson Creek	HEK
11	Hobsonville	HBV
12	Upper Waitemata Harbour	UWH
13	Little Shoal Bay	LSB
14	Shoal Bay North	SBN
15	Shoal Bay East	SBE

The bathymetry of the Regional Harbour Model (RHM), which has been previously calibrated for the ARC (Oldman et al. 2004), was used as the basis for the mesh developed for this study (Figure 2). Bathymetry for the RHM is particularly sparse within the tidal creeks and intertidal areas of the southwest of the harbour. For this application, additional data were required in these areas.

To this end, further topographic data (Figure 3) were added to the RHM bathymetry. These data were collected for the ARC by remote sensing using Light Detection and Ranging imagery (LIDAR). The Waitemata LIDAR image consists of one point per 2 m² (approximately), with height accuracy mostly 0.25 m. Processing of the raw LIDAR data to Chart Datum and into a format readable by the DHI models was carried out as outlined in Appendix 1.

Figure 2

Bathymetry data from the Regional Harbour Model (Oldman et al. 2004).

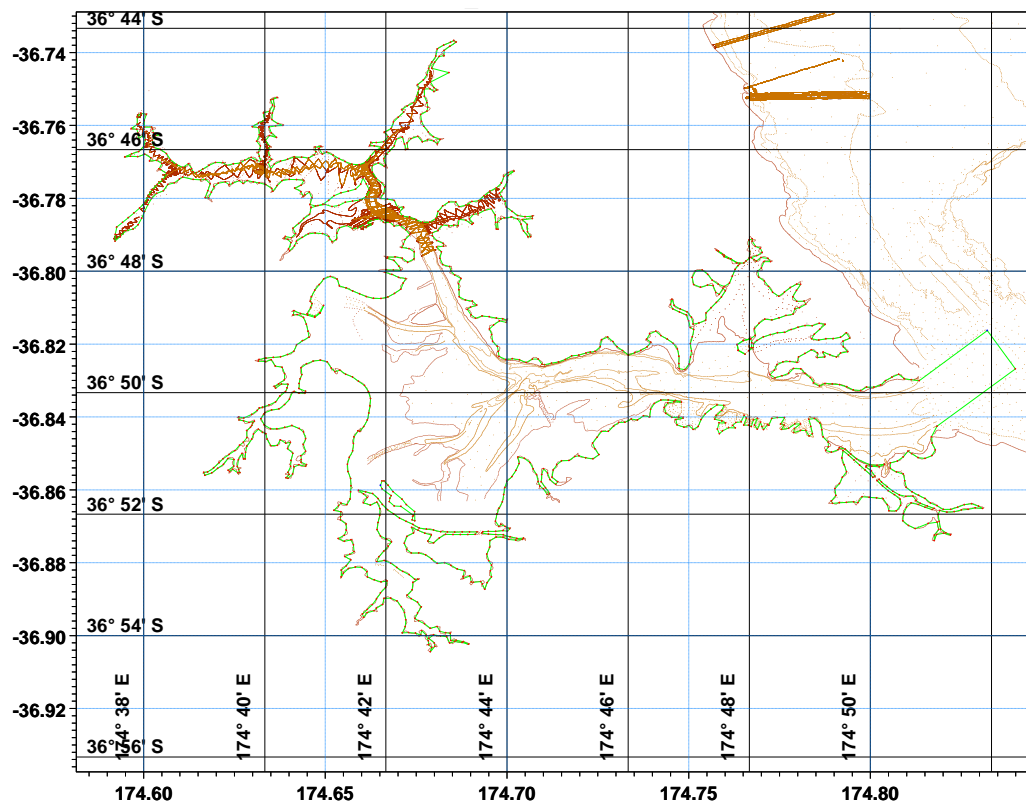
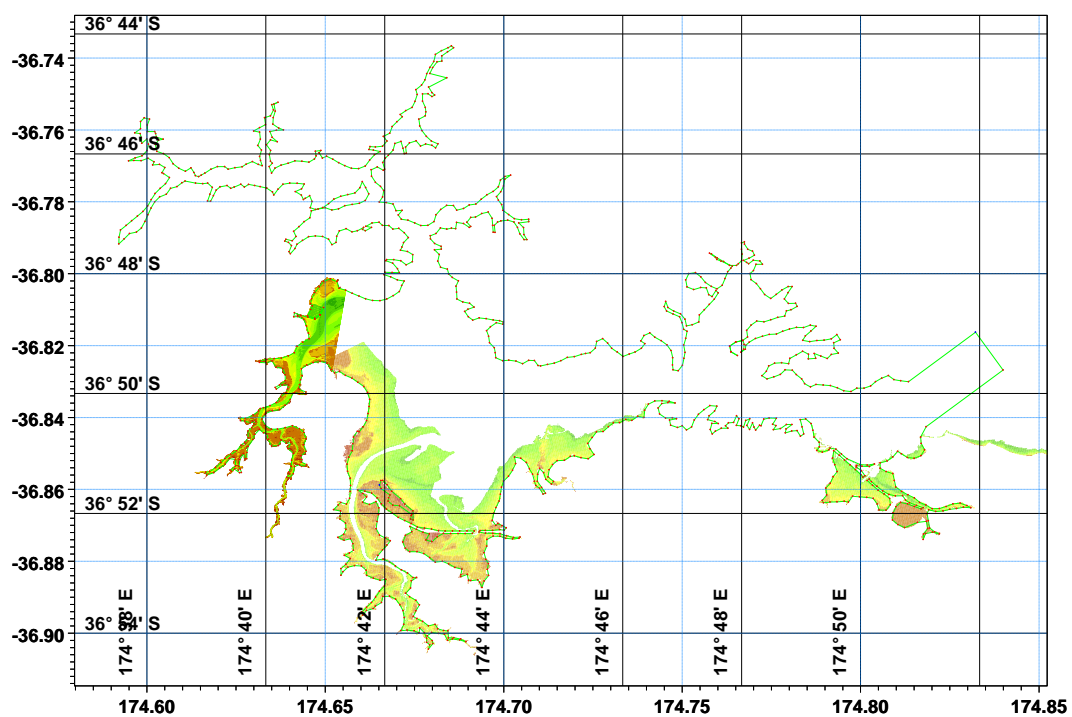


Figure 3

LIDAR data following processing. Interpolated harbour shoreline also shown.



The finite mesh was developed from the combined bathymetry data (Figure 2 and 4) by firstly interpolating the shoreline data every 150 m around the perimeter of the harbour. Gridding was then carried out using a default minimum element angle of 28°, which resulted in the mesh shown in Figure 5. Appendix 2 gives finer-detail plots of the mesh for various sections of the harbour.

Subestuaries for application of the USC model were defined based on catchment outlets and a broad consideration of hydrodynamics and sediment transport (Figure 6). The number of elements and element sizes for each of the subestuaries are shown in Table 2.

Table 2

Subestuary element information.

Subestuary	Subestuary name	Subestuary code	Number of elements	Minimum area (m ²)	Maximum area (m ²)	Total area (m ²)
1	Hobsonville	HBE	74	871	94,552	1,599,323
2	Limeburners Bay	LBY	110	1,689	25,093	834,748
3	Northwestern Intertidal	NWI	124	1,928	188,098	3,052,405
4	Central Subtidal	CNS	22	83,525	314,334	3,677,757
5	Western Intertidal	WSI	339	1,013	222,283	4,693,359
6	Southwestern Intertidal	SWI	462	842	112,041	5,474,497
7	Waterview	WAV	39	2,492	78,809	1,082,372
8	Point Chevalier	PCV	70	7,697	213,490	1,958,963
9	Meola	MEO	78	1,568	47,318	1,079,382
10	Motions	MOT	93	2,260	39,536	1,404,598
11	Shoal Bay	SBY	288	1,026	56,625	6,465,420
12	Hauraki Gulf	HGF	218	2,302	418,390	8,344,738
13	Henderson Creek	HEN	840	278	37,619	2,277,921
14	Whau River	WHR	717	242	5,927	2,116,217
15	Waterview	WAT	153	602	43,922	2,129,185
16	Hobson Bay	HBA	420	457	12,007	2,470,576
17	Upper Waitemata Harbour	UWH	1266	8	51,597	10,086,389
18	Whau Channel	WC	254	718	13,964	500,279
19	Whau Subtidal	WS	25	25,181	139,869	2,031,352
20	Upper Channel	UC	170	597	130,447	4,114,731
21	Middle Channel	MC	447	310	142,863	7,264,518
22	Outer Channel	OC	361	1,030	72,508	6,225,499

Figure 4

Final mesh developed for this study.

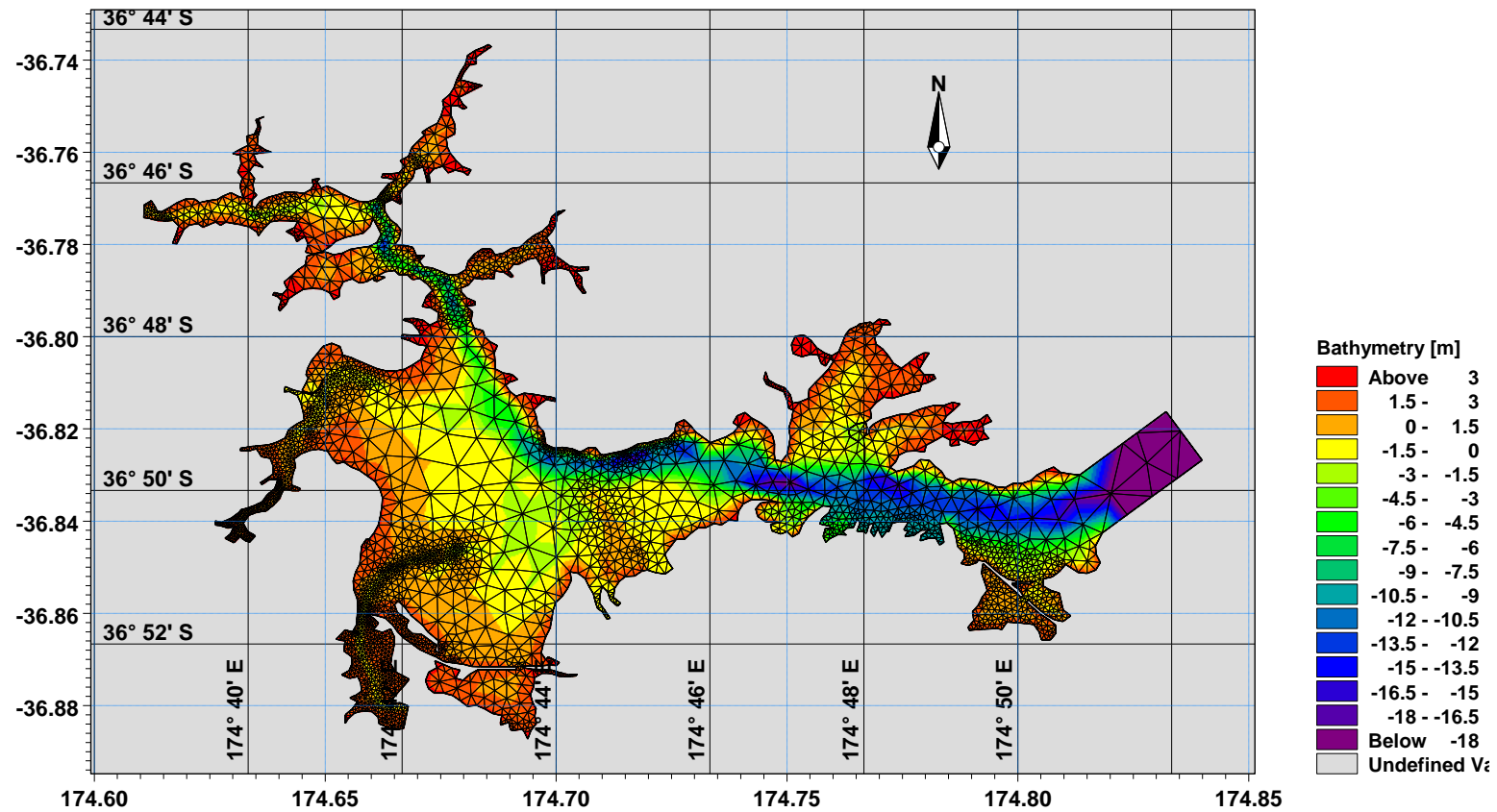
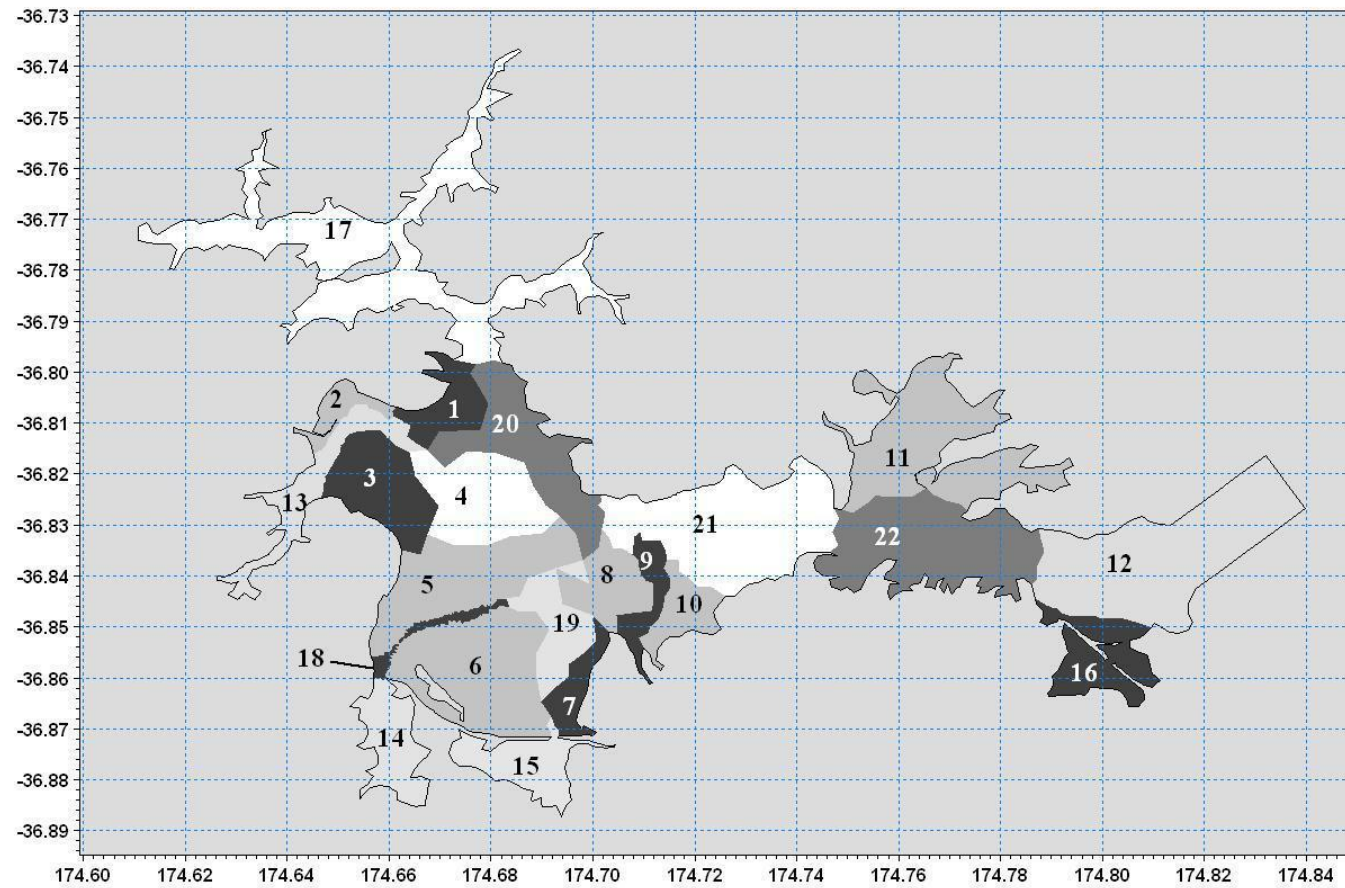


Figure 5

Subestuaries defined for application of the USC model.



4 Formulation of Processes Simulated by the MIKE3 Models

This section outlines the methods used by the MIKE3 FM and MT models to simulate tidal propagation within the harbour, tide- and wind-driven currents, freshwater mixing and sediment transport.

4.1 Mesh flooding and drying

The treatment of flooding and drying is based on the work by Zhao et al. (1994) and Sleight et al. (1998). When the depths are small the problem is reformulated, and only when the depths are very small are the elements/cells removed from the calculation. The reformulation is made by setting the momentum fluxes to zero and only taking the mass fluxes into consideration.

The depth in each element/cell is monitored and the elements are classed as dry, partially dry or wet. Also, the element faces are monitored to identify flooded boundaries.

An element face is classed as flooded if the water depth at one side of the face is less than the tolerance depth h_{dry} , the water depth at the other side of the face is larger than the tolerance depth h_{flood} and the sum of the water depth at the side for which the water depth is less than h_{dry} and the water depth at the other side is larger than zero.

An element is classed as dry if the water depth is less than h_{dry} and none of the element faces are flooded boundaries. In this case the element is removed from the calculation.

An element is classed as partially dry if the water depth is larger than h_{dry} and less than the tolerance depth h_{wet} or when the depth is less than h_{dry} and one of the element faces is a flooded boundary. In this case, the momentum fluxes are set to zero and only the mass fluxes are calculated.

An element is classed as wet if the water depth is greater than h_{wet} . In this case, both the mass fluxes and the momentum fluxes are calculated.

When an element is removed from the calculation, water and sediment are removed from the computational domain. The water and sediment mass in the element are saved and then reused when the element becomes flooded again.

4.2 Bed shear stress

MIKE3 FM uses a quadratic friction law to define the bed shear stress due to the current:

$$\frac{\bar{\tau}_b}{\rho_0} = c_f \bar{u}_b |\bar{u}_b| \quad (1)$$

where c_f is the drag coefficient, \bar{u}_b is the time-averaged current speed at a distance Δz_b above the bed, and ρ_0 is the density of water. The drag coefficient is defined in terms of a logarithmic profile between the seabed and the point Δz_b above the seabed:

$$c_f = 1 \frac{1}{\left(\frac{1}{\kappa} \ln \left(\frac{\Delta z_b}{z_0} \right) \right)^2} \quad (2)$$

where $\kappa=0.4$ is von Karman's constant and z_0 is the bed roughness length, which is typically varied to calibrate the model.

The enhancement of the current-related bed shear stress by any waves that may be present is accounted for use in the calculation of sediment transport. The method used is a parameterised version of Fredsøe's (1984) method, which was derived by Soulsby et al. (1993). The mean and maximum combined wave-current bed shear stresses are given as follows:

$$\frac{\tau_{wc,mean}}{\tau_c + \tau_w} = \frac{\tau_c}{\tau_c + \tau_w} \left(1 + b \left(\frac{\tau_c}{\tau_c + \tau_w} \right)^p \left(1 - \frac{\tau_c}{\tau_c + \tau_w} \right)^q \right) \quad (3)$$

$$\frac{\tau_{wc,max}}{\tau_c + \tau_w} = \left(\frac{\tau_c}{\tau_c + \tau_w} \right)^m \left(1 - \frac{\tau_c}{\tau_c + \tau_w} \right)^n \quad (4)$$

where b, p, q, a, m, n constants:

$$\begin{aligned} a &= a1 + a2 \cos \gamma_i + (q3 + q4 \cos \gamma_j) \log_{10}(r) \\ b &= b1 + b2 \cos \gamma_j + (b3 + b4 \cos \gamma_i) \log_{10}(r) \\ m &= m1 + m2 \cos \gamma_i + (m3 + m4 \cos \gamma_j) \log_{10}(r) \\ n &= n1 + n2 \cos \gamma_i + (n3 + n4 \cos \gamma_j) \log_{10}(r) \\ p &= p1 + p2 \cos \gamma_j + (p3 + p4 \cos \gamma_i) \log_{10}(r) \\ q &= q1 + q2 \cos \gamma_j + (q3 + q4 \cos \gamma_i) \log_{10}(r) \end{aligned}$$

and $a1, a2$, etc. are given in the Table 3 below, γ is the angle between the waves and currents with $i = 0.8, j = 3.0$ and $r = 2 f_w/f_c$.

Table 3

	<i>a</i>	<i>m</i>	<i>n</i>	<i>b</i>	<i>p</i>	<i>q</i>
1	-0.06	0.67	0.75	0.29	-0.77	0.91
2	1.70	-0.29	-0.27	0.55	0.10	0.25
3	-0.29	0.09	0.11	-0.10	0.27	0.50
4	0.29	0.42	-0.02	-0.14	0.14	0.45

f_w is the pure-wave wave friction factor, given by Swart (1974) as:

$$f_w = \exp\left(5.213\left(\frac{a}{k}\right)^{-0.194} - 5.977\right) \quad (5)$$

where k is the bed roughness and a is the wave-orbital semi-excursion at the bed.

Also, f_c is the pure-current friction factor, given by the logarithmic resistance law:

$$f_c = 2\left(2.5\left(\ln\left(\frac{30h}{k}\right) - 1\right)\right)^{-2} \quad (6)$$

where h is the water depth.

4.3 Currents

The influence of the wind on currents is treated in terms of the wind-induced shear stress that acts on the sea surface:

$$\tau_w = \rho_a c_d |u_w| \overline{u_w} \quad (7)$$

where ρ_a is the density of air, c_d is the drag coefficient and u_w is the wind speed 10 m above the sea surface. The model is typically calibrated by adjusting c_d . Local variations in winds can be accounted for in the model by spatially varying the applied winds. In the absence of appropriate scale wind data, the mean wind from a number of weather stations was applied across the whole model domain.

The turbulent transfer of momentum by eddies gives rise to an internal fluid friction which is resolved in the horizontal and vertical dimensions by use of an eddy viscosity formulation.

In the vertical, the eddy viscosity is derived from the following log-law formulation:

$$\nu_t = U_\tau h \left(c_1 \frac{z+d}{h} + c_2 \left(\frac{z+d}{h} \right)^2 \right) \quad (8)$$

Here, $U_\tau = \max(U_{\tau s}, U_{\tau b})$, c_1 and c_2 are constants, d is the still-water depth, h is the total water depth, and $U_{\tau s}$ and $U_{\tau b}$ are the friction velocities associated with the surface and seabed shear stresses, respectively. The model is typically calibrated by adjusting the constants c_1 and c_2 and by defining the upper and lower limits of the vertical eddy viscosity.

For the horizontal eddy viscosity, the Smagorinsky formulation was applied, which gives the subgrid-scale eddy viscosity as:

$$A = c_s^2 l^2 \sqrt{2S_{ij}S_{ij}} \quad (9)$$

where c_s is a constant, l is the characteristic length (approximated by the minimum edge length for each element) and the deformation rate (S_{ij}) is given by

$$S_{ij} = \frac{1}{2} \left(\frac{\partial u_i}{\partial x_j} + \frac{\partial u_j}{\partial x_i} \right) \quad (10)$$

Using this formulation, the model can be calibrated by adjusting the constant c_s and by defining the upper and lower limits of the horizontal eddy viscosity.

4.4 Salinity

In baroclinic mode MIKE3 FM requires coefficients for vertical and horizontal dispersion. These can be constant or they can be proportionally scaled to the eddy viscosity. For the implementation of the model here a scaled dispersion coefficient was used.

4.5 Sediment transport

MIKE3 MT can simulate the erosion, transport and deposition of up to eight different particle size fractions. For each particle size a fall velocity (w_s) is assigned.

MIKE3 MT can include the effects of flocculation and hindered settling at high suspended sediment concentrations. Oldman et al. (2008) showed that measured concentrations were, for the majority of the deployment period, much less than 0.5 kg m^{-3} . This is too low for hindered settling of sediments. Therefore, this process has not been included in the modelling. Data from the field programme have shown that salinities within the main body of the harbour rarely drop below 20 PSU, and it is only in the upper parts of Henderson Creek and the Whau River that salinities drop below 10 PSU (Figures 4.2, 4.3 and 4.5 in Oldman et al., 2008). Thus, for the majority of the harbour, where salinities are high and suspended sediment concentration is low, the effects of flocculation can be ignored. It is only within the upper reaches of tidal creeks that flocculation may become important. For example, a turbidity maximum might occur, dependent on freshwater input, tidal range, wind conditions, and sediment particle size distribution.

4.5.1 Deposition

Deposition of sediment onto the bed is deemed to occur when and where the bed shear stress (τ_b) is smaller than the critical bed shear stress for deposition (τ_{cd}). A separate τ_{cd} is assigned to each particle size.

The deposition rate ($\text{kg.m}^{-2}.\text{s}^{-1}$) is given separately for each particle size by:

$$D = w_s p_d c_b \quad (11)$$

where p_d is the probability ramp function for deposition defined as:

$$p_d = \max(0, \min(1, 1 - \frac{\tau_b}{\tau_{cd}})) \quad (12)$$

and c_b is the near-bed suspended-sediment concentration for the particle size at hand.

MIKE3 MT gives two choices for determining c_b : the Teeter formulation and the Rouse formulation. The Teeter formulation was chosen for implementation here, which is:

$$c_b = \bar{c} \left(1 + \frac{p_e}{1.25 + 4.75 p_d^{2.5}} \right) \quad (13)$$

where p_e is the Peclet number, defined as:

$$p_e = 6 \frac{w_s}{\kappa U_f} \quad (14)$$

and U_f is the friction velocity.

The calibration process involves selecting the fall velocity and the critical bed shear stress for deposition (τ_{cd}) for each particle size.

4.5.2 Erosion

Erosion of bed material takes place when and where the bed shear stress exceeds the critical shear stress for erosion (τ_{ce}). A single value of τ_{ce} is assigned for the bed sediment as a whole.

The erosion rate ($\text{kg}/[\text{m}^2\text{s}]$) is specified for the bed as a whole as:

$$E = E_i \exp \left(\alpha \left(\tau_b - \tau_{ce} \right) \right) \quad (15)$$

where α is a power term and E_i is the "initial" erosion rate. The total mass of sediment eroded from the bed (which is governed by E) is then distributed amongst the constituent particle sizes by the proportions of the constituent particle sizes in the bed sediment. For example, if constituent particle size #1 makes up 50 % of the bed sediment by mass then 50 % of the sediment eroded by E will be assigned that particle size.

The calibration process involves selecting one value each for τ_{ce} , α and E_i .

5 Model Calibration

Calibration of the MIKE3 FM and MT models consisted of comparing model output and measured water levels, currents, salinities and suspended-sediment concentrations under a range of conditions, and adjusting various model parameters until the comparisons are satisfactory.

The SWAN model was calibrated in the same way against measured wave heights and periods.

5.1 Water surface elevation

Raw water surface elevation (WSE) records in the calibration dataset were converted to depths relative to Chart Datum (CD) by matching mean sea level calculated from the data to published mean sea level at the Ports of Auckland (1.85 m CD). Because Sites 2, 3, 4 and 10 (see Figure 1a) were dry for some part of the record, the offset to adjust the raw record to CD could not be established accurately in those cases. These sites are therefore not included in the WSE calibration.

Bed roughness z_0 was varied to achieve the best fit between measured and predicted water surface elevations. The roughness that gave the best fit is shown in Figure 6.

Figure 7 shows predicted and measured water surface elevations at Sites 1, 5, 7, 8, 9 and 11 (see Figure 1a) using the bed roughness in Figure 10.

Towards the end of the simulation period (around 11-13 May) the model underpredicts water surface elevations at low water except at Sites 8 and 11. This suggests that the tidal constituent data used on the boundary are correct and that the propagation of the tide through the main subtidal channels of the harbour is correct. Increasing the bed roughness would increase the predicted tidal range at sites not in the main harbour. This would result in a better fit between modelled and observed WSE at low water, but this would also be offset by a poorer fit of WSE at high water. Also, an increase in bed roughness would result in a larger phase lag between observed and modelled WSE. Another way to improve predicted WSE at low water would be to apply a spatially varying wind field in the model. For instance, for the period 11–13 May, winds were from the northwest, but wind speed measured at the Whenuapai AWS (near the upper harbour) was up to 30 % stronger than the wind applied in the model. Applying stronger winds in the model would create greater setup along the southern shores of the harbour with a corresponding setdown elsewhere in the harbour. However, given the overall fit between observed and predicted WSE (Table 4) this option was not pursued.

Table 4

Statistics of linear regression between predicted and measured water surface elevation at Sites 1, 5, 7, 8, 9 and 11 (see Figure 1a).

Site	Slope	r-squared
1	1.019	0.959
5	1.008	0.964
7	1.007	0.964
8	0.997	0.986
9	0.957	0.983
11	0.978	0.995

Figure 6

Distribution of bed roughness z_0 (m) that yielded best fit between measured and predicted water surface elevation.

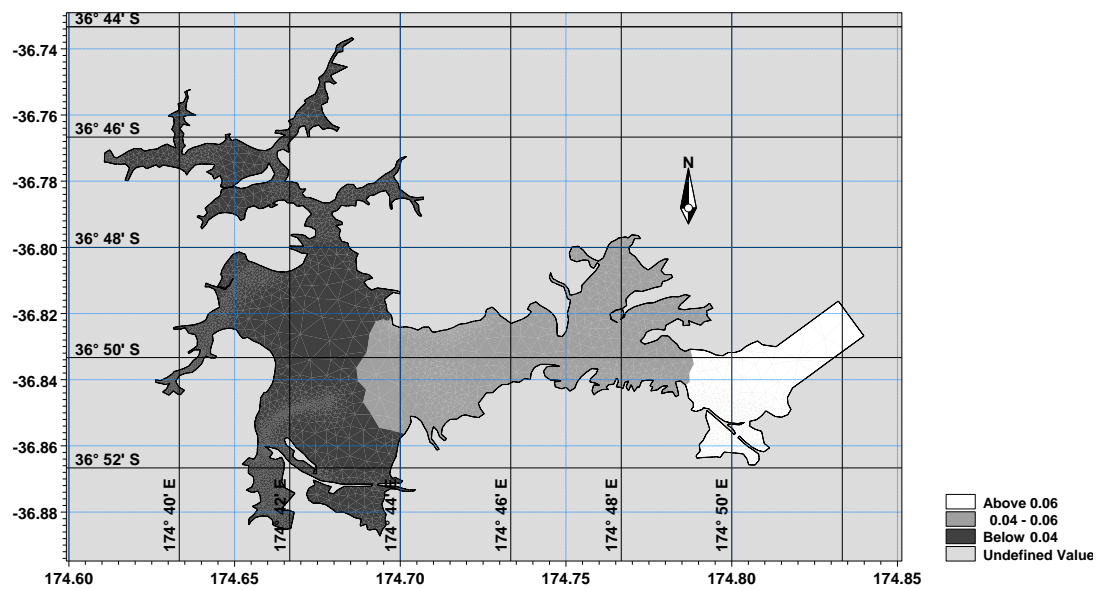


Figure 7

Water surface elevation at Sites 1 (entrance to Upper Waitemata), 5 (Upper Whau), 7 (approach to Whau), 8 (Middle Waitemata), 9 (Shoal Bay) and 11 (Watchman Island). Sites shown in Figure 1a.

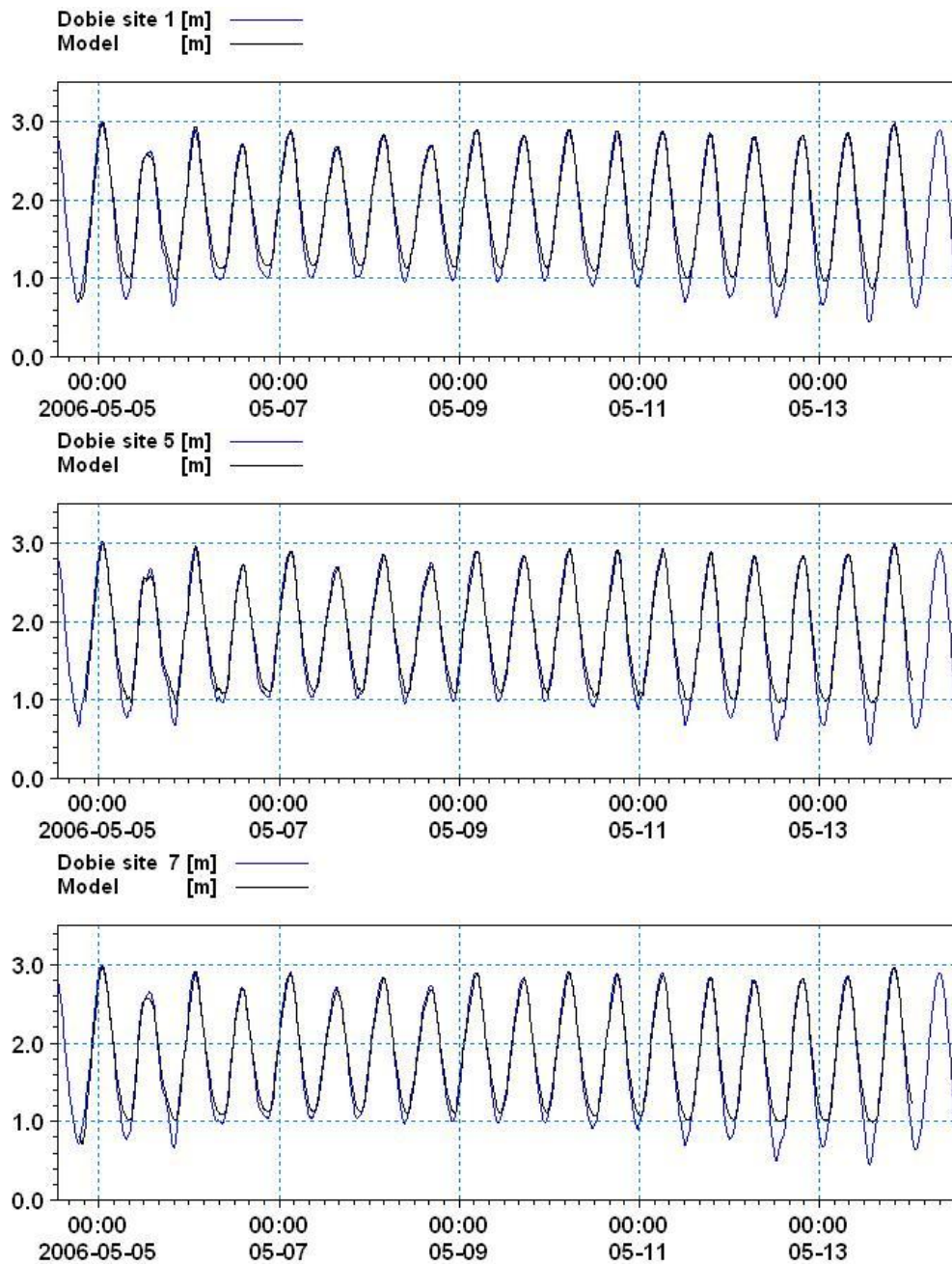
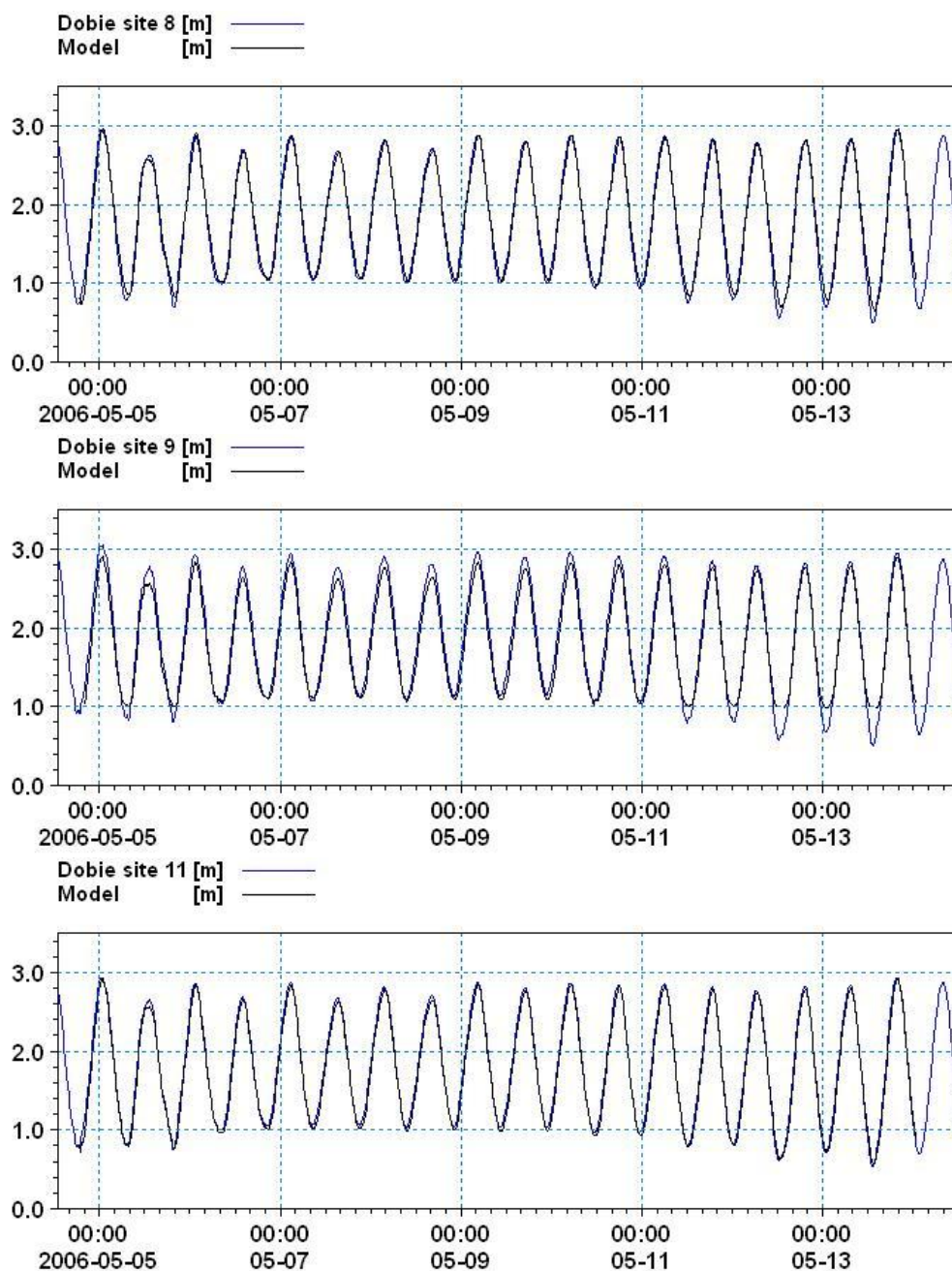


Figure 8

Water surface elevation at Sites 1 (entrance to Upper Waitemata), 5 (Upper Whau), 7 (approach to Whau), 8 (Middle Waitemata), 9 (Shoal Bay) and 11 (Watchman Island). Sites shown in Figure 1a.



5.2 Currents

Having established that the model can accurately predict water levels throughout the harbour, the next step in the calibration process is to determine how well the model can predict tidal and wind-driven currents. Four sites across the harbour were selected to calibrate the model for currents (Figure 1c).

The best overall fit between observed and predicted currents was achieved by using a Smagorinsky coefficient of 0.42 for the horizontal eddy viscosity formulation, with a lower bound of $1.8\text{e-}006 \text{ m}^2 \text{ s}^{-1}$ and an upper bound of $10 \text{ m}^2 \text{ s}^{-1}$. Two of the calibration sites (Paremoremo and Hobsons Bay, see Figure 1a

c) were particularly sensitive to this formulation, because at both of these sites an eddy is formed for part of each tidal cycle. The simulation of the size and strength of these eddies was found to be very sensitive to the horizontal eddy viscosity.

For the vertical eddy viscosity, the constants c_1 and c_2 were set to 0.41 and -0.41, respectively, to give a standard parabolic profile. The upper and lower limits of the vertical eddy viscosity were set to $1.8\text{e-}006 \text{ m}^2 \text{ s}^{-1}$ and $0.4 \text{ m}^2 \text{ s}^{-1}$, respectively, which are the default values used in the MIKE3 FM model. Model tests showed very little difference in predicted currents at any of the sites with adjustments to the vertical eddy viscosity.

The value for the wind-induced surface shear stress drag coefficient (c_d) was increased from the default value of 0.00125 to 0.0018 to achieve a slightly better fit between the observed and predicted currents during periods of higher winds.

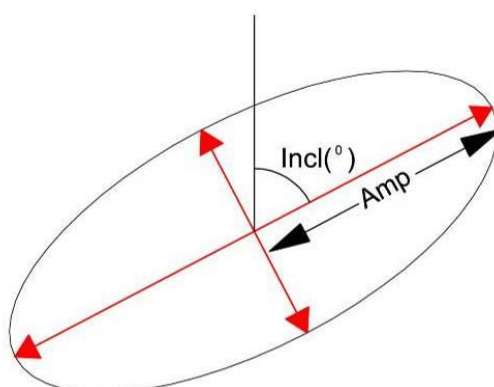
The tidal current constituents calculated from current data at Henderson Creek and off the end of Te Tokoroa Reef (Figure 1c) were compared to those predicted by the model. Because the model simulation duration was only 10 days, only the M_2 , K_1 and M_4 components could be inferred from the model output. Data from the field indicate that these components contribute to over 60 % of the current variance. The next largest component (N_2) would require a 30-day model run to be resolved, and the next largest component (S_2) accounts for less than 6 % of the tidal signal at the two sites.

Tidal ellipses (Figure 9) are defined in terms of the ellipse major amplitude (maximum tidal current along the principal axis of the current), ellipse minor amplitude (maximum tidal current along the minor axis of the current), the ellipse inclination (peak tidal current direction relative to True North), and ellipse phase (time of the peak tidal current relative to NZST). Z_0 value is an estimate of the tidal residual.

Table 6 compares predicted and measured tidal ellipses at Henderson Creek and Te Tokoroa Reef, which indicates that the model is a good predictor of tidal currents at both of those sites. The model slightly overpredicts the tidal residual at both sites. There is an error in maximum peak tidal current of only 2 cm s^{-1} . The tidal ellipse inclinations are within 5° of those observed, and the timing of the peak currents is accurate to within 15 minutes.

Figure 9

Tidal ellipse representation.

**Table 5a**Comparison of measured and predicted tidal ellipses, M_2 currents.

Location	Observed			Modelled			Difference		
	Amplitude (m s^{-1})	Inclination (° True)	Phase (° NZST)	Amplitude (m s^{-1})	Inclination (° True)	Phase (° NZST)	Amplitude (m s^{-1})	Inclination (°)	Phase (°)
Henderson Creek (Site 2)	0.154	52.1	308.3	0.174	47.1	303.6	0.020	-5.0	-4.7
Te Tokoroa Reef	0.424	33.0	325.3	0.411	34.3	330.9	-0.013	1.3	5.6

Table 5bComparison of measured and predicted tidal ellipses, M_2 currents.

Location	Observed			Modelled			Difference		
	Amplitude (m s^{-1})	Inclination (° True)	Phase (° NZST)	Amplitude (m s^{-1})	Inclination (° True)	Phase (° NZST)	Amplitude (m s^{-1})	Inclination (°)	Phase (°)
Henderson Creek (Site 2)	0.039	72.4	336.4	0.037	70.8	330.6	0.007	-5.4	-14.7
Te Tokoroa Reef	0.072	59.8	345.6	0.079	54.4	330.9	-0.010	1.0	4.0

Table 5c

Comparison of measured and predicted tidal ellipses, K_1 currents.

Location	Observed			Modelled			Difference		
	Amplitude (m s^{-1})	Inclination (° True)	Phase (° NZST)	Amplitude (m s^{-1})	Inclination (° True)	Phase (° NZST)	Amplitude (m s^{-1})	Inclination (°)	Phase (°)
Henderson Creek (Site 2)	0.007	153.5	359.1	0.006	148.7	3.4	-0.001	-4.8	4.3
Te Tokoroa Reef	0.018	40.4	274.1	0.015	40.2	273.6	-0.003	-0.2	-0.5

Table 5d

Comparison of measured and predicted tidal residuals (Z).

Location	Observed	Predicted	Difference
	Amp (m s^{-1})	Amp (m s^{-1})	Amp (m s^{-1})
Henderson Creek (Site 2)	0.034	0.039	0.005
Te Tokoroa Reef	0.067	0.081	0.014

Figures 13 to 16 show measured and predicted currents (north–south and east–west components) at Henderson Creek, Te Tokoroa Reef, Hobsons Bay, and at the site near the entrance to Paremoremo Creek (Figure 1c). Table 8 shows the statistics of the linear regression between predicted and measured currents at each site.

At the Henderson Creek site (Figure 14) the model predicts the peak north–south and east–west velocity components reasonably well. The phasing of the north–south component is also reasonably well represented in the model, but the model tends to overpredict the length of the ebbing (positive) east–west velocity component. Given likely strong gradients in the north–south and east–west components near this site (the main channel sweeps through 90° in the space of 800 m), the model predictions are particularly good. Table 6 shows that the model tends to overpredict both components by around 20 %.

At the Hobson Bay site (Figure 11) the model predicts the phasing and amplitudes of the north–south component reasonably well. The smaller-scale fluctuations (particularly noticeable in the east–west velocity component) are not well modelled. This is most likely a consequence of the fact that the model is averaging over a single element with area 13,000 m^2 and depth 0.8 m, whereas the S4 current meter used to obtain the calibration data measures over just a few cubic metres of water. Table 6 shows that the model tends to overpredict both components. The smaller-scale fluctuations in the data result in a relatively low r-squared value for the north-south component.

At the Te Tokoroa Reef site (Figure 12) the model predicts the phasing and amplitudes of both velocity components well. Peak flows during the outgoing tides of 27–28 June were underpredicted by the model slightly. Table 6 shows that the model is a good predictor of currents at this site.

At the Paremoremo Creek site (Figure 13) the model does not predict the observed small-scale fluctuations in currents well. However, Table 6 shows that the predominant north-south component is modelled reasonably well. Given the location of the site (close to the headland along the eastern side of Paremoremo Creek), the fit between observed and predicted currents is acceptable.

Table 6

Statistics of linear regression between predicted (x) and measured (y) currents.

Location	East/West velocity component	North/South velocity component
Henderson Creek	$y = 0.7923x + 0.0229$ r-squared = 0.374	$y = 0.8155x + 0.0382$ r-squared = 0.4902
Hobson Bay	$y = 0.7923x + 0.0029$ r-squared = 0.5808	$y = 0.3222x + 0.0151$ r-squared = 0.2606
Te Tokoroa Reef	$y = 0.8833x + 0.0386$ r-squared = 0.7506	$y = 1.0238x + 0.088$ r-squared = 0.8641
Paremoremo	$y = 0.0719x + 0.0232$ r-squared = 0.0155	$y = 0.7393x + 0.0007$ r-squared = 0.3083

Figure 10

Measured and predicted currents at the site near the mouth of Henderson Creek (see Figure 1c). The blue line shows measured currents and the black line shows predicted currents.

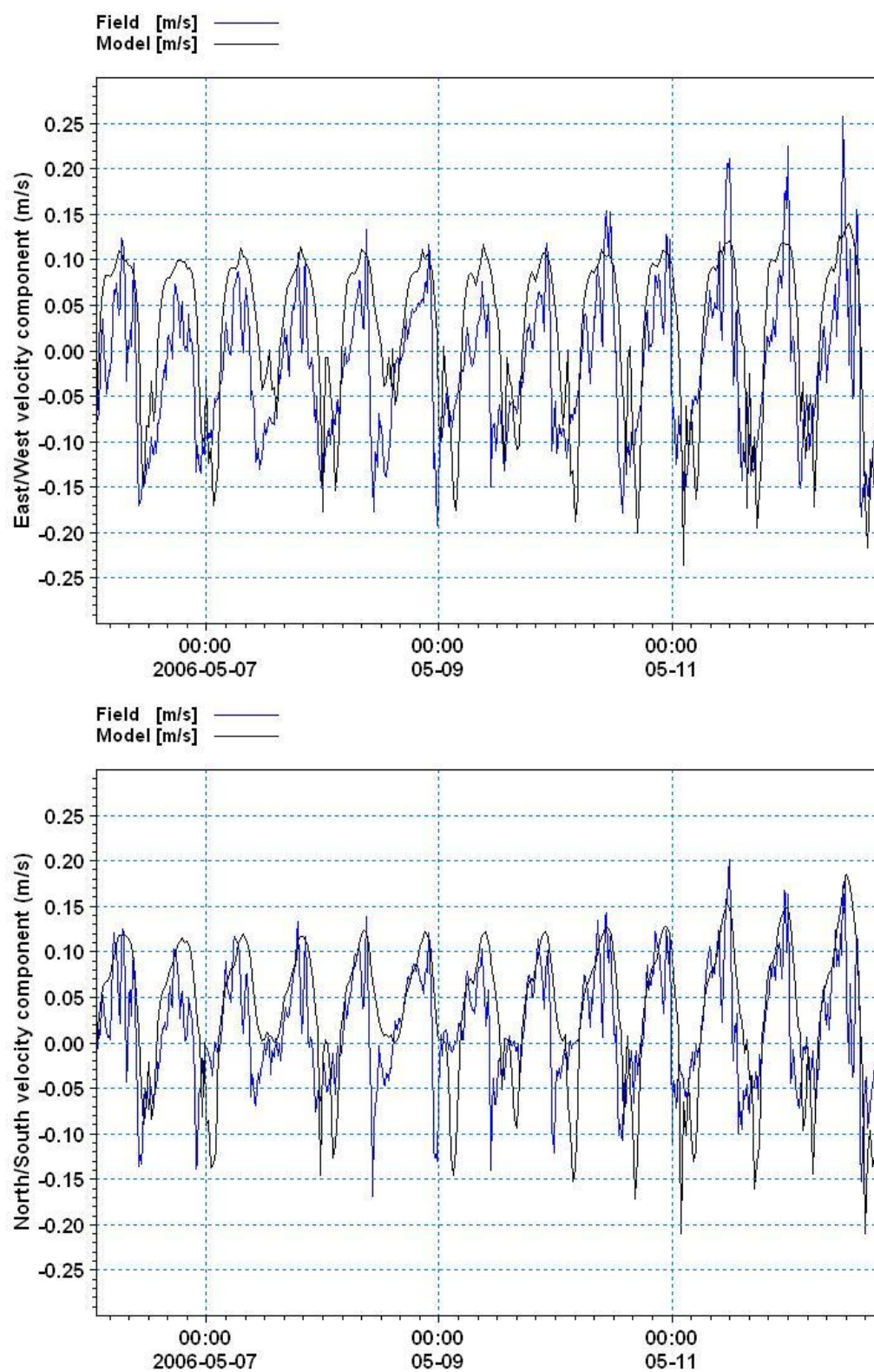


Figure 11

Measured and predicted currents at Hobsons Bay (see Figure 1c). The blue line shows measured currents and the black line shows predicted currents.

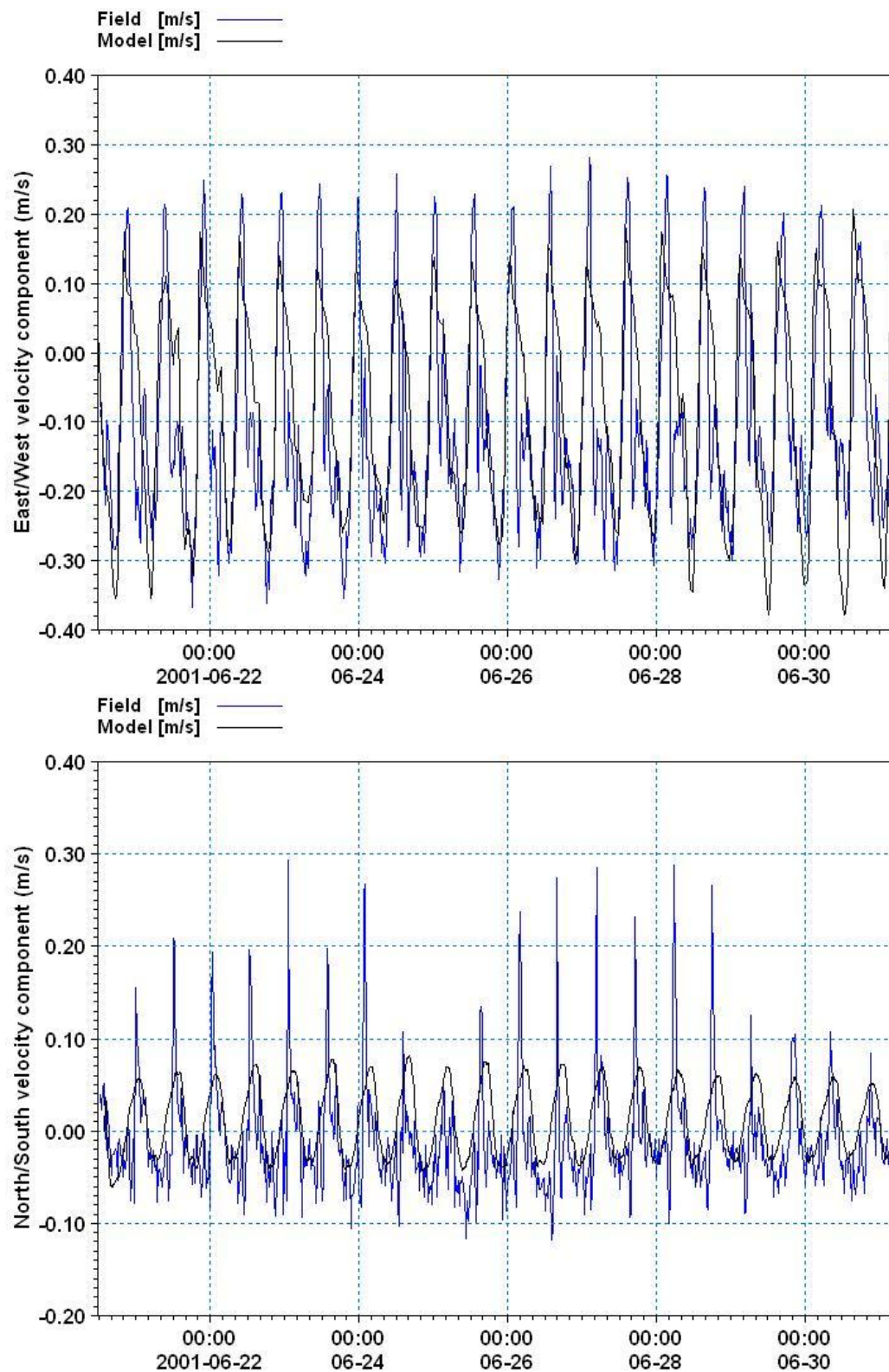


Figure 12

Measured and predicted currents at Te Tokoroa Reef (see Figure 1c). The blue line shows measured currents and the black line shows predicted currents.

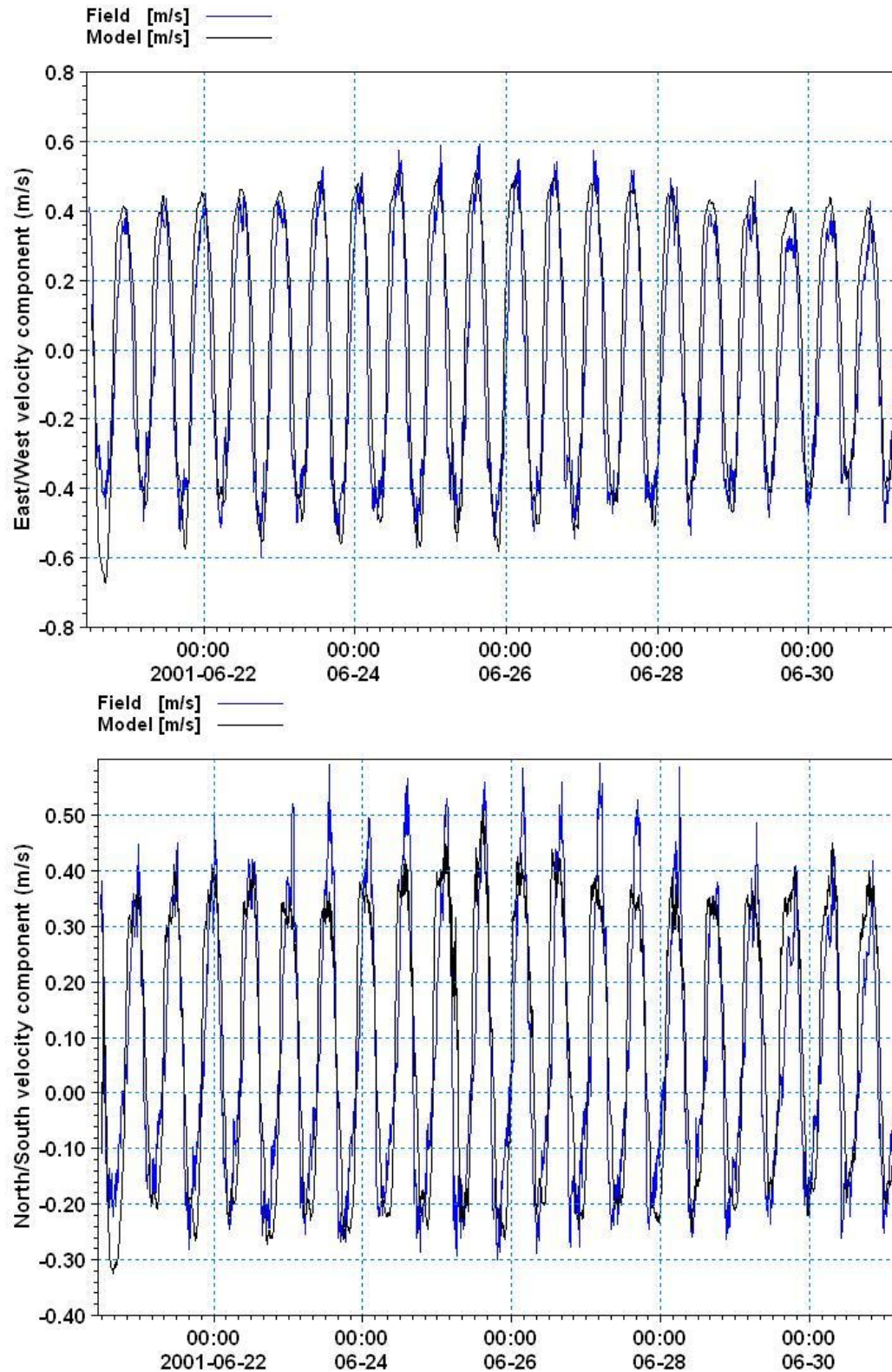
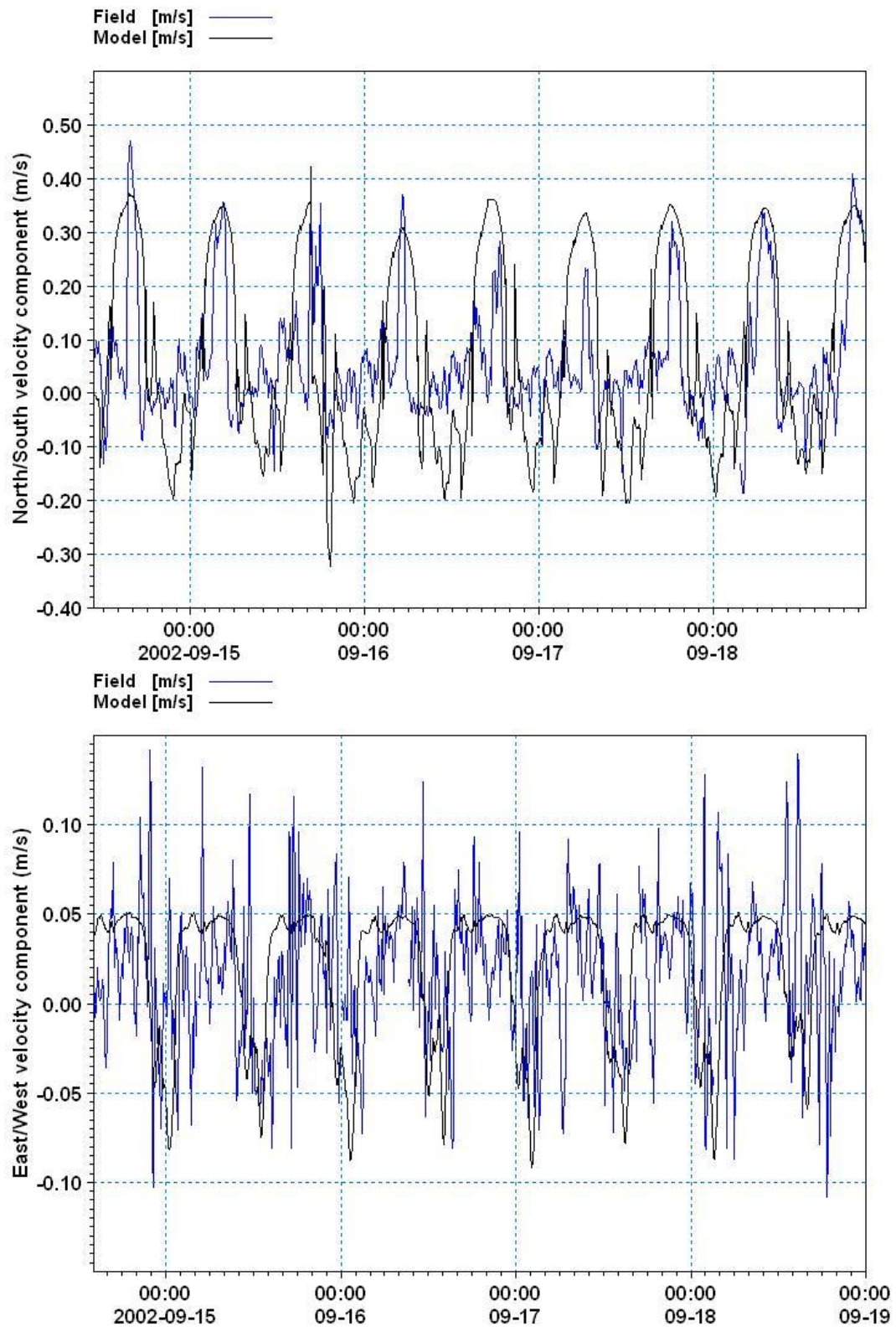


Figure 13

Measured and predicted currents at the site near the mouth of Paremoremo Creek (see Figure 1c). The blue line shows measured currents and the black line shows predicted currents.



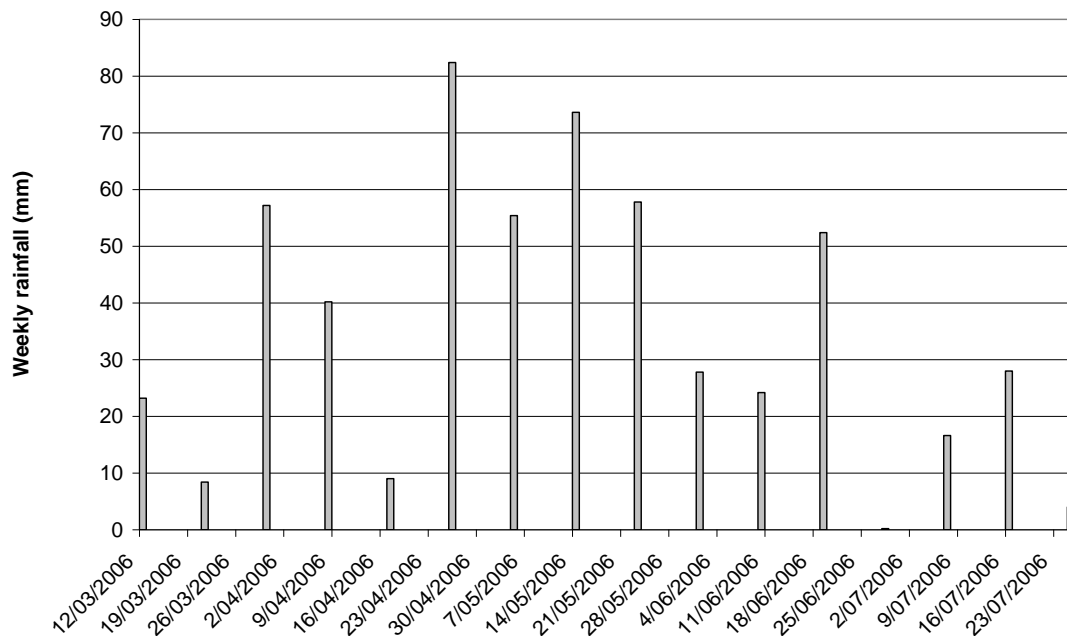
5.3 Salinity

Having determined that the model can predict currents within the harbour, the next step in the calibration process was to determine if the model could adequately simulate the mixing of freshwater inputs to the harbour.

Two periods were modeled: 10–18 May 2006, and 14–16 June 2006. CTD measurements are available in Henderson Creek and the Whau River for both of these periods (Oldman et al. 2008). The first period corresponds to the second wettest week during the 2006 deployment period (Figure 14). Simulating this period provides a good test of the ability of the model to predict harbour-wide mixing of fresh and saline waters.

Figure 14

Weekly rainfall during the 2006 deployment period.



Using the TP108 approach (ARC, 1999) relationships between rainfall and run-off for each catchment surrounding the Central Waitemata Harbour were developed. The relationships were used to derive freshwater inflows during the 2006 deployment period. Figures 18 and 19 show inflows from Henderson Creek and the Whau River so derived.

Figure 15

Mean daily inflows for Henderson Creek during the 2006 deployment derived from TP108.

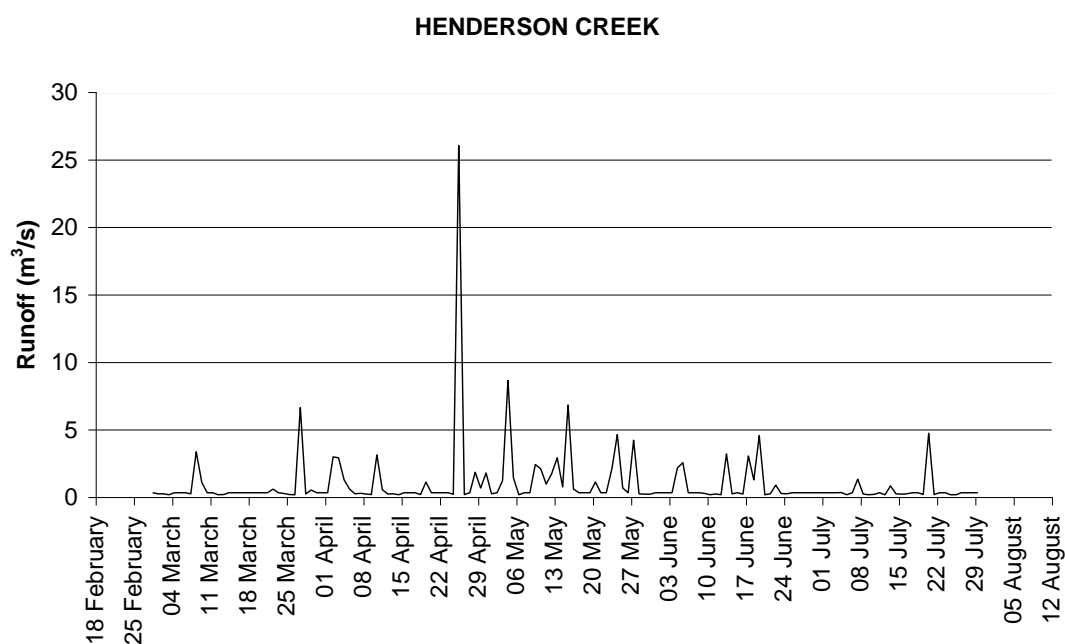
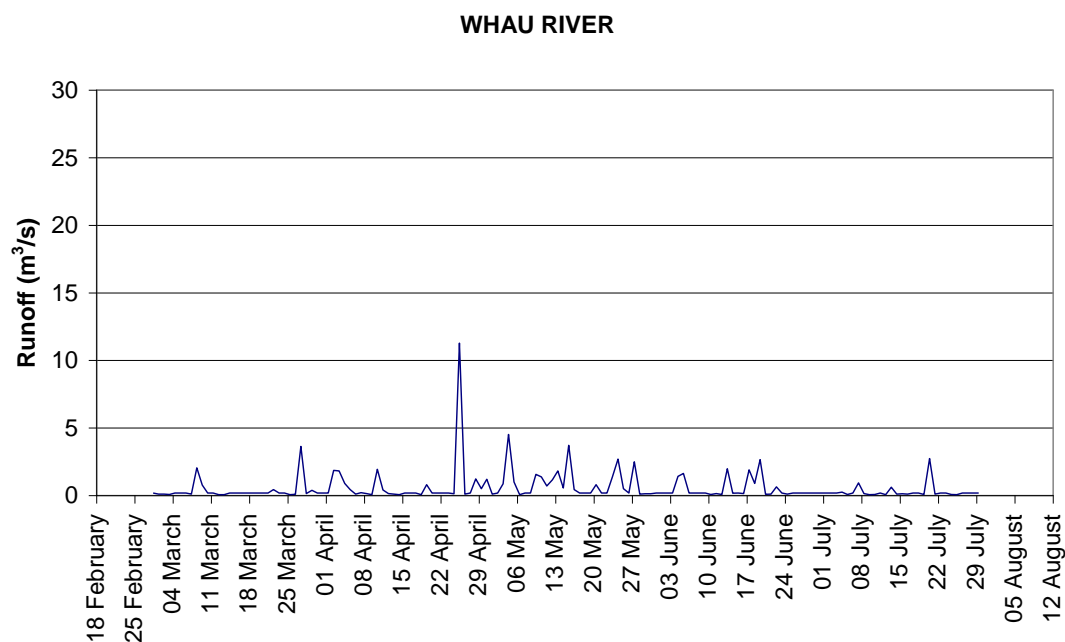


Figure 16

Mean daily inflows for the Whau River during the 2006 deployment derived from TP108.



Initially, the salinity in the model harbour was set to a uniform value of 32 PSU. From this initial condition, the model was run for 14 days with nominal freshwater inflows of $0.1 \text{ m}^3 \text{ s}^{-1}$ from all sources. At the end of the warm-up period, freshwater inflows

derived from TP108, measured tides, and measured winds were used to predict salinity in the harbour for the two periods 10–18 May 2006 and 14–16 June 2006.

Both the vertical and horizontal dispersion coefficients for salinity were applied using the scaled eddy viscosity formulation. The best overall fit between observed and predicted salinity was obtained by applying a scale factor of 1.1 in both the horizontal and vertical dimensions. Lower values led to lower vertical mixing, and observed transitions to a vertically well-mixed situation were not well reproduced. Higher values led to rapid mixing in the horizontal, causing a much larger variation in salinity at sites away from freshwater sources.

Figures 17 to 24 show the observed salinity values (from surface to bed) and the model data (interpolated onto 0.5 m depth intervals) for the period 14–16 June 2006.

The observed vertical salinity structure within the main tidal creeks of the harbour is well simulated by the model. On occasions (eg, Figure 22D) the model overpredicts salinity, which relates to the discrepancy between model averaging over a full element compared to the more localised field sampling.

Table 7 shows that the model tends to slightly over predict observed salinity, and the difference between observed and predicted salinity is greater at lower salinity.

Table 7

Statistics of linear regression between predicted (x) and measured (y) salinity at CTD sites shown in Figure 1b for the period 14–16 June 2006.

Location	Linear regression
CTD Site 1	$y = 0.7973x + 6.5393$, r-squared = 0.5851
CTD Site 2	$y = 0.9448x + 2.1157$, r-squared = 0.9932
CTD Site 3	$y = 0.919x + 3.3178$, r-squared = 0.9796
CTD Site 4	$y = 0.848x + 5.3203$, r-squared = 0.9087
CTD Site 5	$y = 0.5497x + 14.141$, r-squared = 0.9659
CTD Site 6	$y = 0.6691x + 10.713$, r-squared = 0.8663
CTD Site 7	$y = 0.8276x + 5.939$, r-squared = 0.9468
CTD Site 8	$y = 0.8695x + 4.9526$, r-squared = 0.9594

Figure 17

Observed salinity (● - from surface to bed) and predicted salinities (interpolated onto 0.5 intervals – o plus dashed line) at CTD Site 1 (see Figure 1b) for the 14–16 June 2006. Plots for 14 June show observed and predicted salinities at high water (A) and during peak ebbing currents (B). Plots for 16 June show observed and predicted salinities at high water (C) and during peak ebbing currents (D) and low water (E).

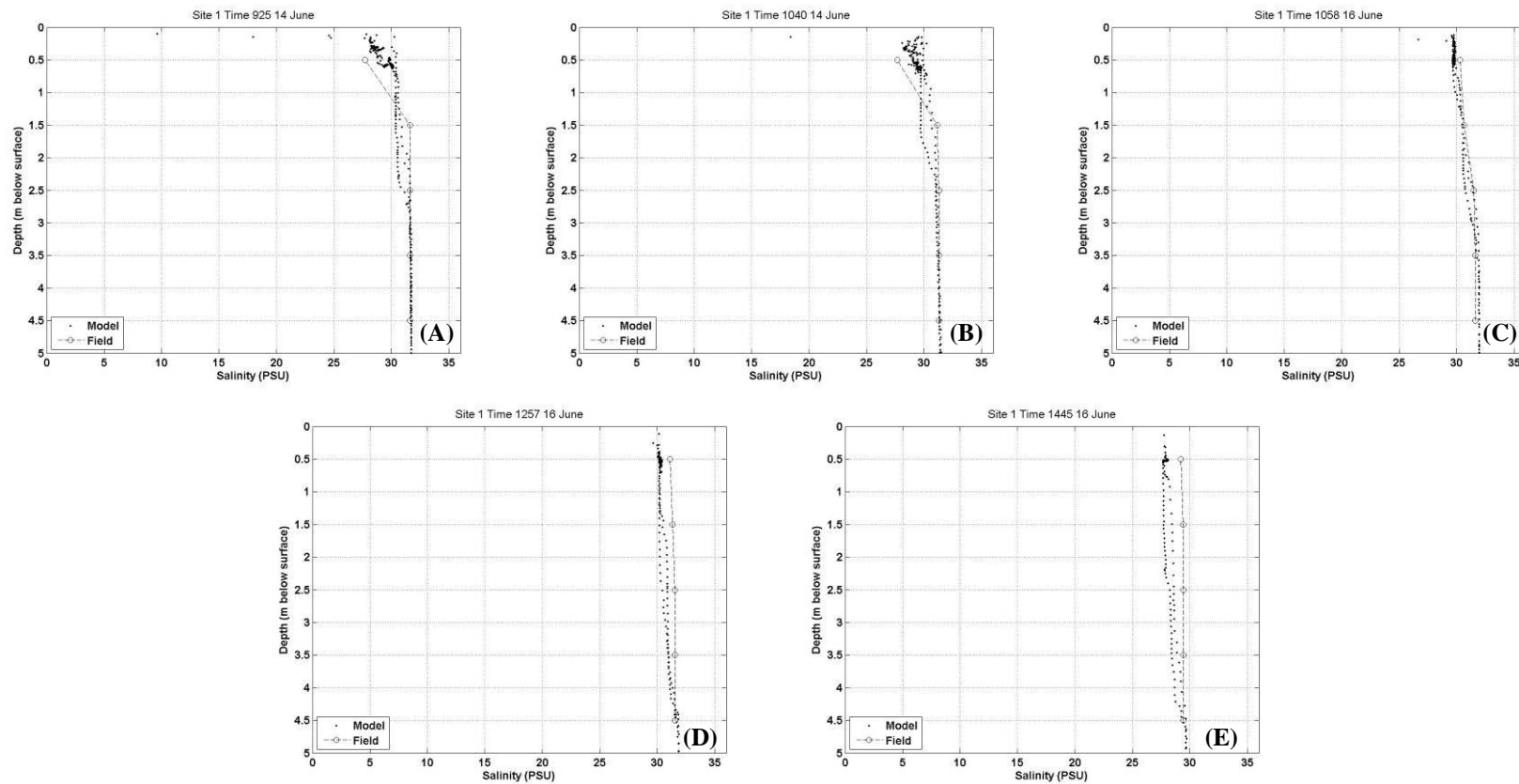


Figure 18

Observed salinity (● - from surface to bed) and predicted salinities (interpolated onto 0.5 intervals - o plus dashed line) at CTD Site 2 (see Figure 1b) for the 14–16 June 2006. Plots for 14 June show observed and predicted salinities at high water (A) and during peak ebbing currents (B). Plots for 16 June show observed and predicted salinities at high water (C) and during peak ebbing currents (D) and low water (E).

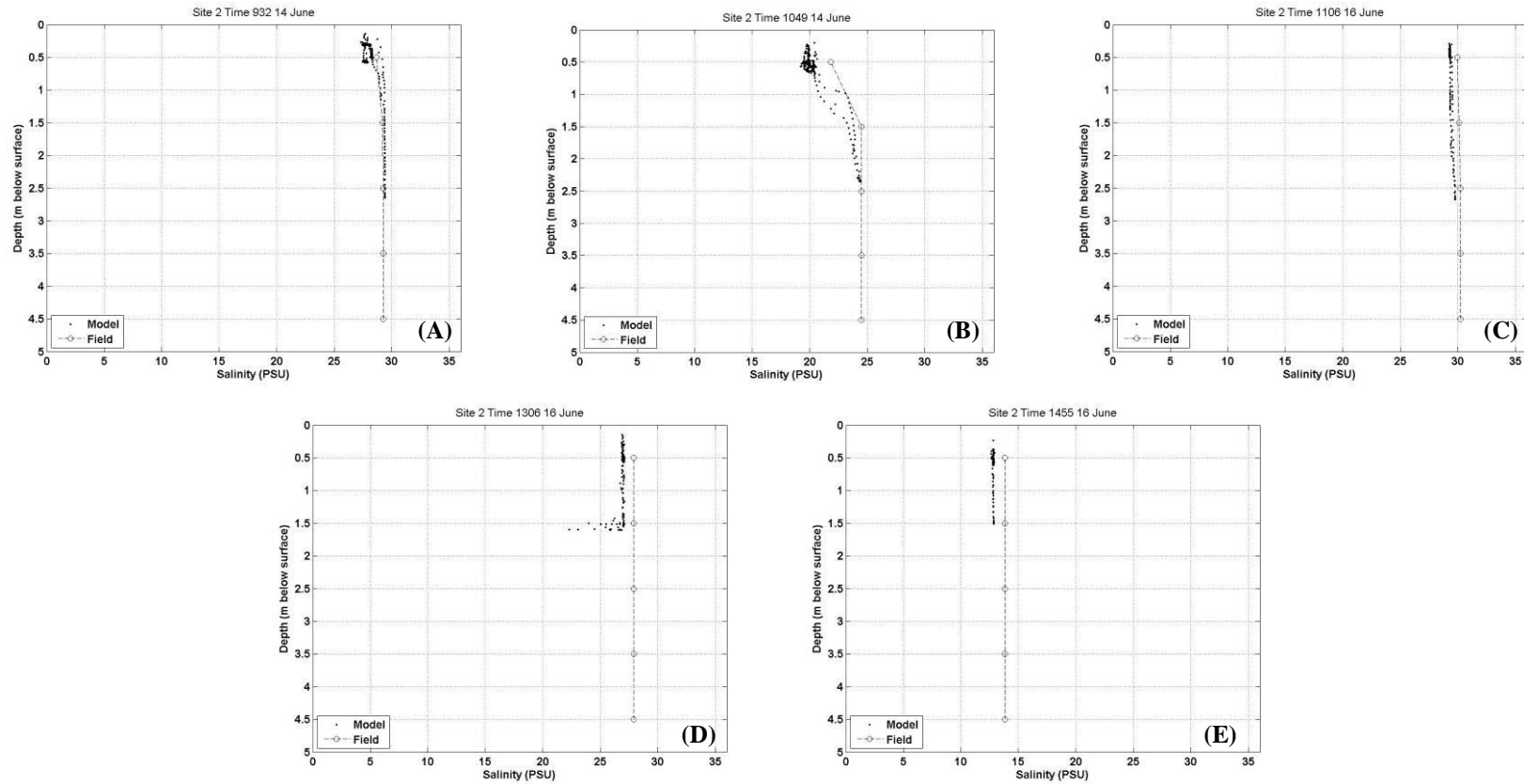


Figure 19

Observed salinity (● - from surface to bed) and predicted salinities (interpolated onto 0.5 intervals – o plus dashed line) at CTD Site 3 (see Figure 1b) in the middle reach of the Henderson Creek for the 14–16 June 2006. Plots for 14 June show observed and predicted salinities at high water (A) and during peak ebbing currents (B). Plots for 16 June show observed and predicted salinities at high water (C) and during peak ebbing currents (D) and low water (E).

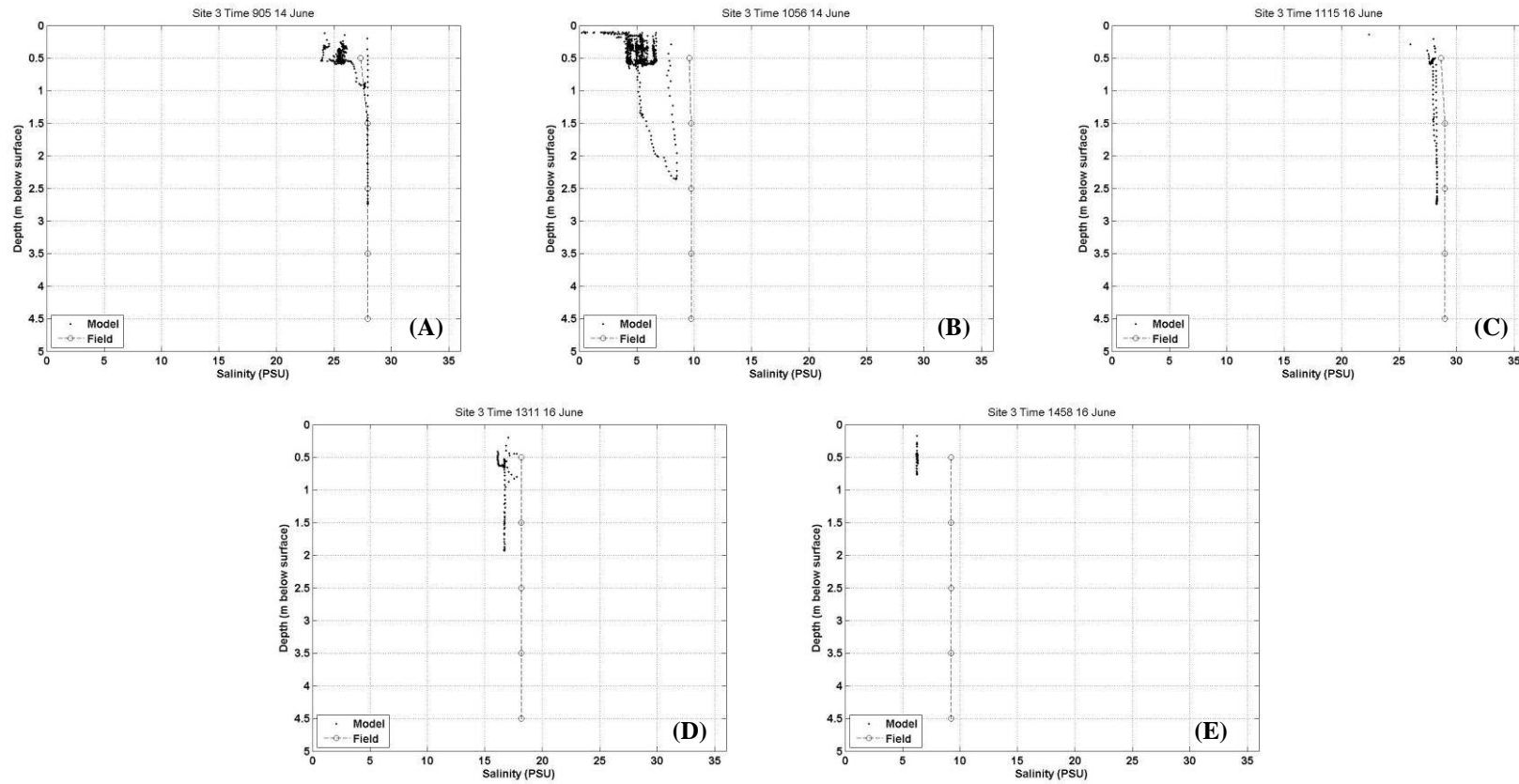


Figure 20

Observed salinity (● - from surface to bed) and predicted salinities (interpolated onto 0.5 intervals - o plus dashed line) at CTD Site 4 (see Figure 1b for upper reach of the Henderson Creek for the 14–16 June 2006. Plots for 14 June show observed and predicted salinities at high water (A) and during peak ebbing currents (B). Plots for 16 June show observed and predicted salinities at high water (C) and during peak ebbing currents (D) and low water (E).

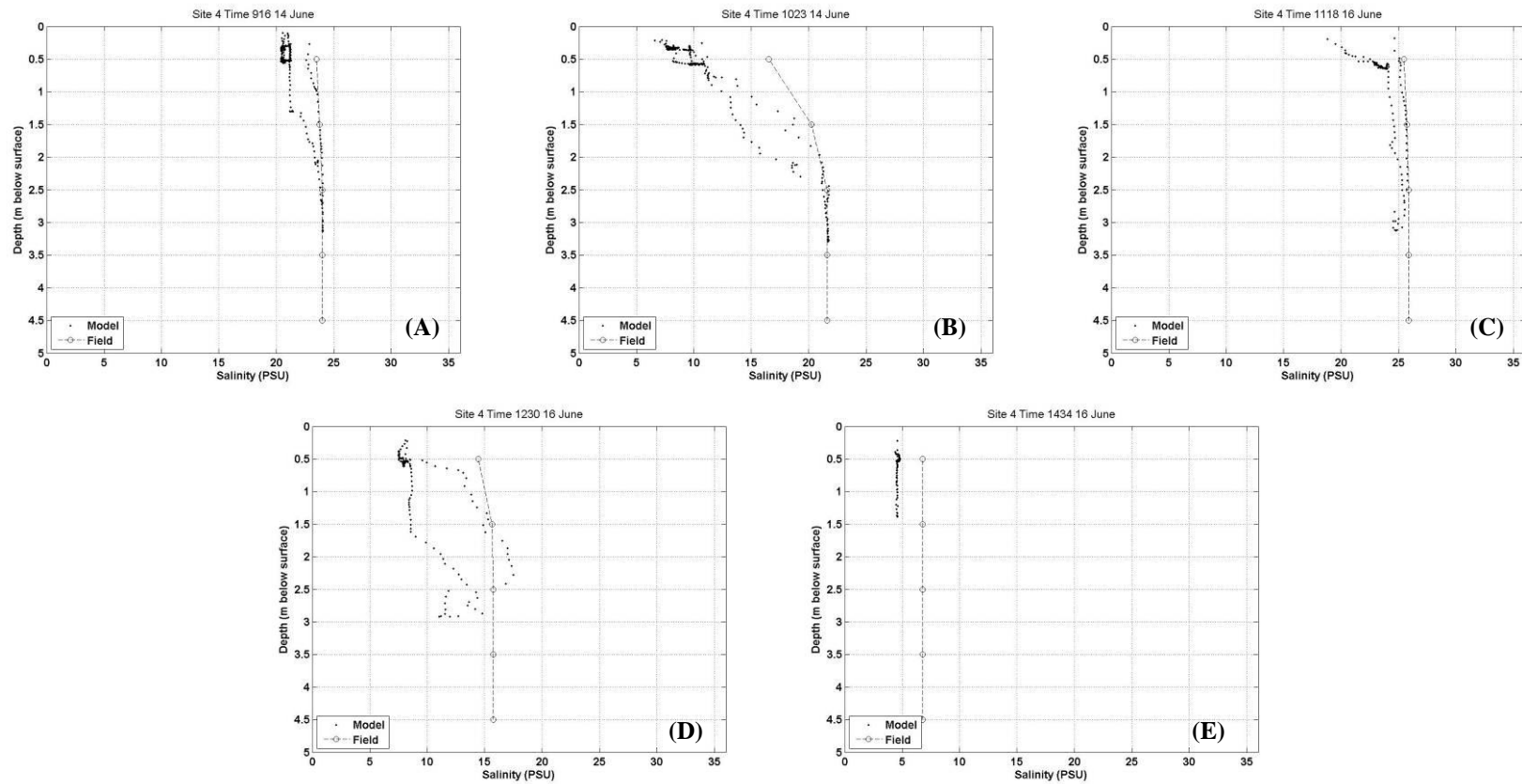


Figure 21

Observed salinity (● - from surface to bed) and predicted salinities (interpolated onto 0.5 intervals - o plus dashed line) at CTD Site 5 (see Figure 1b) for the 15 June 2006. Plots show observed and predicted salinities at high water (A), peak ebb tide currents (B) and low water (C).

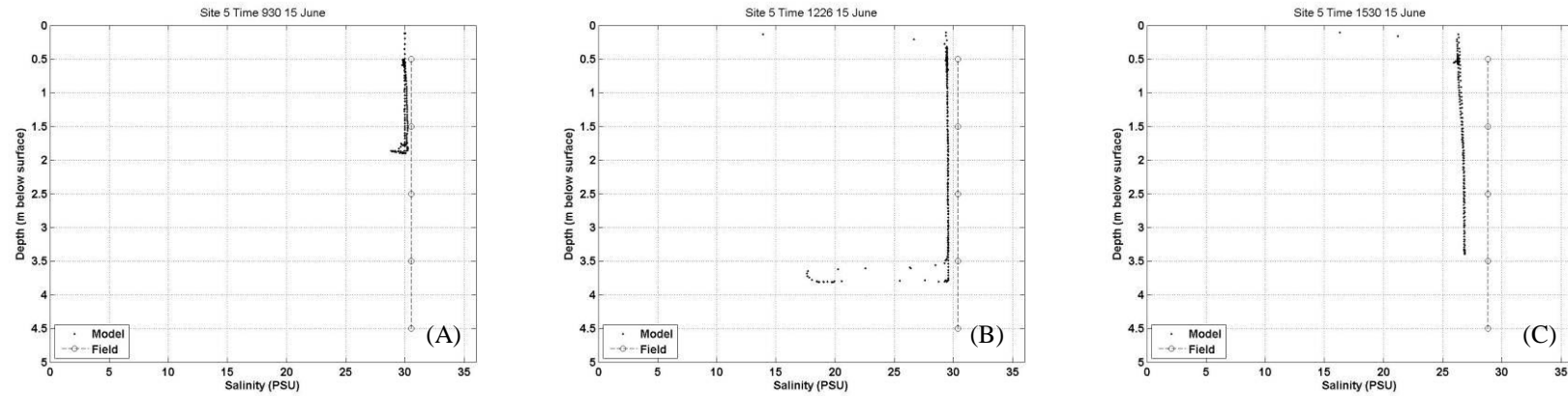


Figure 22

Observed salinity (● - from surface to bed) and predicted salinities (interpolated onto 0.5 intervals - o plus dashed line) at CTD Site 6 (see Figure 1b) for the 15 June 2006. Plots show observed and predicted salinities at high water (A), peak ebb tide currents (B) and low water (C).

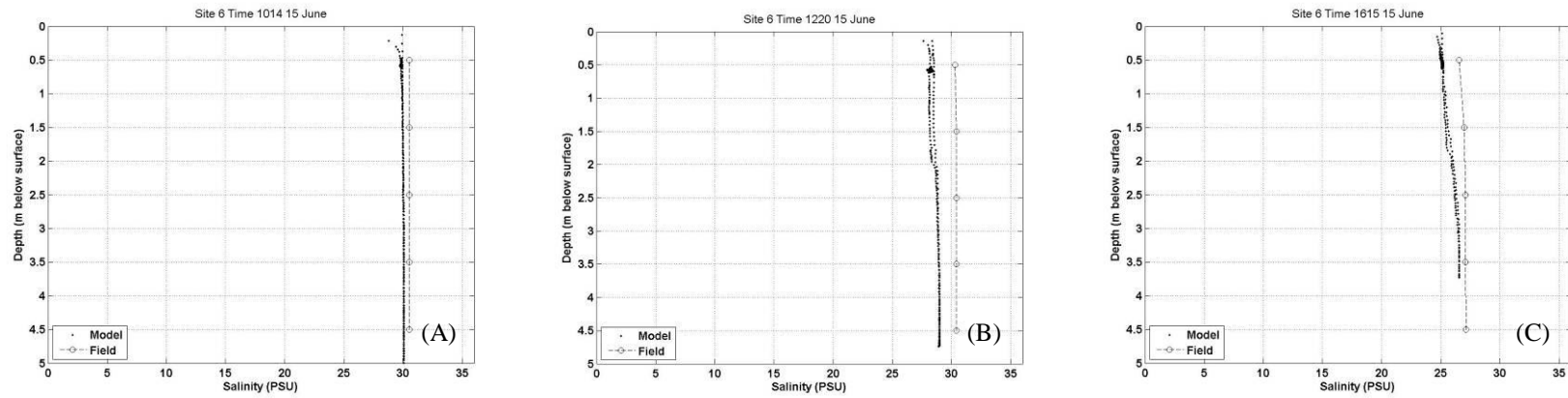


Figure 23

Observed salinity (● - from surface to bed) and predicted salinities (interpolated onto 0.5 intervals - o plus dashed line) profiles at CTD Site 7 (see Figure 1b) for the 15 June 2006. Plots show observed and predicted salinities at high water (A), peak ebb tide currents (B) and low water (C).

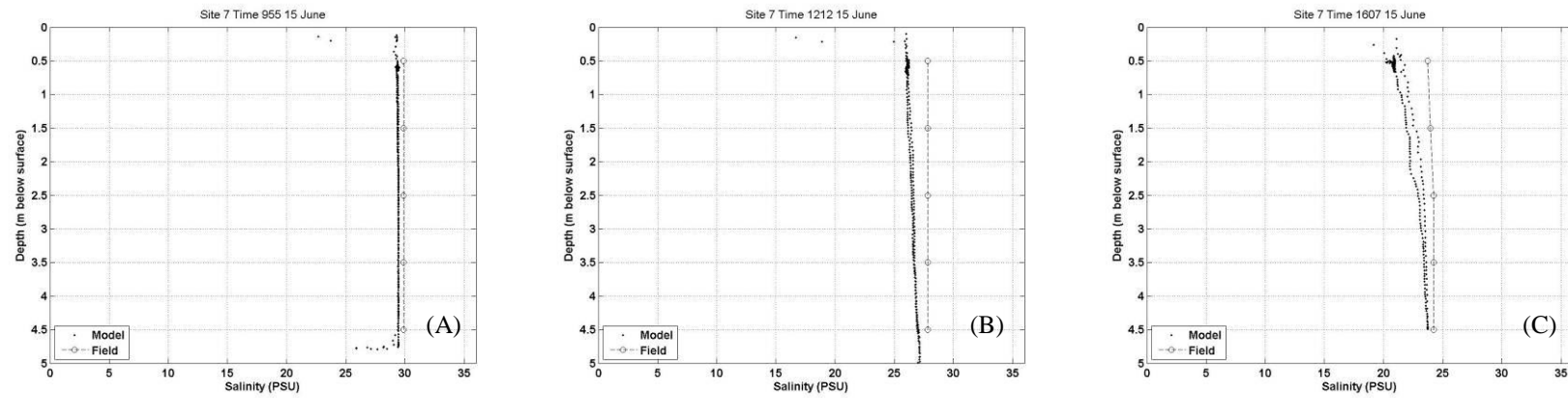
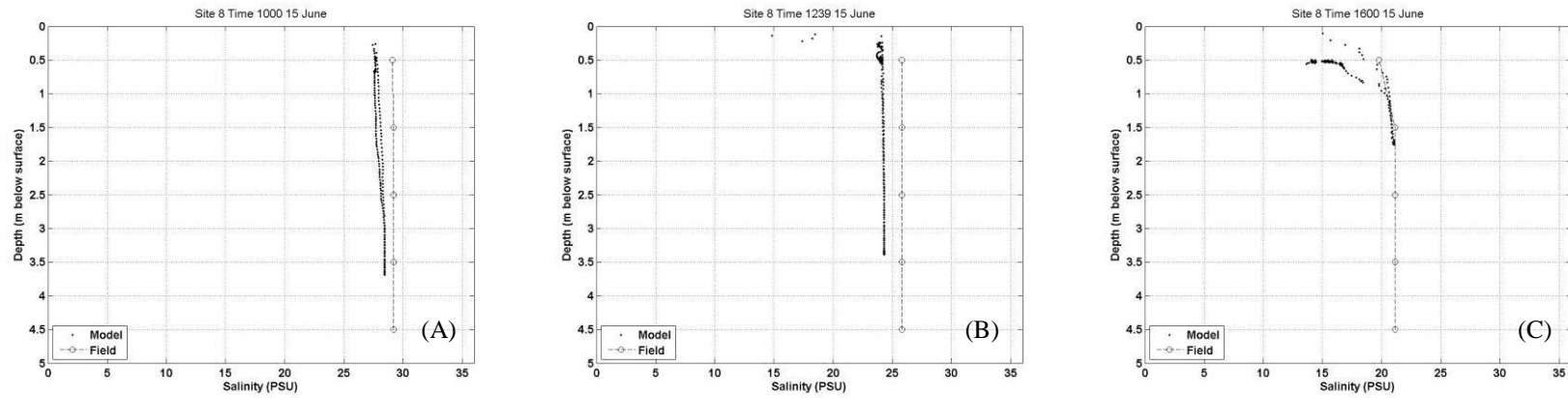


Figure 24

Observed salinity (● - from surface to bed) and predicted salinities (interpolated onto 0.5 intervals - o plus dashed line) CTD at Site 8 (see Figure 1b) for the 15 June 2006. Plots show observed and predicted salinities at high water (A), peak ebb tide currents (B) and low water (C).



Figures 25 to 28 show measured near bed salinity and the predicted salinity in the near bed layer of the model at DOBIE Sites 2, 5, 7 and 8 in the period 10–18 May 2006, which was the second wettest week during the 2006 deployment season with 74 mm falling.

Table 8 shows that at Sites 5, 7 and 8 the model is reasonably good at predicting tidal fluctuations of salinity. At Site 2, the model predicts salinity reasonably well between peak flood and peak ebb tide (ie, salinities above ~22 PSU), but for predictions around low water (ie, <22 PSU) the model often predicts much lower salinity than observed. The discrepancy between observed and predicted low water salinity at Site 2 could be due to: too much freshwater in Henderson Creek; poor schematisation of the subtidal bathymetry of Henderson Creek; too much horizontal dispersion within Henderson Creek. The good fit between observed and predicted salinity at Site 5 in the upper reaches of the Whau River suggests that the method of estimating freshwater inflows is reasonably accurate. The current calibration at Site 5 (see Figure 10 and Table 7) suggests that the bathymetry is good. Thus, the discrepancy between observed and predicted low-water salinity at Site 2 can be attributed to excessive freshwater dispersion within Henderson Creek. Applying a lower horizontal dispersion coefficient within Henderson Creek could lead to a better fit between observed and predicted low-water salinity. However, given the overall fit between observations and predictions (Table 7), this option was not pursued.

Table 8

Statistics of linear regression between predicted (x) and measured (y) salinity at DOBIE sites (Figure 1a) for the period 10–18 May 2006.

Location	Linear regression
2	$y = 0.481x + 14.192$, r-squared = 0.727
2 (data below 22 PSU)	$y = 0.5443x + 13.602$, r-squared = 0.2605
2 (data above 22 PSU)	$y = 1.0383x - 0.973$, r-squared = 0.7291
5	$y = 0.759x + 3.982$, r-squared = 0.681
7	$y = 0.651x + 9.095$, r-squared = 0.643
8	$y = 0.996x - 0.002$, r-squared = 0.826

Figure 25

Measured and predicted salinity at Site 2 (near the mouth of Henderson Creek) from 10–18 May 2006.

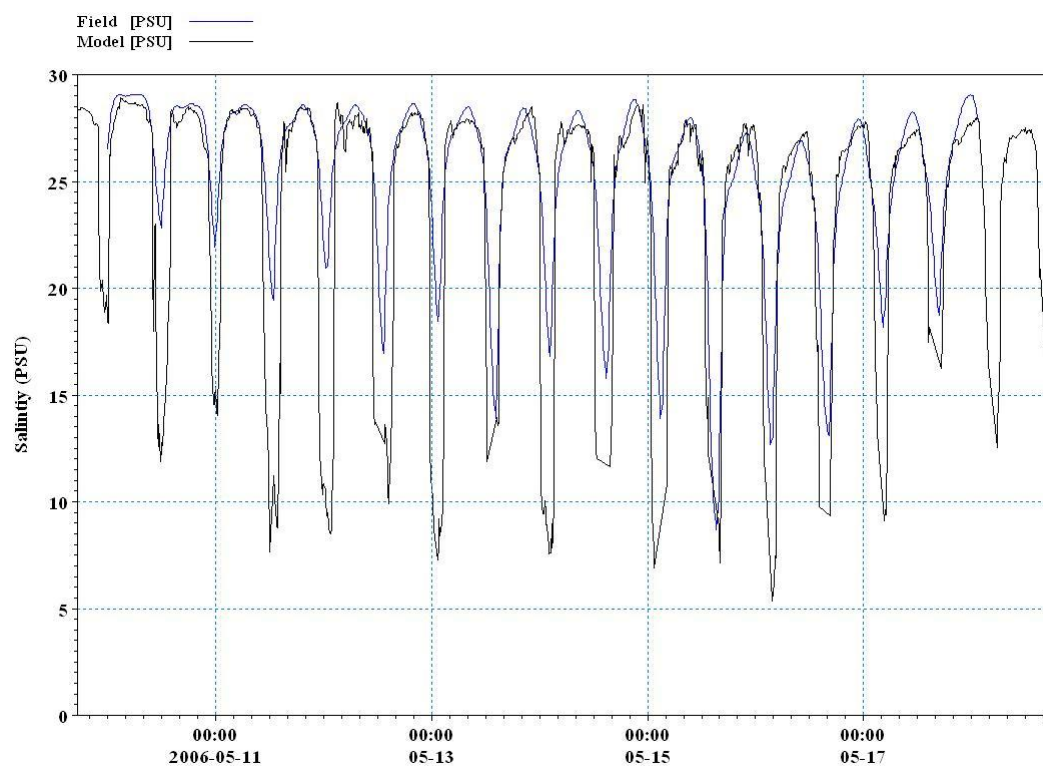


Figure 26

Measured and predicted salinity at Site 5 (near the upper reaches of the Whau River) from 10–18 May 2006.

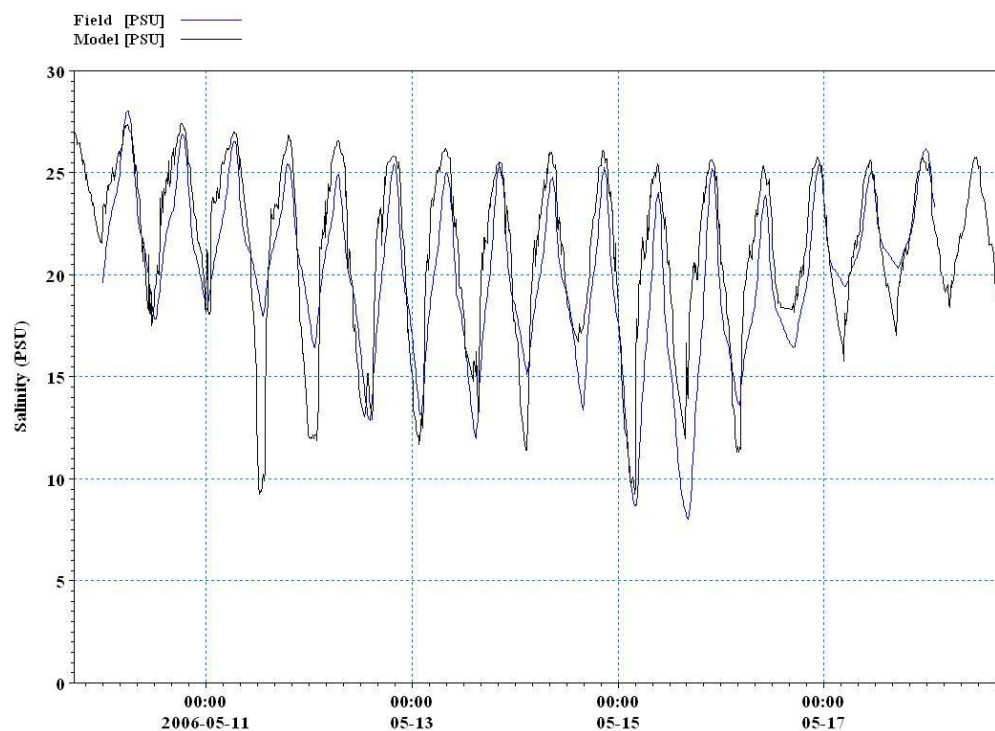


Figure 27

Measured and predicted salinity at Site 7 (Whau River near Pollen Island) from 10–18 May 2006.

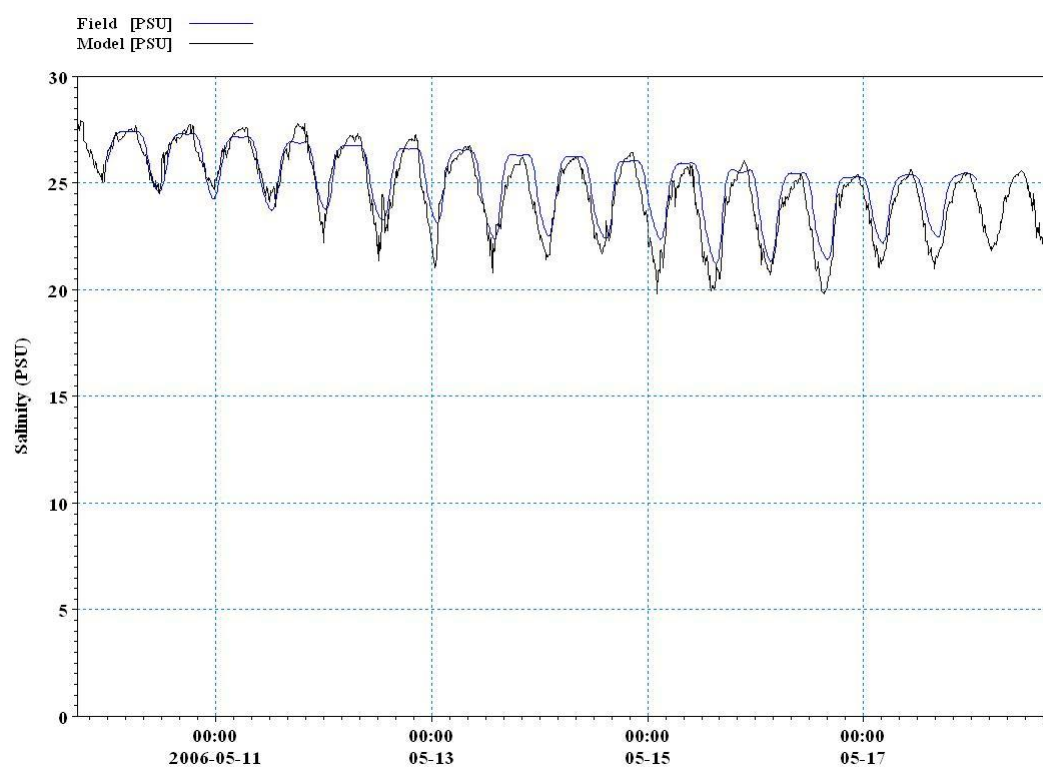
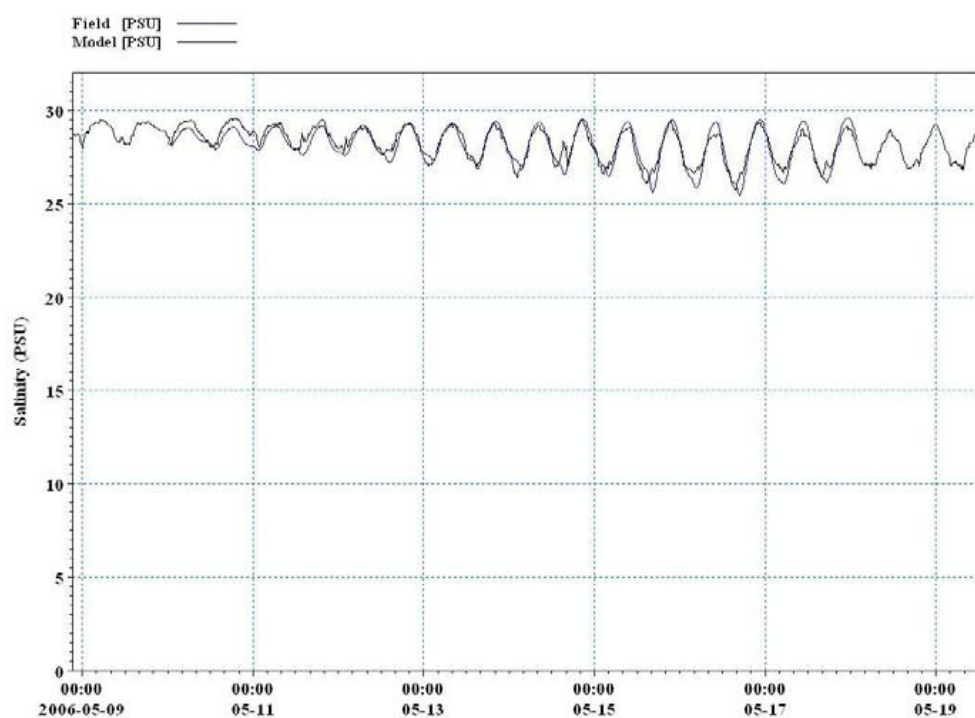


Figure 28

Measured and predicted salinity at Site 8 (in the middle basin of the Waitemata) from 10–18 May 2006.



5.4 Waves

The SWAN model (Booij et al. 1999; Ris et al. 1999) is a spectral wave model particularly intended for shallow-water applications in coastal and estuarine environments. It describes the sea state at each time (t) and position (x, y) within a defined region in terms of the amount of energy associated with each wave frequency (f) and propagation direction (θ). The model computes the evolution of the wave spectrum $F(f, \theta)$ by accounting for the input, transfer and loss of energy through various physical processes. These processes include:

- wave generation by wind stress;
- wave propagation;
- refraction by the seabed and/or currents;
- transfer of energy between interacting waves of different frequencies and directions (a nonlinear effect);
- dissipation by white-capping;
- depth-induced breaking; and
- bottom friction.

The model takes inputs specifying relevant environmental conditions, including:

- wind speed and direction;
- water depth;
- current speed and direction; and
- incident wave conditions at the domain boundary.

In the most general case, the above parameters can be given as a function of position (x, y) and time (t), although sometimes a “stationary” simulation is done, where the equilibrium sea state is computed assuming time-invariant conditions.

5.4.1 SWAN model application to the Central Waitemata Harbour

A model domain was established covering the Central Waitemata Harbour. A latitude/longitude grid was used, with 250 longitude cells from 174.6260°E to 174.8501°E, and 107 latitude cells from 36.8873°S to 36.7919°S, at 100-m resolution in both directions. The spectral grid had 32 discrete frequencies logarithmically placed between 0.10 Hz and 2.00 Hz, and 24 direction bins at 15° increments. All other model settings were SWAN defaults as described in the manual (Holthuijsen et al. 2000).

5.4.2 Calibration simulations

The model was first applied in a nonstationary (time-varying) simulation covering the 120-hour period starting at 00:00 NZST on 19 June 2006. Each simulation used water levels and currents, varying in space and time, provided by a MIKE3 simulation. Time-varying wind fields were derived from data recorded at the meteorological stations

listed in Table 9. A spatially uniform wind field formed from the vector average of all stations was used. No wave boundary conditions were applied.

Table 9

Meteorological stations from which wind data were sourced for wave model calibration simulations.

Name	Latitude (degrees)	Longitude (degrees)	Altitude (m)
Wiri	-36.993	174.870	18
Onehunga	-36.930	174.801	5
Henderson	-36.863	174.632	35
North Shore	-36.786	174.736	20
Owairaka	-36.893	174.726	41
Musick Pt Ews	-36.850	174.901	18
Auckland Aero	-37.007	174.789	33
Khyber Pass	-36.868	174.771	81
Lincoln Road	-36.869	174.629	25
Pakuranga	-36.907	174.893	15
Penrose	-36.904	174.816	30
Mangere	-36.963	174.775	5
Whenuapai	-36.793	174.624	26

5.4.3 Comparison with measurements

Wave measurements during the simulation period were available from a set of deployments of DOBIE wave-recording pressure sensors (see Figure 1a). Usable data during the simulation period were available at DOBIE Sites 2, 4, 8, 9 and 10 (see Figure 1a). Pressure time series from the DOBIEs were used to compute estimates of statistics including significant wave height, mean water depth, peak and mean wave period, and root-mean-square bed orbital velocity, as follows. These are compared with corresponding statistics output from the SWAN simulations at the corresponding locations.

Wave data recorded (or computed from a model) at a single point are usually discussed in terms of the variance spectrum $S(f)$ of the sea-surface elevation. The DOBIE, however, does not directly measure the sea-surface elevation, but instead records a time series of pressure, from which a variance spectrum $S_p(f)$ can be obtained. The two spectra are related as:

$$S_p(f) = \rho g A(f) S(f) \quad (16)$$

where $\rho = 1025 \text{ kg.m}^{-3}$ (density of sea water), $g = 9.81 \text{ m.s}^{-2}$ (gravitational acceleration), and $A(f)$ is a frequency-dependent attenuation function:

$$A(f) = \left(\frac{\cosh(k(z+h))}{\cosh(kh)} \right)^2 \quad (17)$$

Here, h is water depth and z is the instrument's vertical elevation above mean water level. The wave number k is related to the frequency f by a dispersion relation:

$$(2\pi f)^2 = gk \tanh(kh) \quad (18)$$

The attenuation function $A(f)$ becomes very small when kh is large, ie, at frequencies for which the wavelength is much smaller than the water depth. In that case, the part of the high-frequency pressure signal contributed by surface waves becomes small relative to the noise level. To limit the effect of amplification of noise at high frequencies, it is normal to apply a frequency cutoff when estimating $S(f)$.

From the computed spectral energy density $S(f)$, the peak frequency f_p and peak energy $S_p = S(f_p)$ of the spectrum are located. Spectral moments

$$M_j = \int_0^{f_{cut}} f^j S(f) df \quad (19)$$

are computed, allowing further statistics to be defined, including:

- significant height $H_s = 4\sqrt{M_0}$
- first moment mean period $T_{m01} = M_0 / M_1$
- second moment mean period $T_{m02} = \sqrt{M_0 / M_2}$

The root-mean-square bed-orbital velocity is calculated as:

$$U_{rms}^2 = \int_0^{f_{cut}} 2\pi f A(f) S(f) df \quad (20)$$

Results from the final calibration run are plotted against DOBIE data obtained from Sites 2, 4, 8, 9 and 10 on 23 June 2006 in Figures 32 to 36.

There were discrepancies between the simulated and measured mean water levels relating to the actual depths at the DOBIE sites and the interpolated depths used in the SWAN grid. As noted above, the SWAN model used a 100-m regular grid which was interpolated from the MIKE3 FM mesh, which in turn was interpolated from raw bathymetry data. For example, Site 9 shows a serious discrepancy with respect to measured and predicted water levels not evident during the calibration of MIKE3 FM (Figure 7). This suggests that the depths used in the mesh (and regular grid) may not be correct². Less dramatically, DOBIE records at Site 4 indicate drying at low water at midday on 23 June, while the simulation maintains some 30 cm depth.

² For the MIKE3 calibration, the raw water surface elevation is firstly converted to Chart Datum, so any discrepancies in the underlying grid would not be evident.

Significant wave heights from the simulations are generally close to those measured, though they show somewhat weaker variation with depth. This may be partly linked to inaccuracies in the modelled water depth noted above.

As noted previously, a high-frequency cutoff is used in computing wave statistics from pressure data. Typically, values of about 1 Hz would be appropriate for 1 m water depth, and about 0.5 Hz for 3 m water depth, typical of the depth ranges at the DOBIE measurement sites. The estimation of mean period from the spectral moments is particularly sensitive to the higher frequency range of the spectrum, and applying a cut-off can significantly increase the estimated mean periods. This probably largely accounts for model mean periods being generally below estimates from DOBIE data, noting that the discrepancies are least at times of lower water depth, when the attenuation effect is less marked. At 3 m depth, typical of high tide records, the mean periods estimated from DOBIE data are about two seconds, corresponding to frequencies of 0.5 Hz which are close to the attenuation limit.

Figure 29

Comparison of data recorded by DOBIE wave recorder at Site t2 (+) with output for the same location from the SWAN simulation (black lines). From top to bottom: significant wave height (H_{sig}), mean water depth, peak wave period (T_{peak}), mean (dotted line: first moment, solid line: second moment) wave period, root-mean-square bed orbital velocity. This simulation runs from 12:00NZST on 22 June 2006 (time = 172.5 days) to 00:00NZST on 24 June 2006 (time = 174 days).

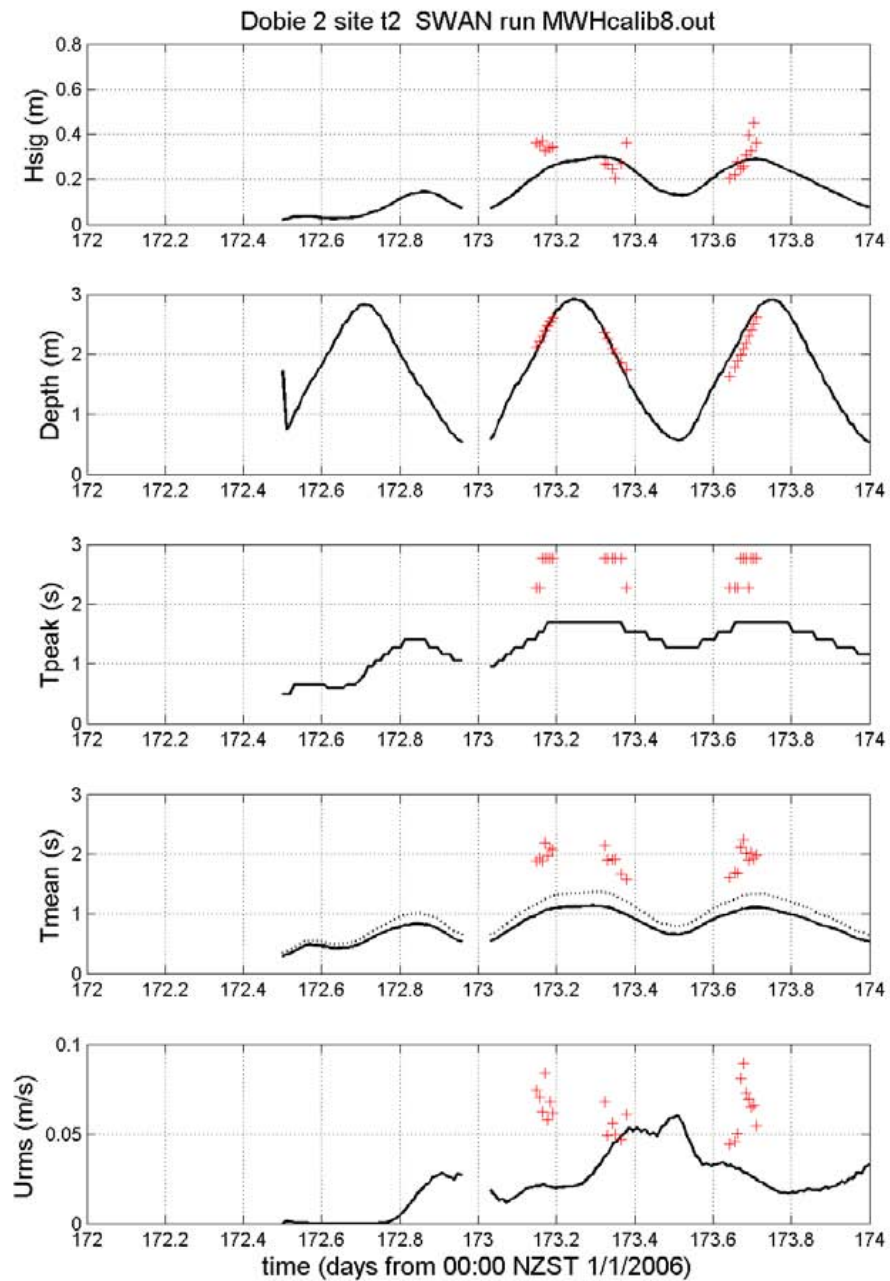


Figure 30

Comparison of data recorded by DOBIE wave recorder at Site t4 (+) with output for the same location from the SWAN simulation (black lines). From top to bottom: significant wave height (Hsig), mean water depth, peak wave period (Tpeak), mean (dotted line: first moment, solid line: second moment) wave period, root-mean-square bed orbital velocity. This simulation runs from 12:00NZST on 22 June 2006 (time = 172.5 days) to 00:00NZST on 24 June 2006 (time = 174 days).

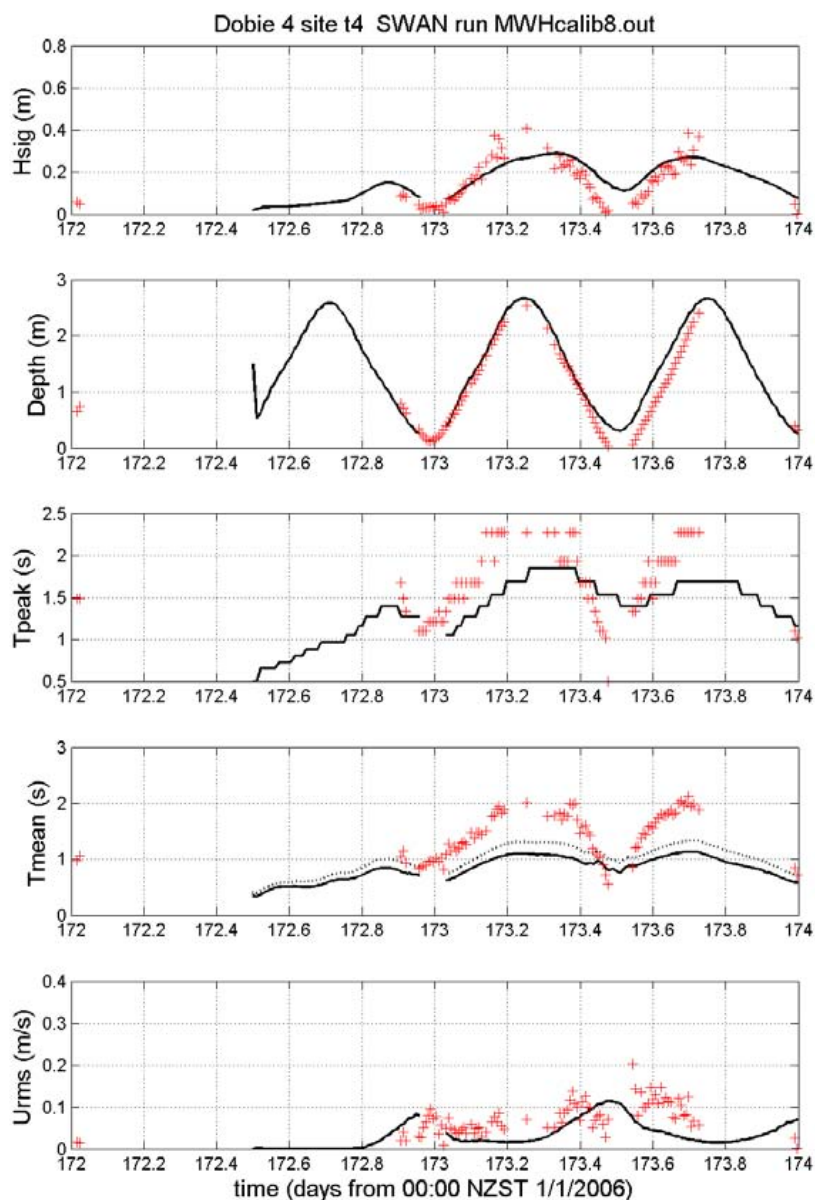


Figure 31

Comparison of data recorded by DOBIE wave recorder at Site t7 (+) with output for the same location from the SWAN simulation (black lines). From top to bottom: significant wave height (Hsig), mean water depth, peak wave period (Tpeak), mean (dotted line: first moment, solid line: second moment) wave period, root-mean-square bed orbital velocity. This simulation runs from 12:00NZST on 22 June 2006 (time = 172.5 days) to 00:00NZST on 24 June 2006 (time = 174 days).

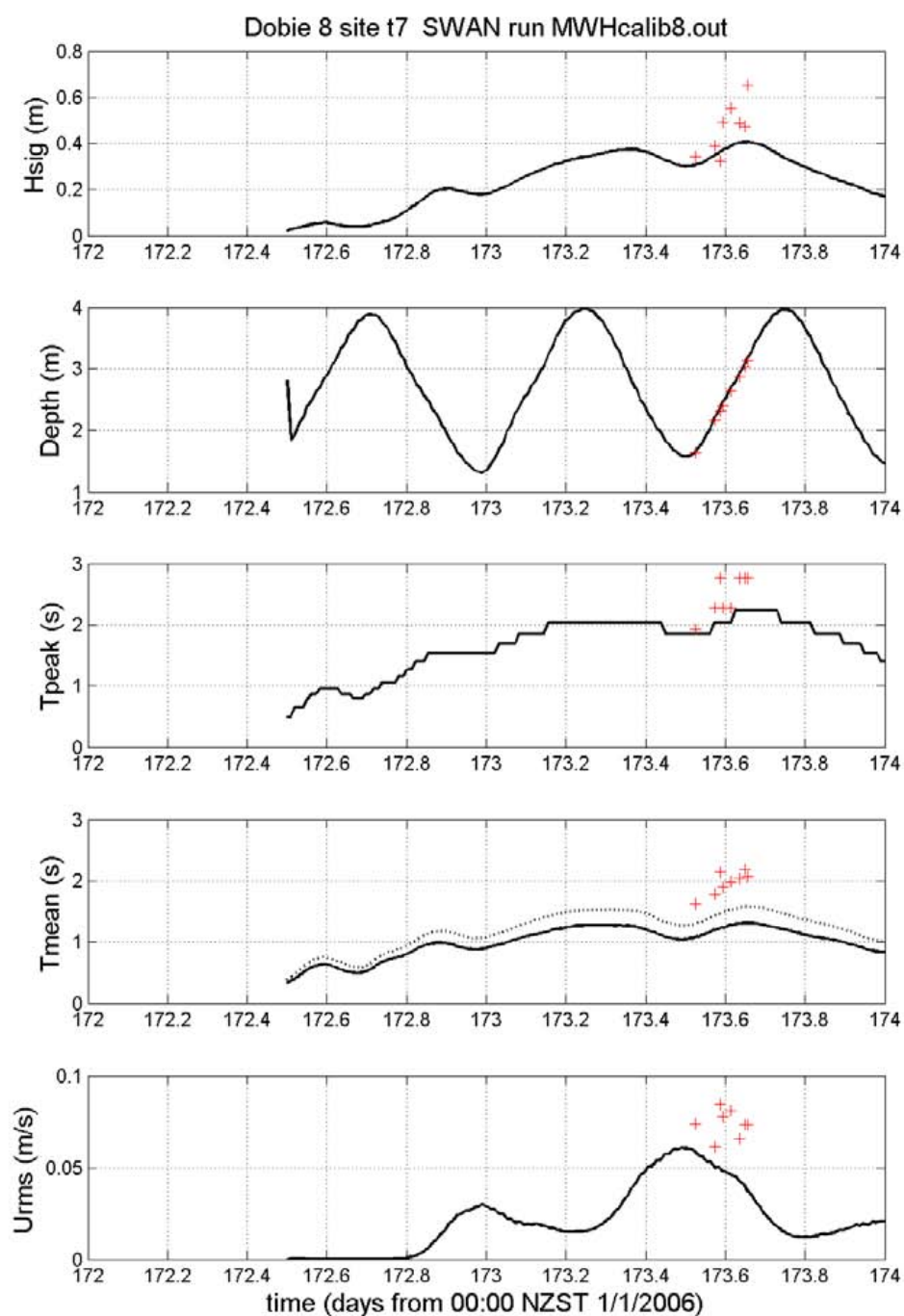


Figure 32

Comparison of data recorded by DOBIE wave recorder at Site t8 (+) with output for the same location from the SWAN simulation (black lines). From top to bottom: significant wave height (Hsig), mean water depth, peak wave period (Tpeak), mean (dotted line: first moment, solid line: second moment) wave period, root-mean-square bed orbital velocity. This simulation runs from 12:00NZST on 22 June 2006 (time = 172.5 days) to 00:00NZST on 24 June 2006 (time = 174 days).

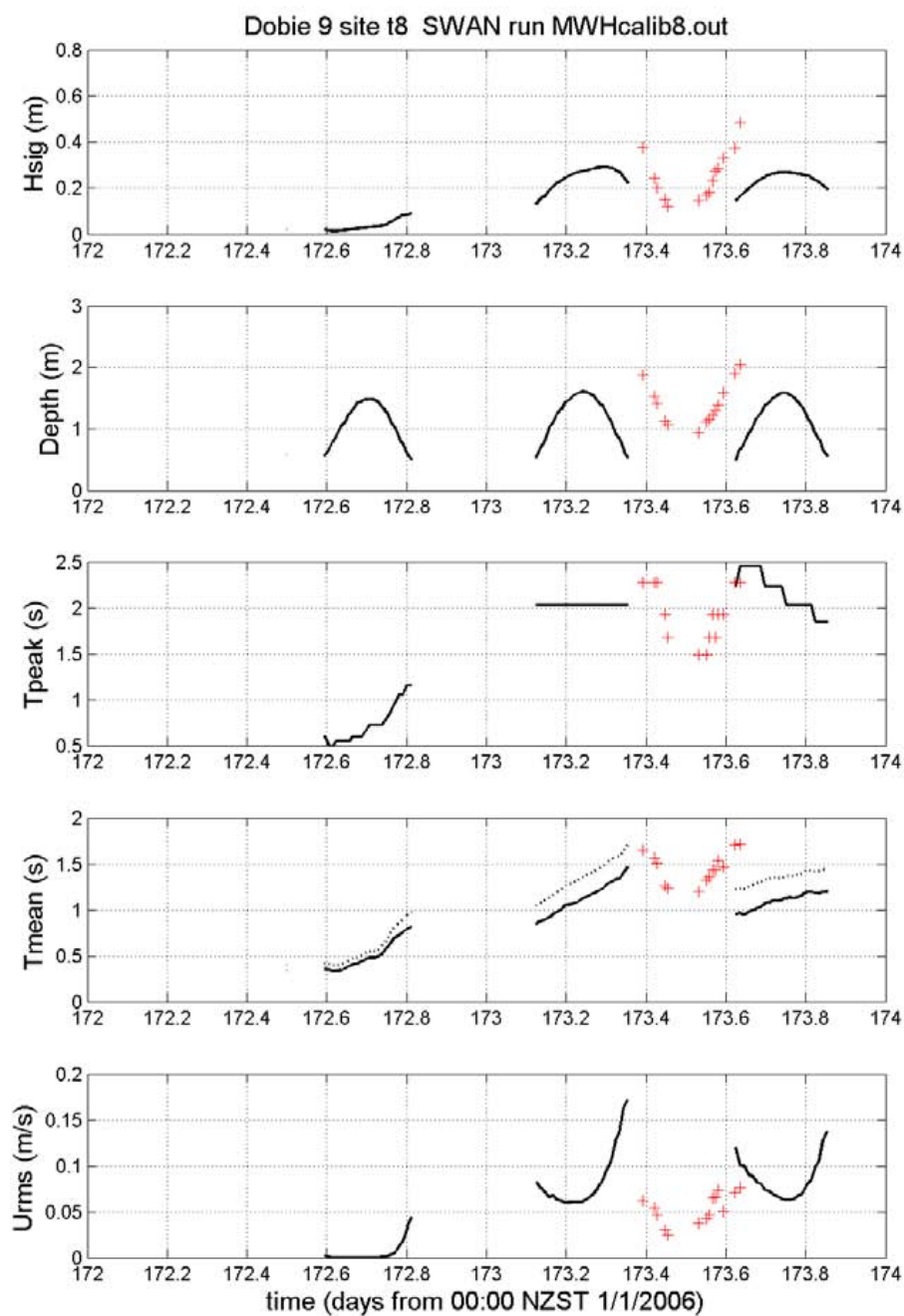
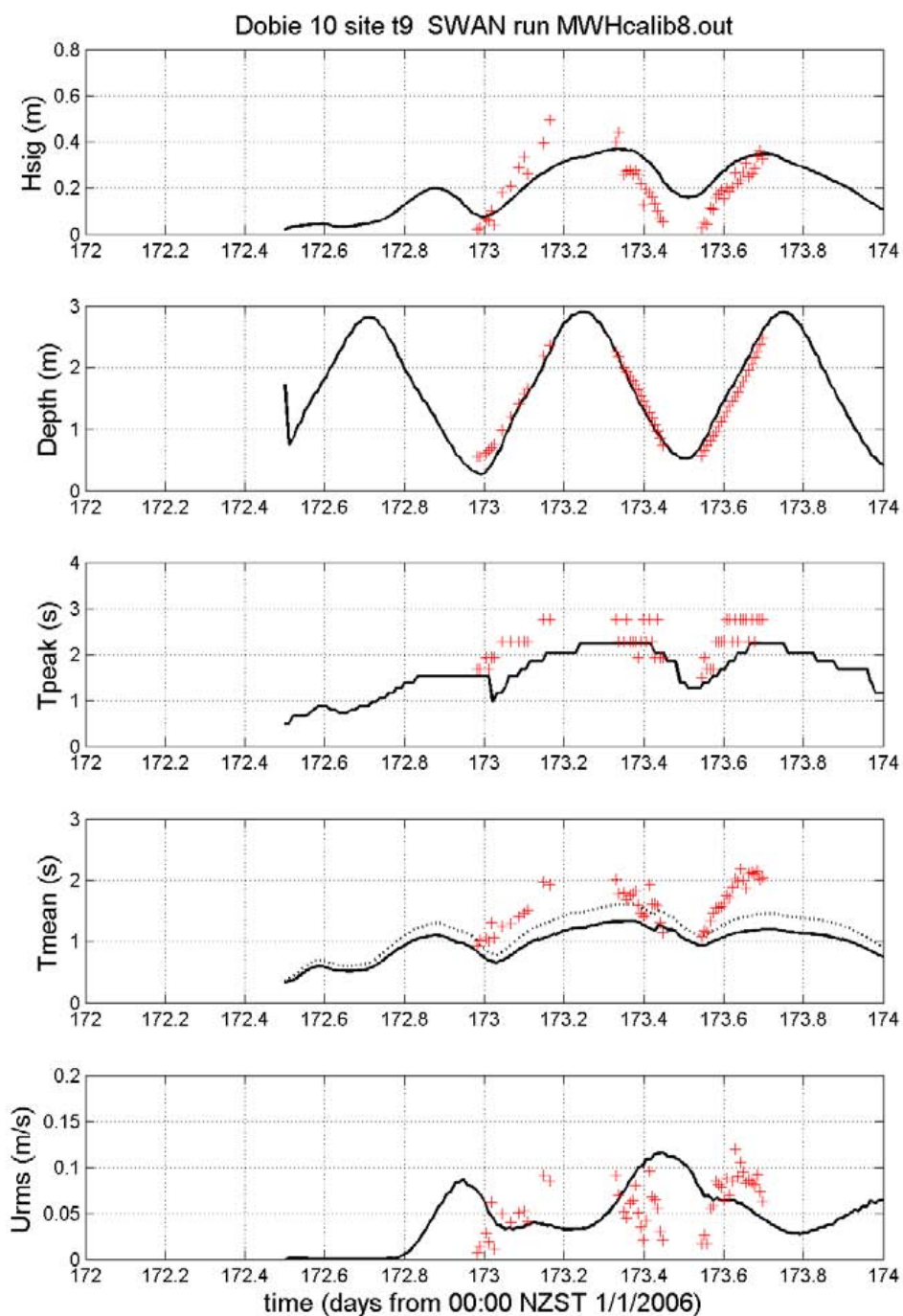


Figure 33

Comparison of data recorded by DOBIE wave recorder at Site t9 (+) with output for the same location from the SWAN simulation (black lines). From top to bottom: significant wave height (Hsig), mean water depth, peak wave period (Tpeak), mean (dotted line: first moment, solid line: second moment) wave period, root-mean-square bed orbital velocity. This simulation runs from 12:00NZST on 22 June 2006 (time = 172.5 days) to 00:00NZST on 24 June 2006 (time = 174 days).



5.5 Suspended sediment concentration

The final step in the calibration process was to calibrate the MIKE3 MT sediment transport model against measured suspended sediment concentrations (SSC). The measurements, which are described in detail in Oldman et al. (2008), were made between 30 to 80 cm above the bed. The measurements were made with optical backscatter sensors, which are more sensitive to fine sediments than coarse sediments.

Seven sites (2, 4, 7, 8, 9, 10 and 11; Figure 1a) were used to compare predicted and measured SSC. Sites 1, 3 and 5 were excluded from the calibration process as these were used to derive the boundary conditions for the model.

Three periods were chosen for the calibration:

- The **first** (6–8 May 2006) had relatively small inputs of sediment from the catchment and light winds averaging less than 2.0 m s^{-1} . This period was modelled with no waves.
- The **second** period (18–21 June 2006) consisted of moderate inputs of sediment from the catchment with winds averaging 3.0 m s^{-1} . This period was modelled with no waves, but the slightly higher winds during this period did lead to increased wind shear stress and a corresponding adjustment in the predicted currents within the harbour.
- The **third** period (26–28 May 2006) had moderate inputs of sediments from the catchment and a significant wave event.

In combination, these events and sites tested the model's capabilities to simulate the transport of sediment under a range of hydrodynamic conditions and sediment loadings.

For the calibration, the bed of the harbour is assumed to be composed of three particle sizes: 12, 40 and $125 \text{ }\mu\text{m}$. These represent fine silt, coarse silt and fine sand, respectively.

Swales et al. (2008), in the report on harbour bed sediments for the Central Waitemata Harbour Study, found each of these modes present in harbour bed sediments. However, bed-sediment median particle size exceeded $125 \text{ }\mu\text{m}$ in the more exposed parts of the harbour, which indicates the presence of a mode that is larger than $125 \text{ }\mu\text{m}$. There are no measurements of the typical particle size of suspended sediments in the CWH (the instrument intended to be used by Swales et al. for this purpose failed), but other studies in comparable harbours (eg, Green et al., 2007) indicate that sediment coarser than fine sand is not likely to be mobilised in any significant way by waves and currents in enclosed harbours. Hence, any sediment coarser than fine sand is considered here to be "relict", and does not contribute to the suspended-sediment load.

The Stokes fall speed assuming sediment density of 2.65 g m^{-3} (quartz) was assigned to each particle size: 0.0001 m s^{-1} , 0.001 m s^{-1} and 0.01 m s^{-1} , respectively, for the 12, 40 and $125 \text{ }\mu\text{m}$ fractions. Because the Stokes fall speed is assigned on the assumption

of quartz density, the 12, 40 and 125 μm particles are implied to be, as a result, in an unaggregated state. Unaggregated sediment particles are treated in the model because (1) mud content of harbour bed sediment is typically <16 % (Swales et al., 2008); (2) the harbour is relatively open and energetic, which will tend to cause the breakup of any aggregates that do form, and (3) suspended-sediment concentrations are typically too low (generally <100 mg L^{-1} ; rarely exceeding 1000 mg L^{-1}) to promote aggregation.

Comment is provided below on the applicability of the sediment-transport equations in the MIKE3 MT model to the 12, 40 and 125 μm particle sizes.

As with the salinity calibration, the daily freshwater inflow from each of the catchment outlets was derived by applying the TP108 approach (ARC, 1999) to daily rainfall data.

A relationship between daily rainfall and mean daily SSC was developed using data from the Whau River and Henderson Creek (Figure 37). This relationship was used to determine sediment inputs from each of the other catchment outlets for use as boundary conditions in the MIKE3 MT model.

The MIKE3 manual recommends that the critical bed shear stress for erosion τ_{ce} should be in the range 0.05–0.1 N m^{-2} . As a starting point for the calibration process, τ_{ce} for the bed as a whole was set to 0.05 N m^{-2} .

The MIKE3 manual recommends that the critical bed shear stress for deposition τ_{cd} is normally in the interval 0–0.1 N m^{-2} . As a starting point for the calibration process, τ_{cd} was set to 0.05 N m^{-2} (ie, the same value as τ_{ce}) for each particle size.

The MIKE3 MT model was warmed up for 14 days using mean freshwater inflow and associated sediment inputs. The distribution of sediments on the bed at the end of this time was used as the initial condition for the particle size composition of the bed sediment for the calibration runs. This also provided the initial condition for SSC throughout the harbour. These initial conditions were examined and tested as below.

The calibration process then consisted of adjusting α and E_f until a satisfactory fit between measured and predicted SSC was obtained at the calibration sites for all three simulation periods. The best match was obtained with $E_f = 0.00008 \text{ kg m}^{-2} \text{ s}^{-1}$ and $\alpha = 4$. For $(\tau_b - \tau_{ce}) < 0.4 \text{ N m}^{-2}$, these values for E_f and α yield an erosion rate that falls within the range of published rates (Van Rijn, 1989; Widdows et. al, 1998; Houwing, 1999; Whitehouse, 2000; Andersen and Pejrup, 2001; Wang, 2003) for similar physical settings and particle sizes. The calibrated erosion rate begins to diverge from published rates for higher values of $(\tau_b - \tau_{ce})$ (Figure 38).

The calibrated value for α lies on the bottom end of the DHI recommended range (4–23), while E_f is higher than the value DHI recommends for soft mud beds (0.00002 $\text{kg m}^{-2} \text{ s}^{-1}$). Using a higher value for α in the calibration tests caused the model to overpredict SSC when waves were present (ie, when $(\tau_b - \tau_{ce})$ was high), and using higher values for E_f caused overprediction when there were no waves.

The next step was to adjust τ_{cd} for the 12 and 125 μm fractions to further improve the fit between measured and predicted SSC. The best fit between measured and predicted SSC was sought by lowering τ_{cd} for the 12 μm fraction from the initial value of 0.05 N m^{-2} , and raising τ_{cd} for the 125 μm fraction (also from the initial value of 0.05

N m^{-2}). The best fit was obtained with $\tau_{\text{cd}} = 0.0225$ for the $12 \mu\text{m}$ fraction and $\tau_{\text{cd}} = 0.09$ for the $125 \mu\text{m}$ fraction.

Finally, a small change in τ_{ce} from 0.05 N m^{-2} to 0.047 N m^{-2} , matched by a reduction in τ_{cd} for the $40 \mu\text{m}$ fraction, completed the calibration process.

As a final check of the calibration process, the 14-day warm-up period was re-run using all of the calibration values determined this far, which provided another initial condition for the particle size composition of the bed sediment and the SSC. The calibrated model, together with these new initial conditions, was then used to predict SSC for the calibration periods. This is intended to test the way the model was warmed up. The output from the model so obtained for Sites 2, 4, 7, 8, 9, 10 and 11 is shown in Figures 39–58.

Under tides only (Figure 36–42) measured SSC is quite low (less than 0.05 kg m^{-3}). The model captures reasonably well the small tidal fluctuations in SSC.

Under stronger winds, the model captures the high SSC associated with sediment inputs from Henderson Creek, (Figure 43), mixing across the middle harbour (Figures 44 to 45), and relatively low SSC in the middle basin (Figure 46).

For the third calibration period, the model predicts reasonably well the elevated SSC in the main basin of the harbour (Figures 50 to 55), as well as the advection of the sediment plumes from the Whau River and Henderson Creek under stronger winds and waves.

The linear regression for all three calibration periods combined (Table 10) indicates that the model underpredicts measured SSC by $\sim 30\%$. Note, however, that peak SSC is generally very well predicted (eg, Figures 44, 45, 47 and 48). Note also that the predictions for Site 2 (in the entrance to Henderson Creek) give one of the better fits with the observed data. Hence, the possible over-estimation of dispersion within Henderson Creek that became apparent in the salinity calibration (see Section 5.3) does not seem to adversely affect the predictions of SSC.

Table 11 shows the average (over all calibration periods) particle size composition of the predicted suspended-sediment load integrated over the water column at each site. The $12 \mu\text{m}$ fraction contributed most to the predicted load, and the $125 \mu\text{m}$ fraction contributed typically less than 10% of the predicted load.

The erosion and deposition equations used in the MIKE3 MT model explicitly treat the sediment entrainment flux, which transports sediment away from the bed, and the sediment settling flux, which transports sediment back to the bed. The sediment entrainment flux is expressed in terms of an erosion rate, and the sediment settling flux is expressed in terms of a deposition rate. If these balance, then the special case of “equilibrium” arises, in which the SSC reaches a steady state. This results in disturbance of the bed only down to the fixed depth needed to supply the corresponding equilibrium suspended-sediment load. If the entrainment flux exceeds the settling flux, the bed will deflate. Deflation will occur until more consolidated layers in the bed sediment become exposed, which shuts down the erosion process. Without the bed “intervening” in this way, erosion may continue indefinitely.

The simulation of fine-sediment transport typically requires explicit treatment of the entrainment and settling fluxes, because fine sediments are not likely to attain

equilibrium. In that sense, the MIKE3 MT model is a fine-sediment model. Nevertheless, equilibrium concentrations may still arise from explicit treatment of entrainment and settling fluxes, but that is not bound to happen. For simulation of coarser sediment, a reference-concentration formulation is normally used for the bottom boundary condition. This implicitly assumes a balance (or equilibrium) between the entrainment and settling fluxes. A widely used reference-concentration model, applicable to sand for which there is an implicit balance between the entrainment and settling fluxes, is that of Nielsen (1984).

The 12 μm fraction used in the simulations here falls into the category of fine sediments that do not readily achieve equilibrium. Hence, the MIKE3 MT model is properly constituted for this fraction. The 40 μm fraction behaves more like a fine sediment, but the 125 μm fraction may not.

Nevertheless, reasonable concentrations for the 125 μm fraction may still arise through the MIKE3 MT formulation, and two factors suggest that this is indeed the case here: (1) a good calibration of the model against the **total** (all fractions) suspended-sediment concentration was achieved using the entrainment/settling-flux equations applied to all three fractions, and (2) the 125 μm fraction was found to contribute only a small part of the modelled total suspended-sediment load (Table 10), which is expected.

Figure 56a-c provides a check on the predicted 125 μm concentrations by plotting them against the predicted bed shear stress. Specifically, the predicted bed shear stress in that figure is represented as the nondimensional skin friction, θ' , which is given by:

$$\theta' = \tau'_{wc} / [(\rho_s - \rho_f)gD] \quad (21)$$

where τ'_{wc} is the combined wave-current skin friction acting on the 125 μm fraction, predicted by the DHI FM model. Overlaid on the same plot is a curve showing concentration of the 125 μm fraction predicted by Nielsen's (1984) reference-concentration model:

$$C = C_0 \exp(-z/l) \quad (22)$$

where z is elevation above the bed (which is chosen to be the same level at which the DHI MT predictions shown in the figure are specified), l is the mixing length, taken here to be 4 cm, which is approximately the height of wave-generated ripples, and C_0 is the concentration at the bed:

$$C_0 = 0.005\rho_s\theta'^3 \quad (23)$$

For all calibration periods the DHI MT model is seen to overpredict concentration of the 125 μm fraction compared to predictions by Nielsen's reference-concentration model, with the discrepancy being smallest for the third calibration period (Figure 56c), when waves were present. Nevertheless, the actual overprediction is very small (typically less than 10 mg L^{-1}) and, as noted previously, the 125 μm fraction constitutes (correctly) only a small fraction of the total suspended-sediment load. It is concluded that, although the MIKE3 MT model is properly constituted only for the 12 and 40 μm fractions, nevertheless, the 125 μm concentrations predicted by the MT model are satisfactory.

Table 10

Statistics of linear regression between predicted (x) and measured (y) suspended sediment concentrations at Sites 2, 4, 7, 8, 9, 10 and 11 (see Figure 1a). All three calibration periods are combined to give the overall performance of the model under the range of conditions modelled.

Site	Linear regression
2	$y = 0.7014x + 0.009$, r-squared = 0.6167
4	$y = 0.7601x + 0.0069$, r-squared = 0.655
7	$y = 0.7368x + 0.0047$, r-squared = 0.4391
8	$y = 0.5992x + 0.0058$, r-squared = 0.4665
9	$y = 0.6245x + 0.0106$, r-squared = 0.2875
10	$y = 0.6476x + 0.0027$, r-squared = 0.721
11	$y = 0.637x + 0.0051$, r-squared = 0.4979

Table 11

Average (over all calibration periods) particle size composition of the predicted suspended-sediment load integrated over the water column at each site.

Site	Fraction	Average contribution to predicted depth-integrated SSC
2	12 µm	71 %
4	12 µm	68 %
7	12 µm	57 %
8	12 µm	53 %
9	12 µm	73 %
10	12 µm	59 %
11	12 µm	52 %
2	40 µm	23 %
4	40 µm	26 %
7	40 µm	32 %
8	40 µm	34 %
9	40 µm	23 %
10	40 µm	31 %
11	40 µm	35 %
2	125 µm	5 %
4	125 µm	6 %
7	125 µm	11 %
8	125 µm	13 %
9	125 µm	4 %
10	125 µm	10 %
11	125 µm	14 %

Figure 34

Relationship between measured daily rainfall and mean daily suspended sediment concentration, Whau River and Henderson Creek (Sites 3 and 5, Figure 1a).

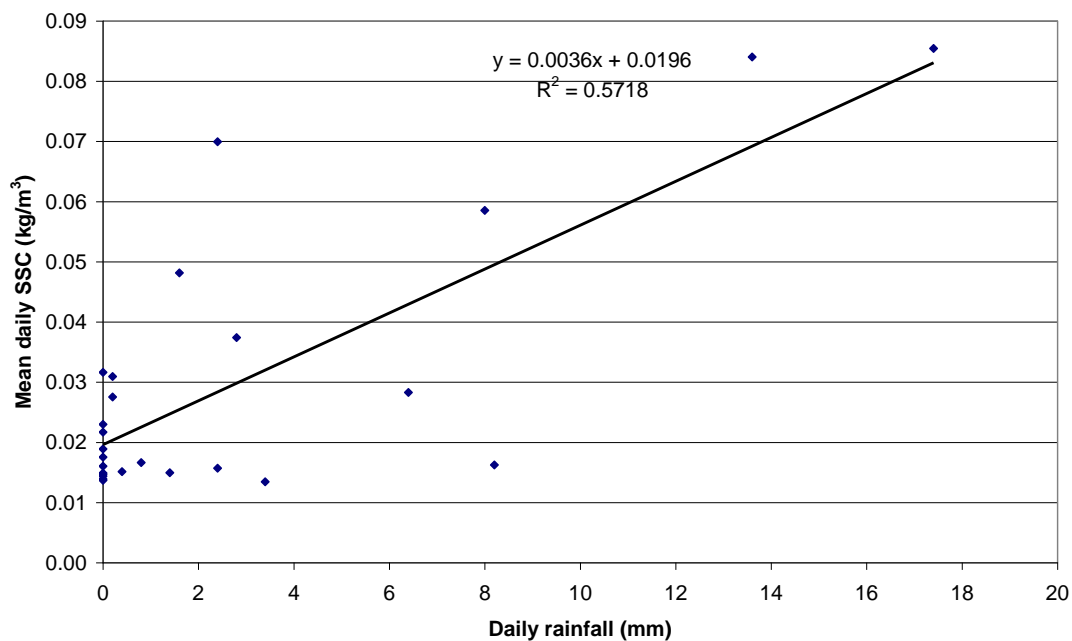


Figure 35

Comparison of published erosion rates and the erosion rate for the MT model calibrated for the Central Waitemata Harbour.

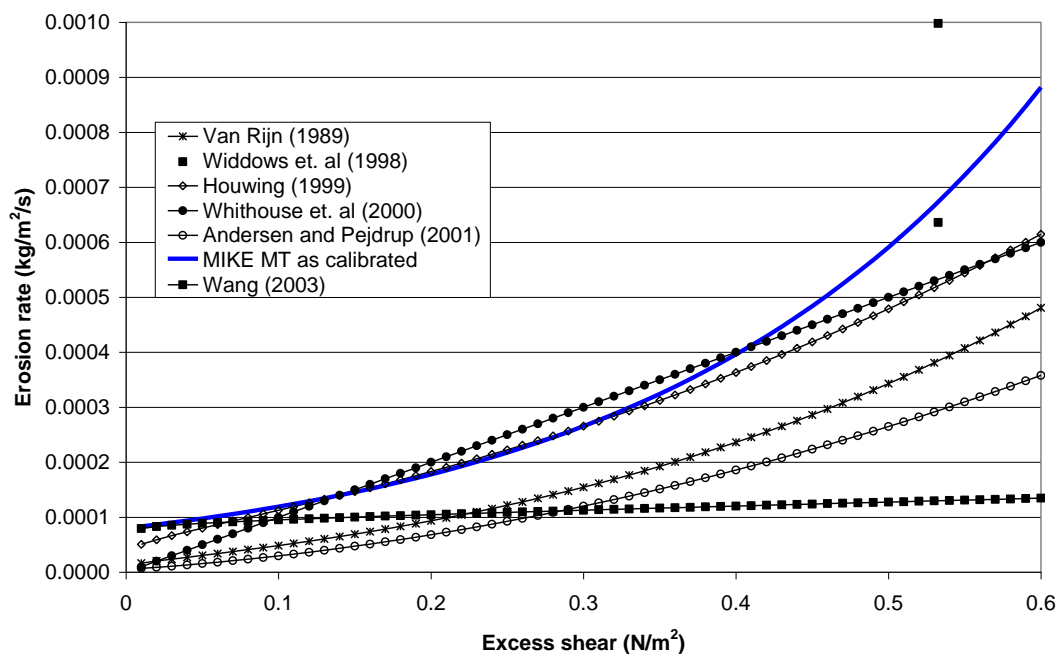


Figure 36

Predicted and measured suspended sediment concentration at Site 2 (Figure 1a) for the period 6–8 May 2006.

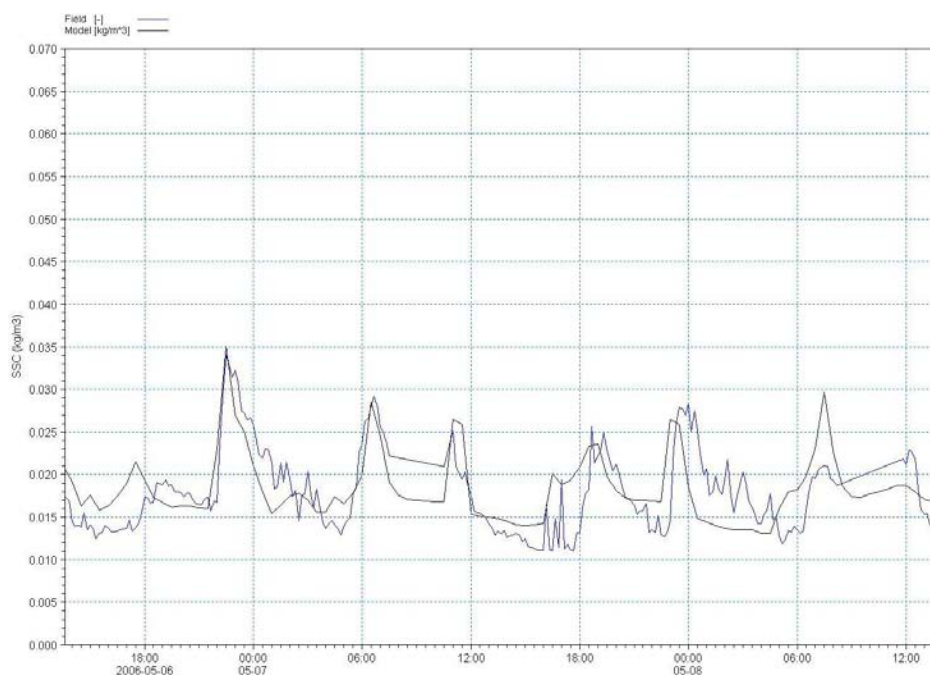


Figure 37

Predicted and measured suspended sediment concentration at Site 4 (Figure 1a) for the period 6–8 May 2006.

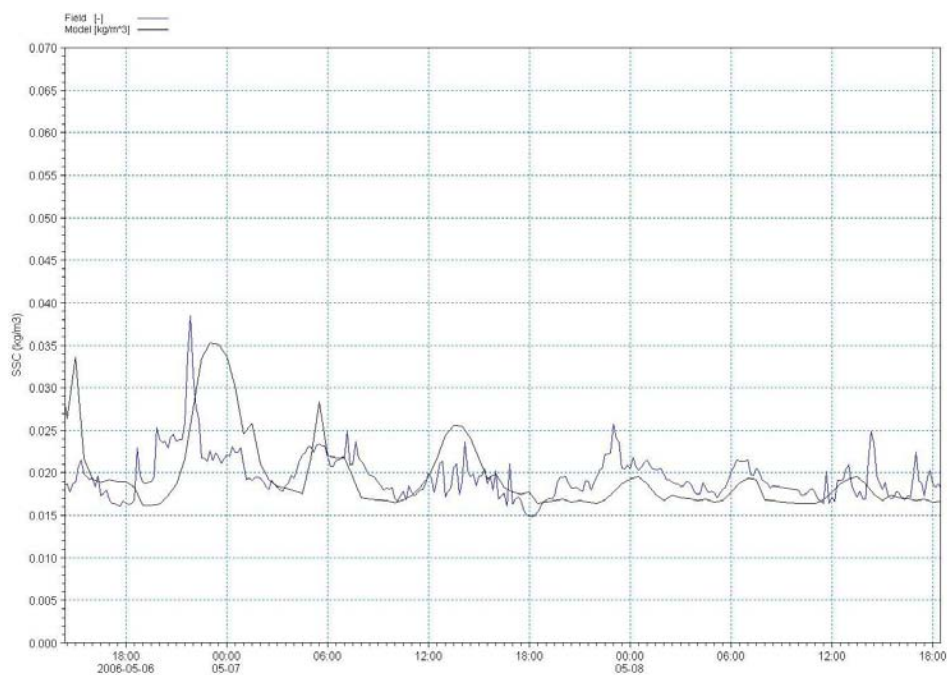


Figure 38

Predicted and measured suspended sediment concentration at Site 7 (Figure 1a) for the period 6–8 May 2006.

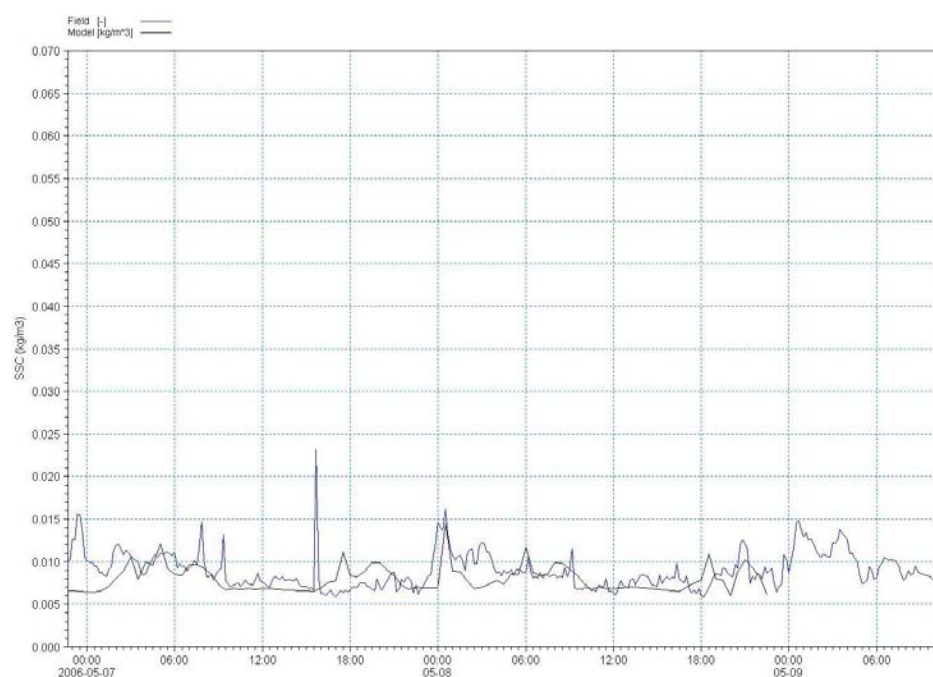


Figure 39

Predicted and measured suspended sediment concentration at Site 8 (Figure 1a) for the period 6–8 May 2006.

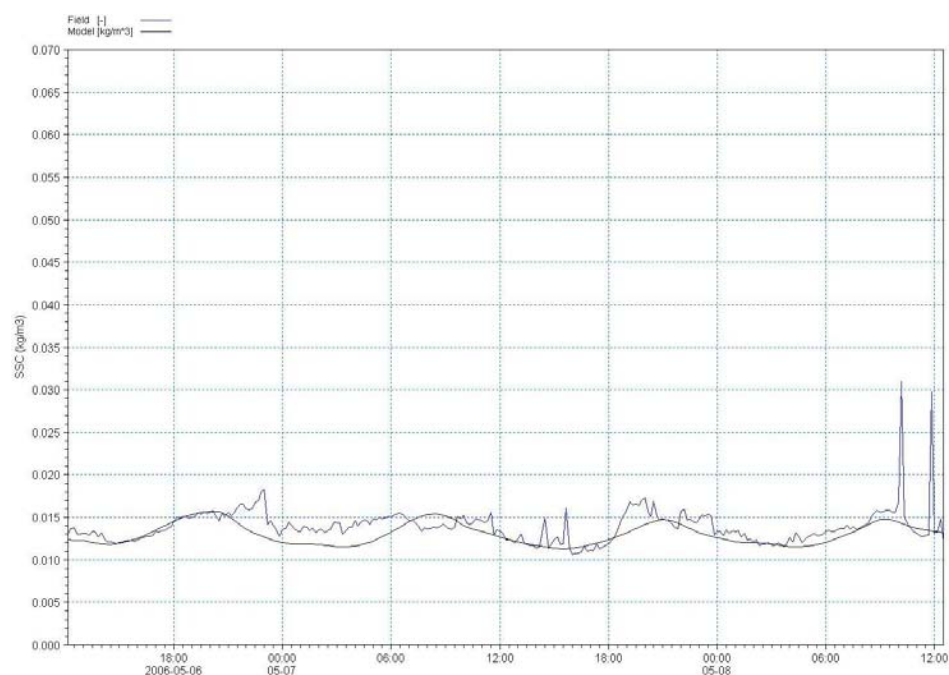


Figure 40

Predicted and measured suspended sediment concentration at Site 9 (Figure 1a) for the period 6–8 May 2006.

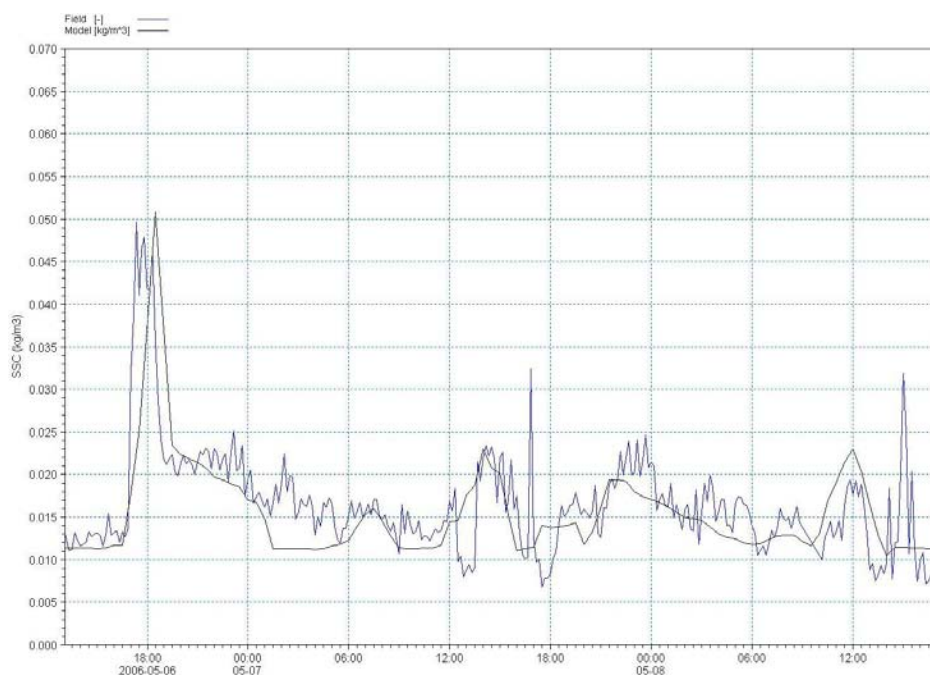


Figure 41

Predicted and measured suspended sediment concentration at Site 10 (Figure 1a) for the period 6–8 May 2006.

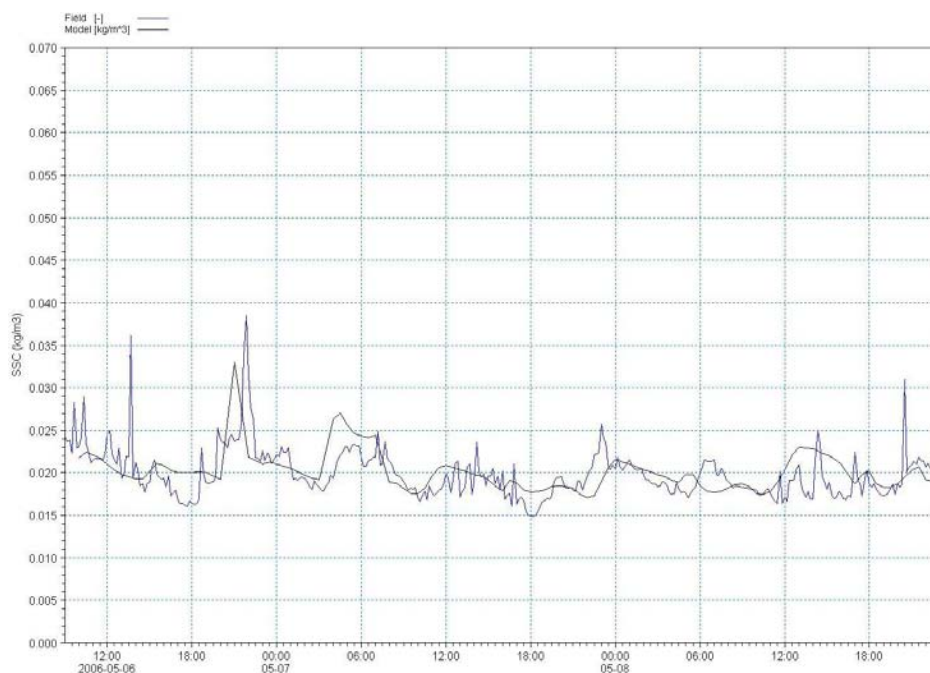


Figure 42

Predicted and measured suspended sediment concentration at Site 11 (Figure 1a) for the period 6–8 May 2006.

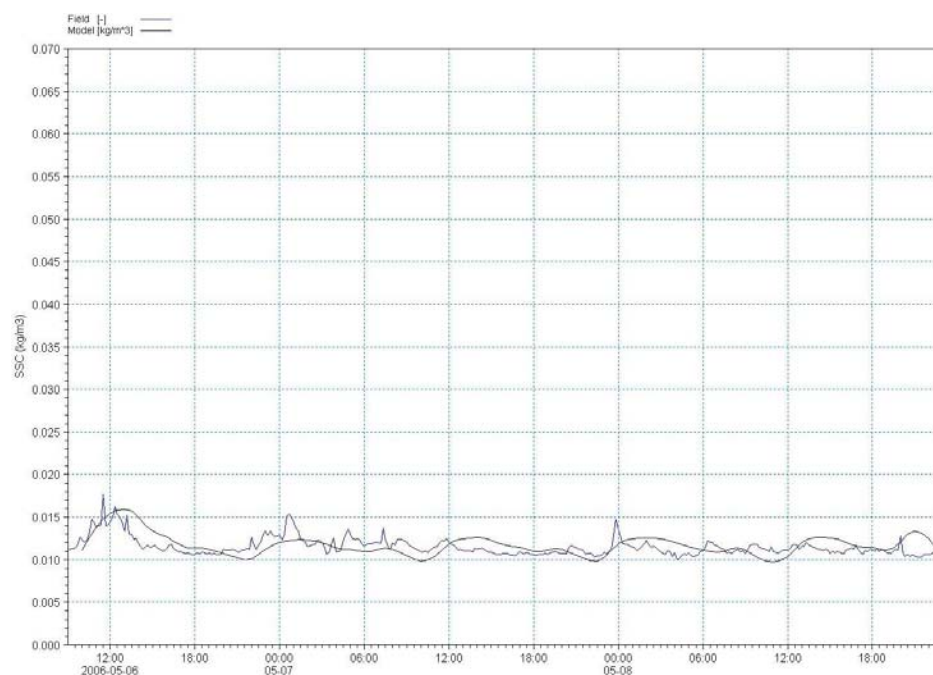


Figure 43

Predicted and measured suspended sediment concentration at Site 2 (Figure 1a) for the period 18–21 June 2006.

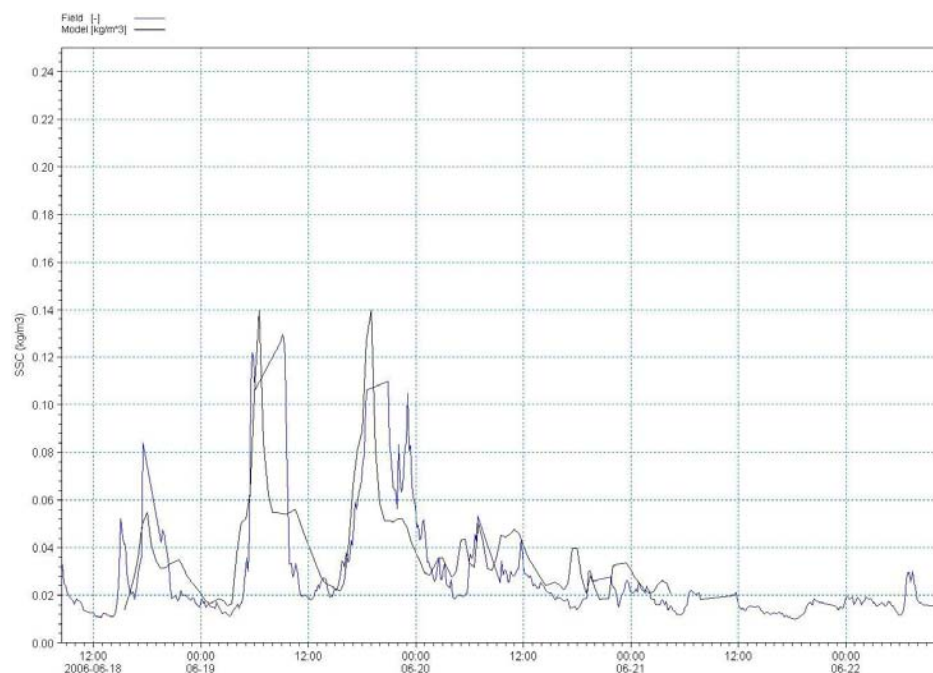


Figure 44

Predicted and measured suspended sediment concentration at Site 4 (Figure 1a) for the period 18–21 June 2006.

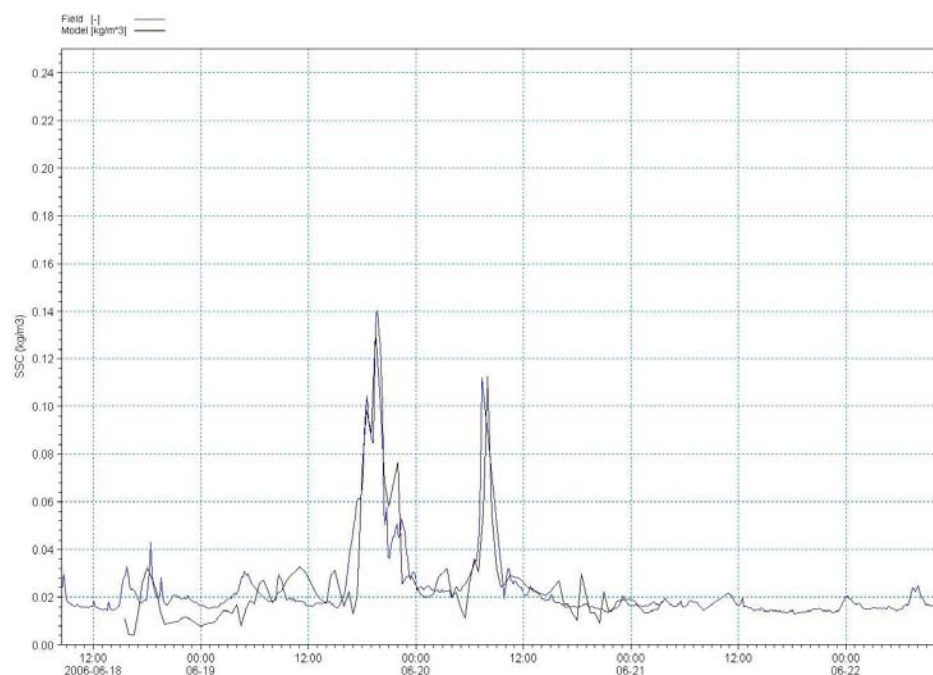


Figure 45

Predicted and measured suspended sediment concentration at Site 7 (Figure 1a) for the period 18–21 June 2006.

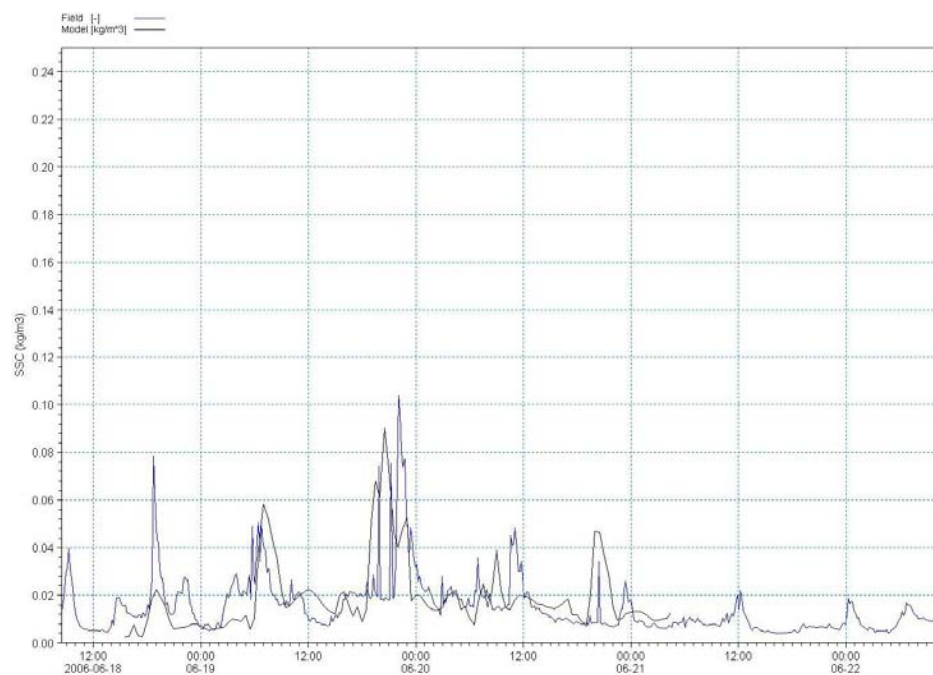


Figure 46

Predicted and measured suspended sediment concentration at Site 8 (Figure 1a) for the period 18–21 June 2006.

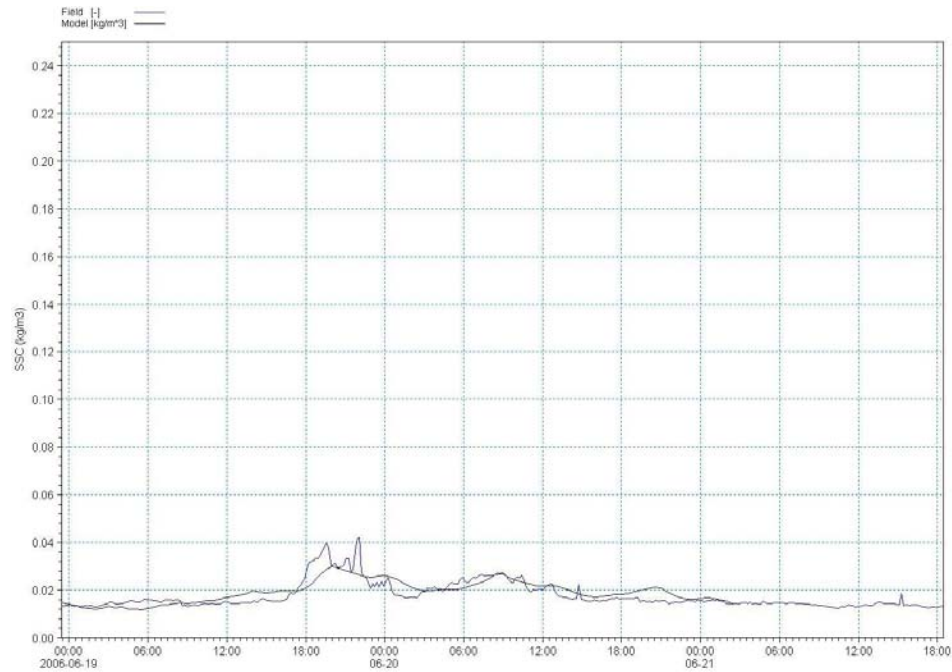


Figure 47

Predicted and measured suspended sediment concentration at Site 9 (Figure 1a) for the period 18–21 June 2006.

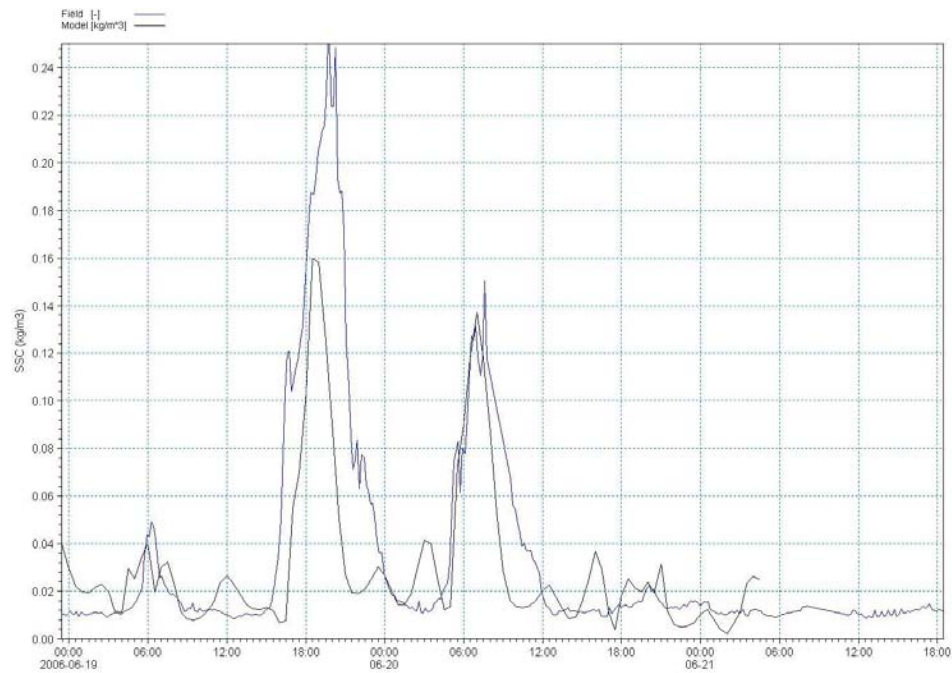


Figure 48

Predicted and measured suspended sediment concentration at Site 10 (Figure 1a) for the period 18–21 June 2006.

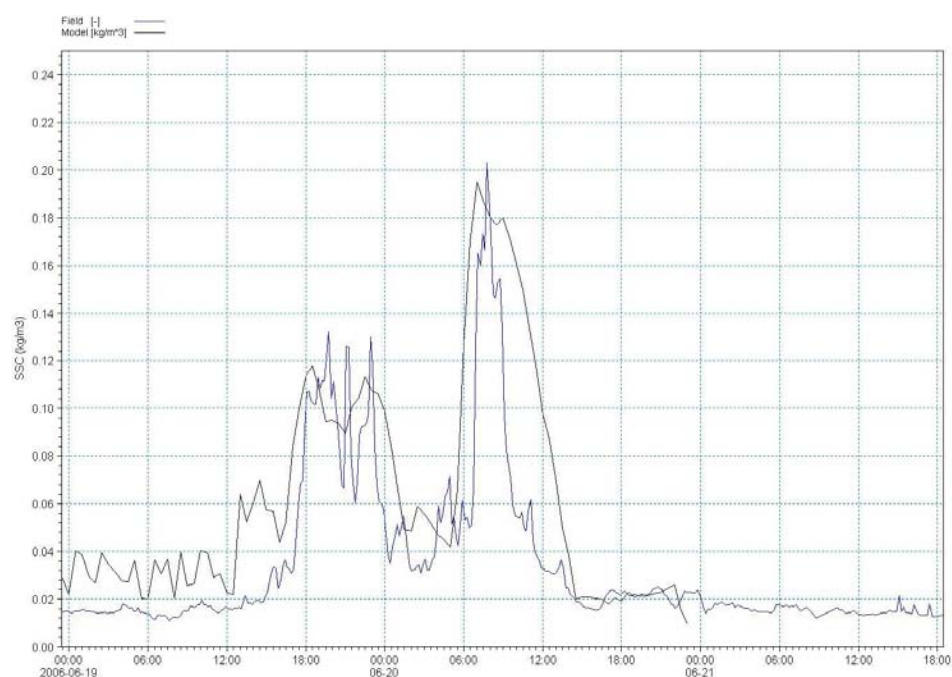


Figure 49

Predicted and measured suspended sediment concentration at Site 11 (Figure 1a) for the period 18–21 June 2006.

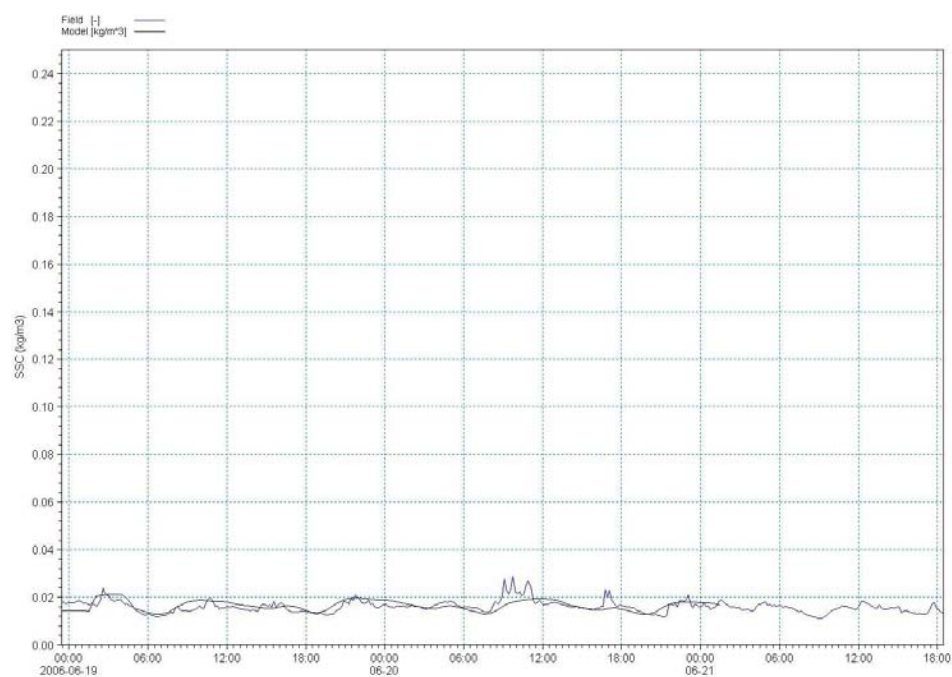


Figure 50

Predicted and measured suspended sediment concentration at Site 2 (Figure 1a) for the period 26–28 May 2006.

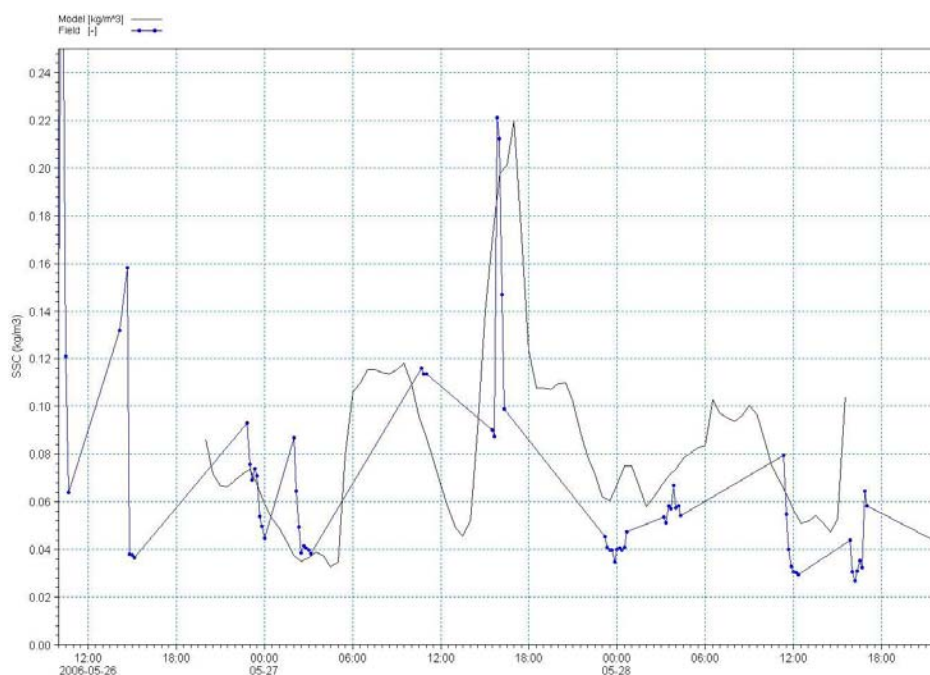


Figure 51

Predicted and measured suspended sediment concentration at Site 4 (Figure 1a) for the period 26–28 May 2006.

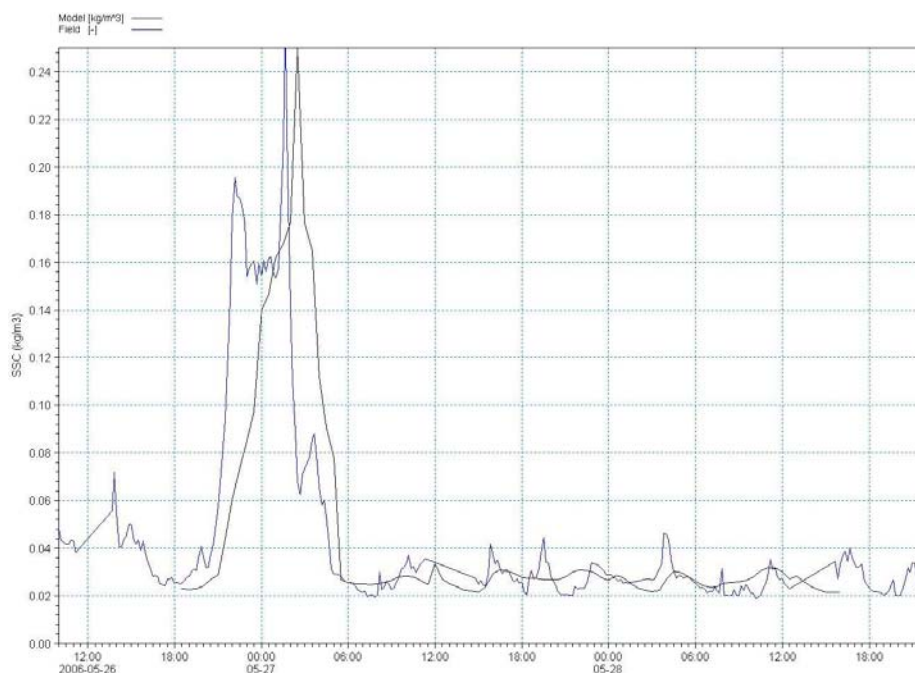


Figure 52

Predicted and measured suspended sediment concentration at Site 7 (Figure 1a) for the period 26–28 May 2006.

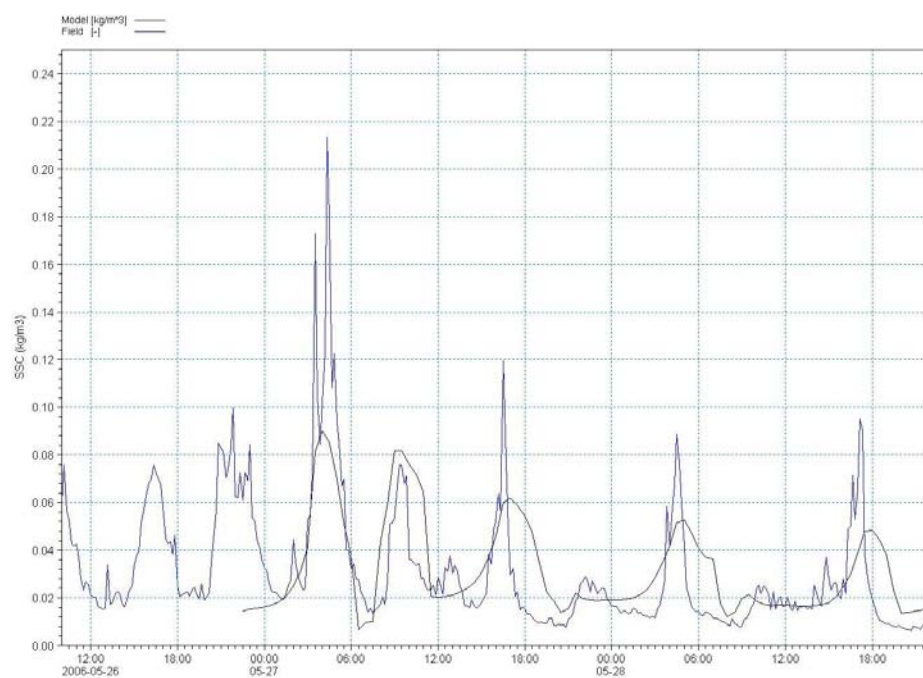


Figure 53

Predicted and measured suspended sediment concentration at Site 8 (Figure 1a) for the period 26–28 May 2006.

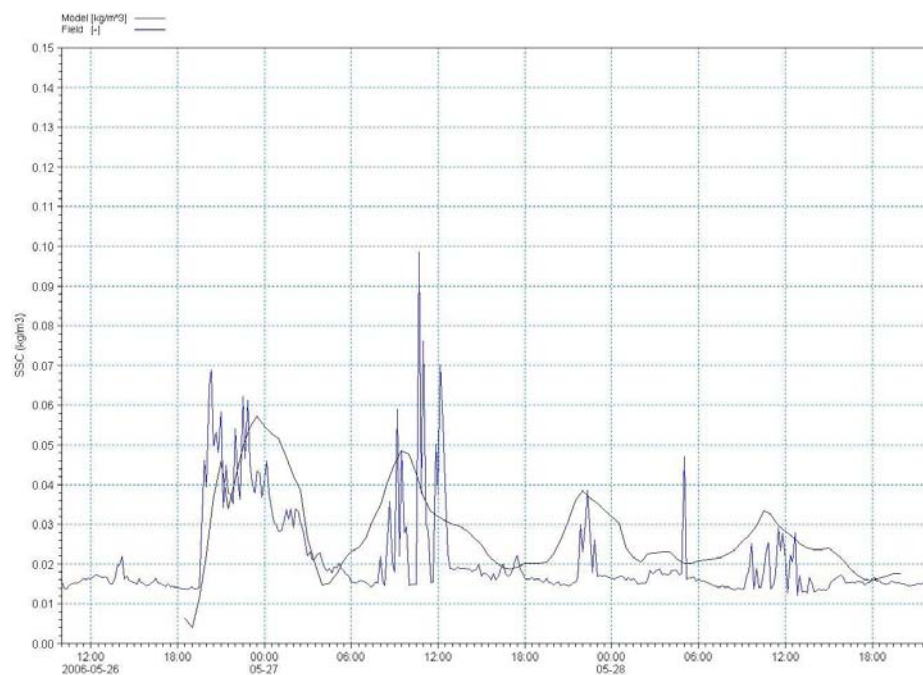


Figure 54

Predicted and measured suspended sediment concentration at Site 10 (Figure 1a) for the period 26–28 May 2006.

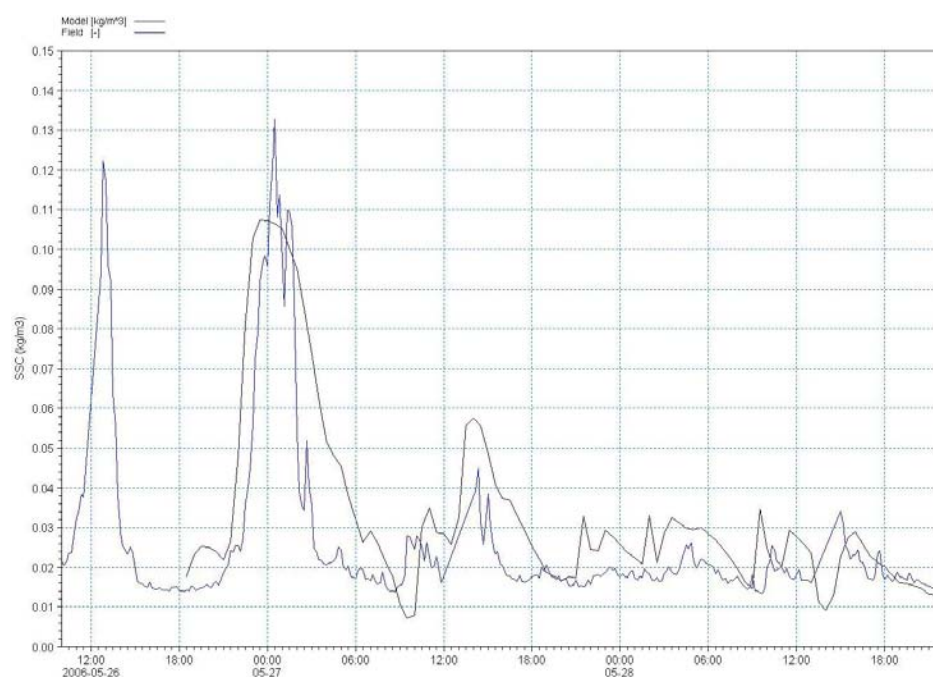


Figure 55

Predicted and measured suspended sediment concentration at Site 11 (Figure 1a) for the period 26–28 May 2006.

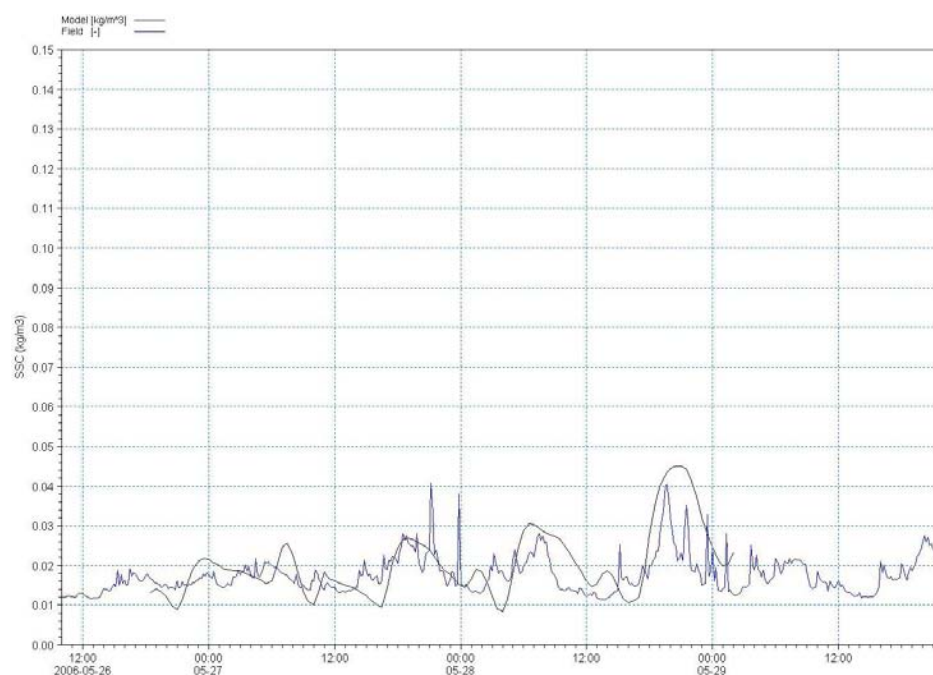


Figure 56a

Suspended-sediment concentration of the 125 μm fraction predicted by the DHI MT model versus nondimensional skin friction predicted by the DHI FM model. Also shown is Nielsen's reference-concentration model. (A) Calibration period 1.

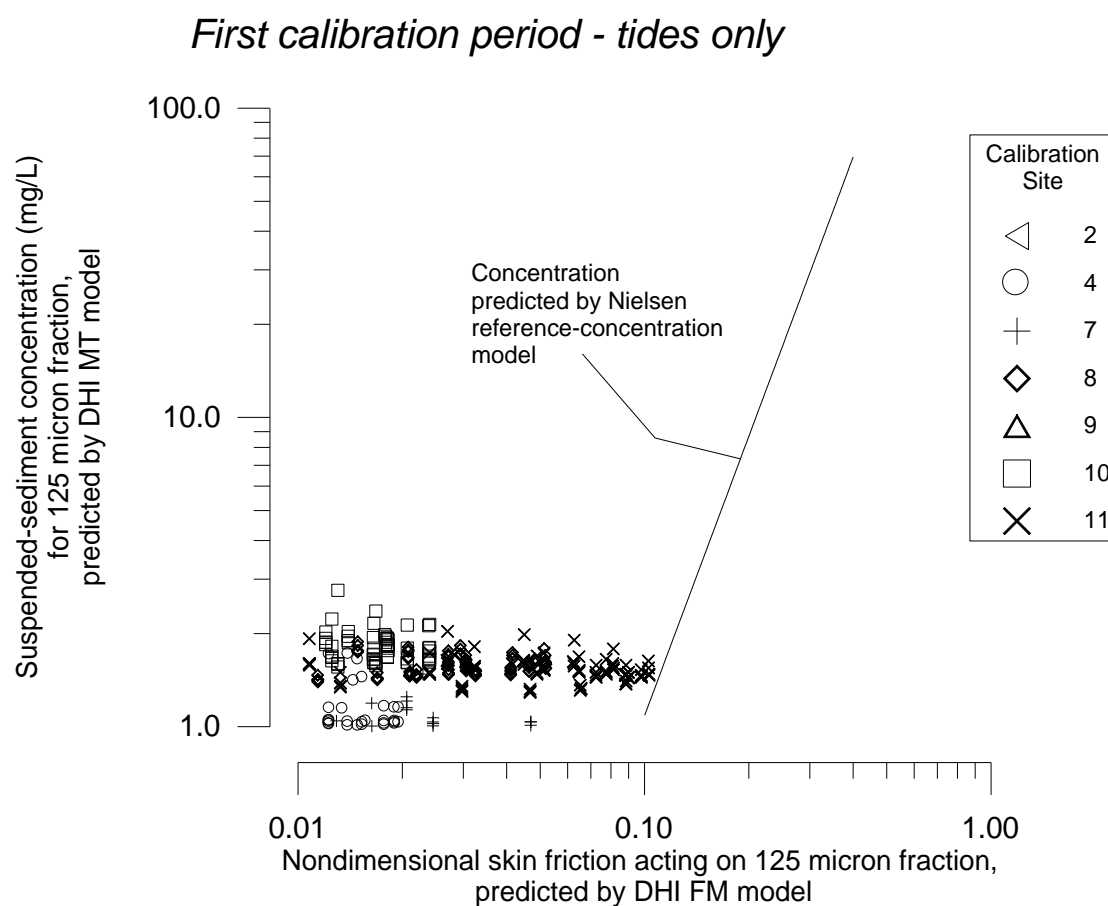


Figure 56b

Suspended-sediment concentration of the 125 μm fraction predicted by the DHI MT model versus nondimensional skin friction predicted by the DHI FM model. Also shown is Nielsen's reference-concentration model. (B) Calibration period 2.

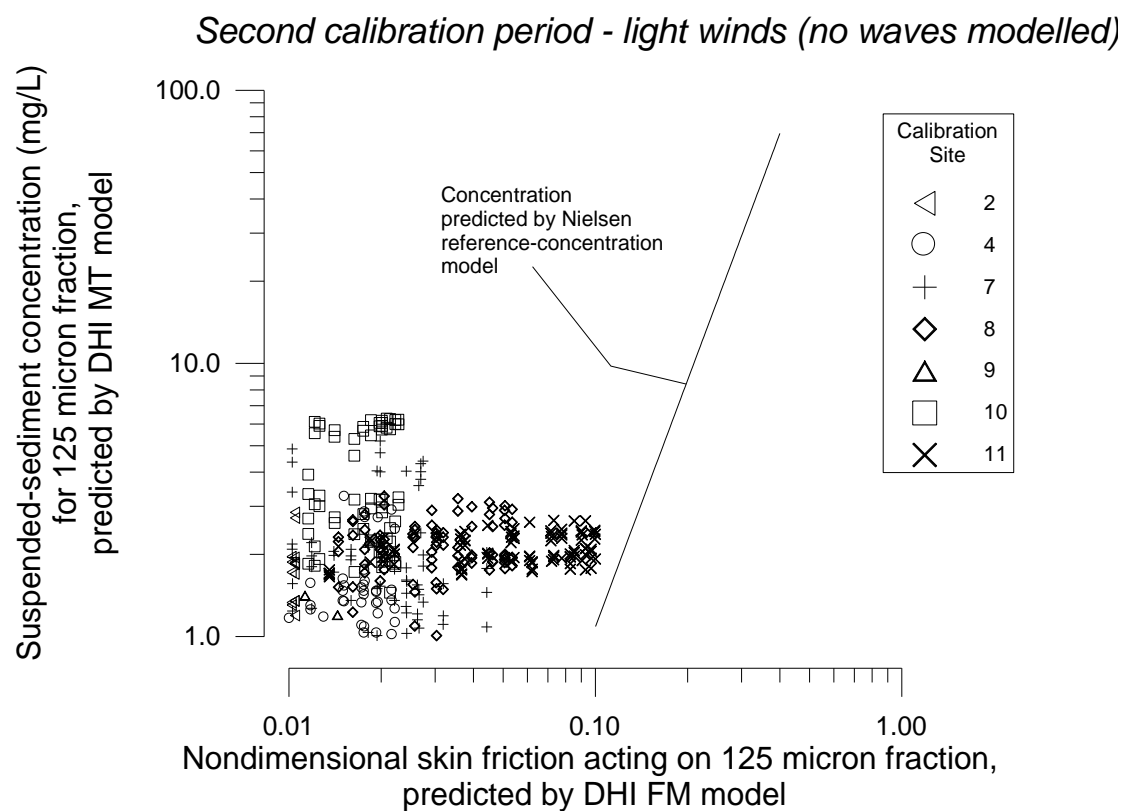
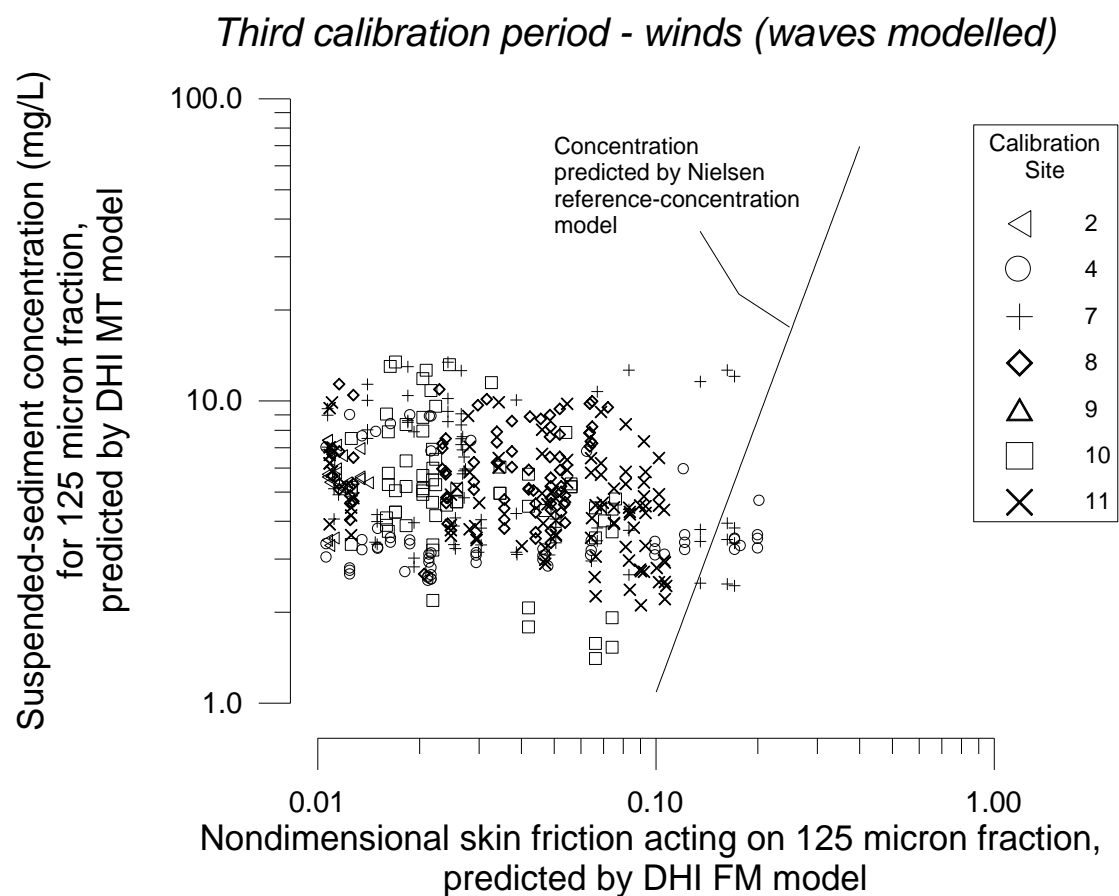


Figure 56c

Suspended-sediment concentration of the 125 μm fraction predicted by the DHI MT model versus nondimensional skin friction predicted by the DHI FM model. Also shown is Nielsen's reference-concentration model. (C) Calibration period 3.



6 References

- ANDERSEN, T.J.; PEJRUP, M., 2001. Suspended sediment transport on a temperate, microtidal mudflat, the Danish Wadden Sea. *Marine Geology* 173: pp. 69-85.
- AUCKLAND REGIONAL COUNCIL, 1999. *Guidelines for stormwater run-off modelling in the Auckland region*, Auckland Regional Council, Technical Publication No. 108, April 1999, ISSN 1172-6415.
- BOOIJ, N.; RIS, R.C.; HOLTHUIJSEN, L.H., 1999. A third generation model for coastal regions. Part I: Model description and validation, *Journal of Geophysical Research*, Vol. 104, No. C4, pp. 7649-7666.
- FREDSØE, J., 1984. Turbulent boundary layer in wave-current motion. *Journal of Hydrological Engineering*, A.S.C.E, Volume 110, HY8, 1103-1120 (1984).
- GREEN, M.O; COCO, G., 2007. Sediment transport on an estuarine intertidal flat: measurements and conceptual model of waves, rainfall and exchanges with a tidal creek. *Estuarine, Coastal and Shelf Science*, 72: 553-569.
- HOLTHUIJSEN, L.H.; BOOIJ, N.; RIS, R.C., 1993. A spectral wave model for the coastal zone, Proceedings of 2nd International Symposium on Ocean Wave Measurement and Analysis, New Orleans, USA, pp. 630-641.
- HOLTHUIJSEN, L.H.; BOOIJ, N.; RIS, R.C.; HAAGSMA, I.G.; KIEFTENBURG, A.T.M.M.; KRIEZI, E.E., 2000. *SWAN Cycle 3 version 40.11 user manual*. Delft University of Technology.
- HOUWING, E.J., 1999. Determination of the critical erosion threshold of cohesive sediments on intertidal mudflats along the Dutch Wadden Sea Coast. *Estuarine, Coastal and Shelf Science* 49: pp. 545-555.
- NIELSEN, P., 1984. Field measurements of time-averaged suspended-sediment concentrations under waves. *Coastal Engineering* 8: 51-72.
- OLDMAN, J.W.; SENIOR, A.; HASKEW, R.; RAMSAY, D., 2004. *Hauraki Regional Harbour Model: Set-up, Calibration and Verification*. NIWA Client Report HAM2004-038. Prepared for Auckland Regional Council.
- OLDMAN, J.; HANCOCK, N.; LEWIS, M., 2008. *Central Waitemata Harbour Contaminant Study. Harbour Hydrodynamics and Sediment-Transport Fieldwork*. Prepared by NIWA Ltd for Auckland Regional Council. Auckland Regional Council Technical Report 2008/036

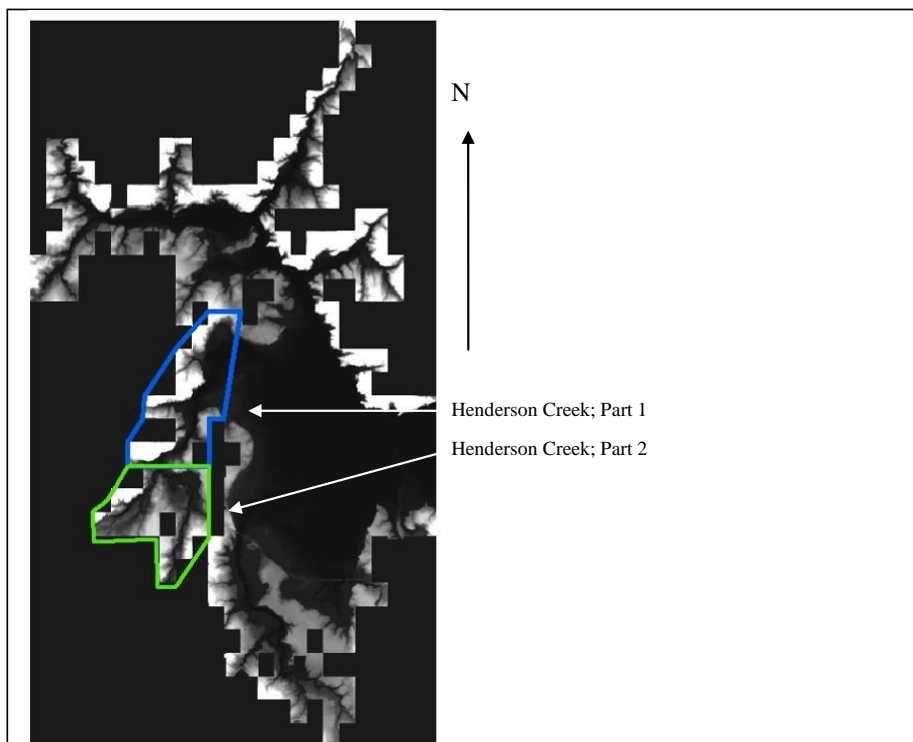
- RIJN, VAN L.C., 1989. *Handbook on Sediment Transport by Current and Waves*. Delft Hydraulics, Report H461, pp. 12.1-12.27.
- RIS, R.C., N. BOOIJ; HOLTHUIJSEN, L.H., 1999. A third-generation wave model for coastal regions. Part II: Verification, *Journal of Geophysical Research*, Vol. 104, No. C4, pp. 7667-7682.
- SLEIGH, P.A.; GASKELL, P.H.; BERSINS, M.; WRIGHT, N.G., 1998, An unstructured finite-volume algorithm for predicting flow in rivers and estuaries. *Computers & Fluids*, Vol. 27, No. 4, 479-508.
- SOULSBY R.L.; HAMM L.; KLOPMAN G.; MYRHAUG D.; SIMONS R.R.; THOMAS G.P., 1993. Wave-current interaction within and outside the bottom boundary layer *Coastal Engineering*, 21, 41-69 (1993).
- SWALES, A.; STEPHENS, S.; HEWITT, J.; OVENDEN, R.; HAILES, S.; LOHRER, D.; HERMANS PHAN, N.; HART, C.; BUDD, R.; WADHWA, S.; OKEY, M., 2008. *Central Waitemata Harbour Study. Harbour Sediments*. Prepared by NIWA Ltd for Auckland Regional Council. Auckland Regional Council Technical Report 2008/034.
- SWART, D.H., 1974. Offshore sediment transport and equilibrium beach profiles. Delft Hydraulic Laboratory Publication 1312, Delft University of Technology, The Netherlands.
- WANG, Y.H., 2003. The intertidal erosion rate of cohesive sediment: a case study from Long Island Sound. *Estuarine, Coastal and Shelf Science* 56. pp. 891–896.
- WHITEHOUSE, R.; SOULSBY, R.; ROBERTS, W.; MITCHENER, H., 2000. *Dynamics of estuarine muds*. Thomas Telford.
- WIDDOWS, J.; BRINSLEY, M.D.; BOWLEY, N.; BARRETT, C., 1998. A Benthic Annular Flume for In Situ Measurement of Suspension Feeding/Biodeposition Rates and Erosion Potential of Intertidal Cohesive Sediments. *Estuarine, Coastal and Shelf Science* 46. pp. 27–38.
- ZHAO, D.H.; SHEN, H.W.; TABIOS, G.Q.; TAN, W.Y.; LAI, J.S., 1994. Finite-volume 2-dimensional unsteady-flow model for river basins. *Journal of Hydraulic Engineering*, ASCE, 1994, 120, No. 7, 863-833.

7 Appendix 1: LIDAR Data Processing

The LIDAR data were supplied to NIWA in raster format, which gives the image shown in Figure 56 when viewed in Arcmap GIS. Due its size (1.1 GB), only small portions of the image could be processed at any one time. For example, the Henderson Creek data were extracted in two parts, creating the image shown in Figure 61.

Figure 57

The grey-scale, high-resolution LIDAR image of the western sector of the Waitemata Harbour.

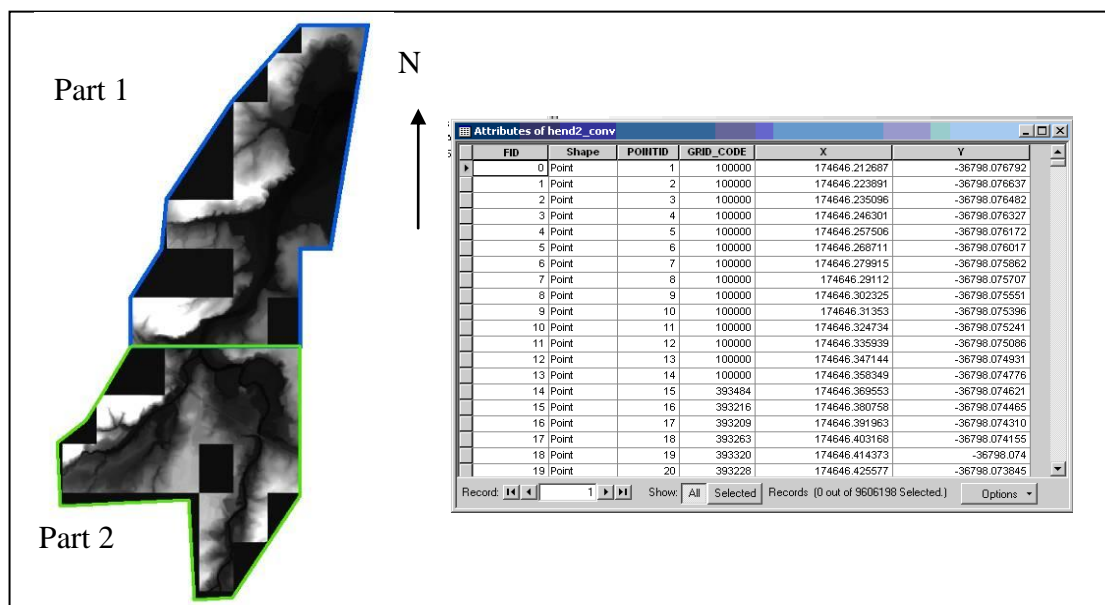


Each of the smaller portions of the raster image were converting into a point file with the co-ordinate system converted to WGS 1984 latitude/longitude, to be consistent with the other bathymetry data. The point file contains the latitude, longitude and height relative to Auckland Vertical Datum -1946 of each of the pixels in the image. The conversion from Auckland Vertical Datum -1946 to Chart Datum consisted of adding 1.743 m to the raw LIDAR data³. Each point file was then converted to a format that could be read by the DHI models.

³ Chart Datum is defined as 1.853 m below the actual mean level of the sea (MLOS) which is 0.11 m above the Auckland Vertical Datum -1946.

Figure 58

The image of Henderson Creek and the associated point file.



8 Appendix 2: Mesh Detail

Figure 59

Detail of mesh within the Upper Waitemata Harbour.

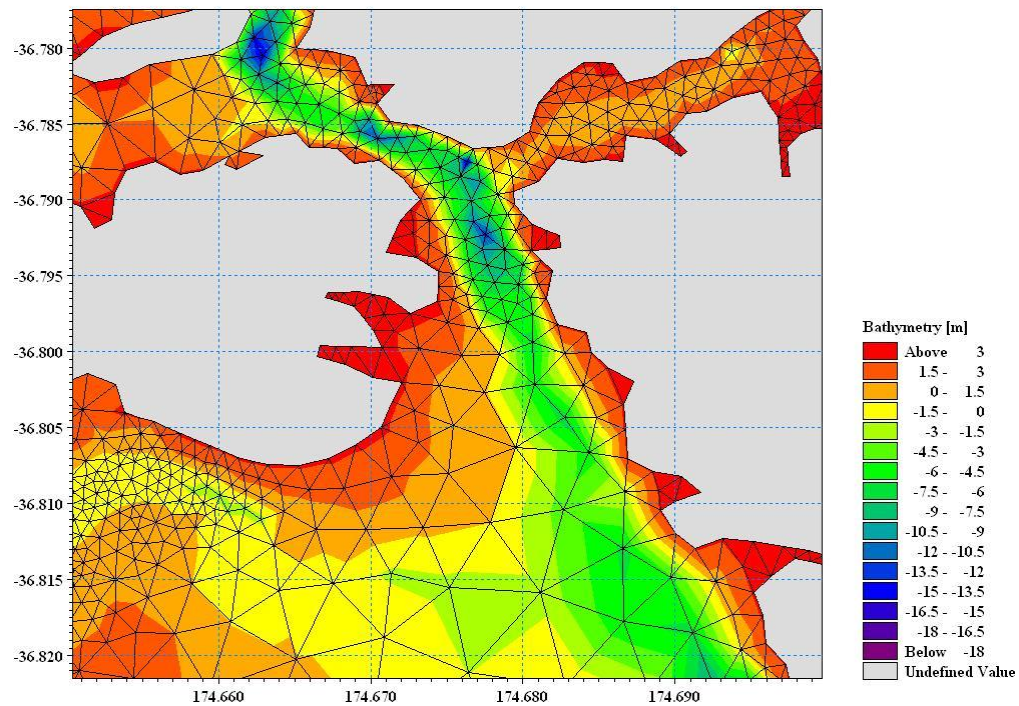


Figure 60

Detail of mesh within the Central Waitemata Harbour.

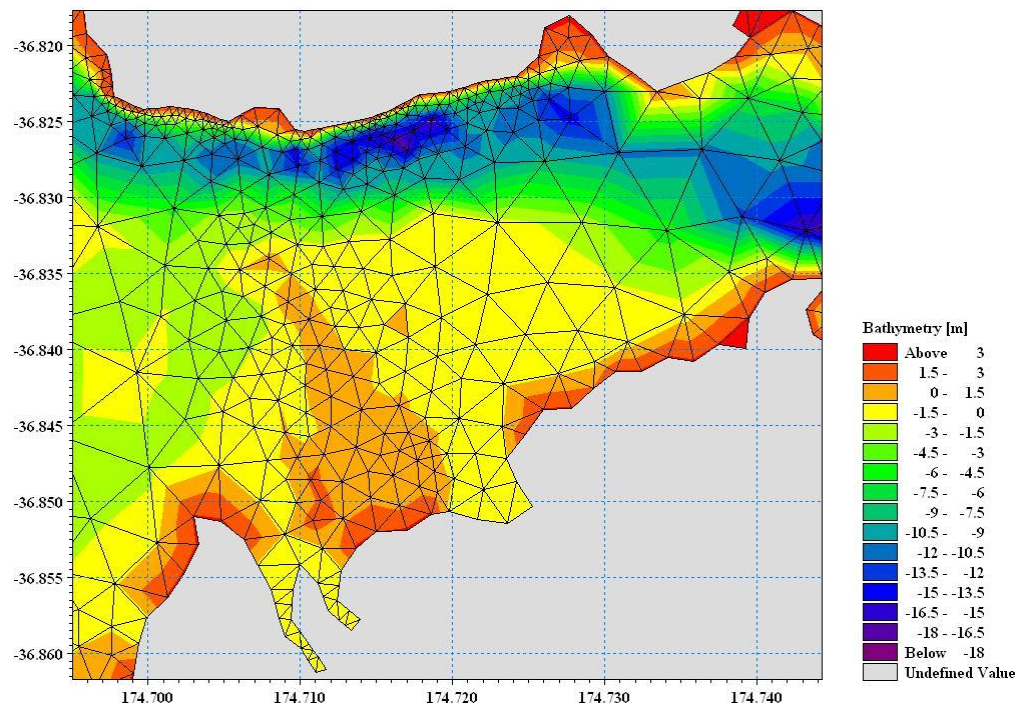


Figure 61

Detail of mesh within the Outer Waitemata Harbour.

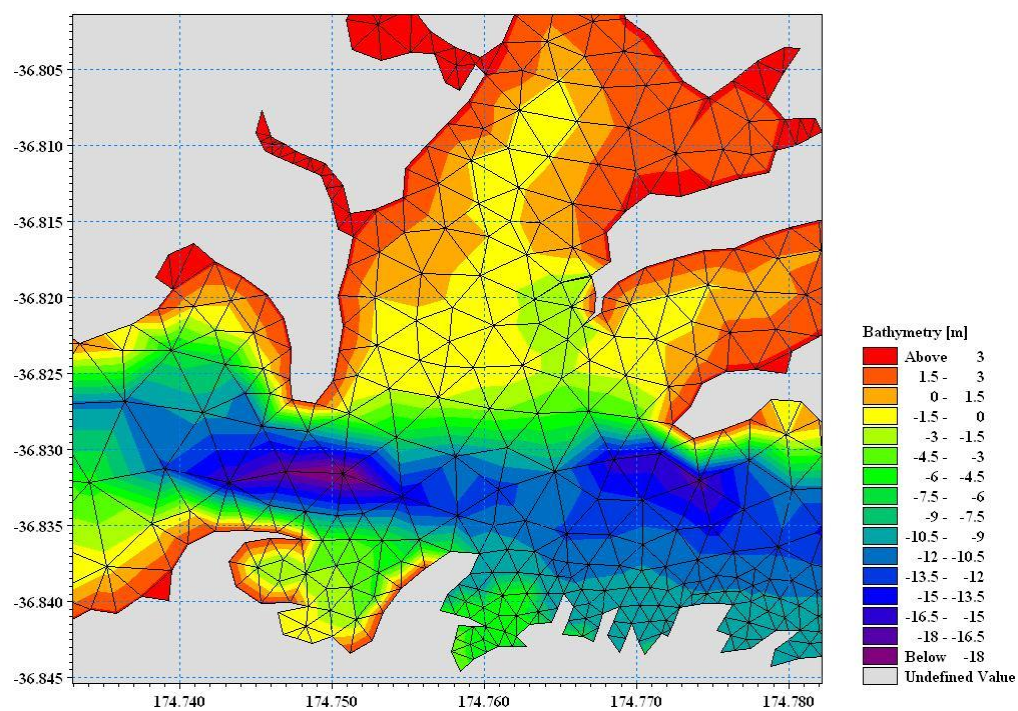


Figure 62

Detail of mesh within the Henderson Creek.

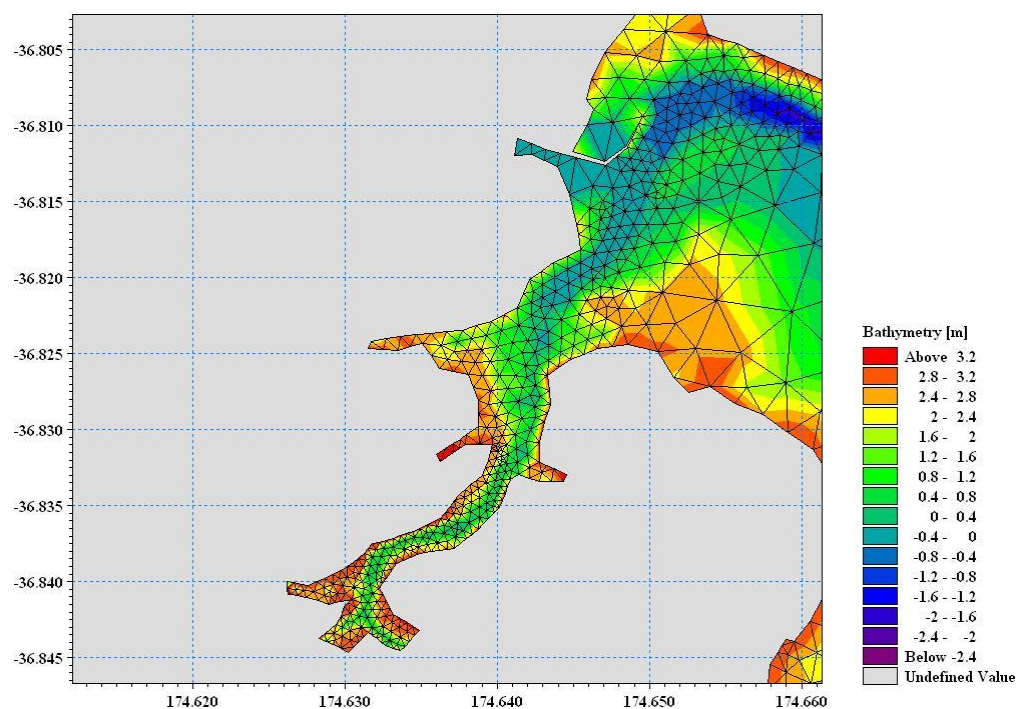


Figure 63

Detail of mesh within the Henderson Creek.

